AN EXPERIMENTAL STUDY OF THE EFFECTS OF CO_2 SEQUESTRATION ON ELECTRICAL PROPERTIES OF CARBONATE ROCKS

BY

Abdulrauf Rasheed Adebayo

A Dissertation Presented to the

DEANSHIP OF GRADUATE STUDIES

KING FAHD UNIVERSITY OF PETROLEUM & MINERALS

DHAHRAN, SAUDI ARABIA

In Partial Fulfillment of the

Requirements for the Degree of

DOCTOR OF PHILOSOPHY

In

PETROLEUM ENGINEERING

March 2015

KING FAHD UNIVERSITY OF PETROLEUM & MINERALS

DHAHRAN- 31261, SAUDI ARABIA

DEANSHIP OF GRADUATE STUDIES

This thesis, written by **ABDULRAUF RASHEED ADEBAYO** under the direction of his thesis advisor and approved by his thesis committee, has been presented and accepted by the Dean of Graduate Studies, in partial fulfillment of the requirements for the degree of **DOCTOR OF PHILOSOPHY IN PETROLEUM ENGINEERING.**

Dr. Hasan Y. Al-Yousef
(Advisor)

Dr. Abdullah S. Sultan
Department Chairman

Dr. Mohamed Mahmoud
(Co-Advisor)

Dr. Salam A. Zummo
Dean of Graduate Studies

عمادة الدراسات العليا
DEANSHIP OF GRADUATE STUDIES

Dr. Sidqi A. Abu Khamsin
(Member)

15/2/15
Date

Dr. Ibnelwaleed Ali Hussein
(Member)

Dr. Hasan S. Al-Hashim
(Member)

This dissertation is dedicated to my loving parents- Alhaji Rashid Adebayo and Alaja Mulikat Adebayo

ACKNOWLEDGMENTS

I sincerely thank my advisor, Dr. Hasan Al-Yousef for his supervision, advices, encouragements, kindness, and patience during this work. I am privileged to be his research student. The guidance and support of my co-advisor, Dr Mohamed Mahmoud is very much appreciated. I am also grateful to the other members of my dissertation committee- Dr. Hasan Al-Hashim, Dr. Sidqi Abu Khamsin of the Petroleum engineering department and also Dr. Ibnelwaleed Ali Hussein of the Chemical engineering department for their suggestions and advices.

I hereby acknowledge the support of King Fahd University of Petroleum & Minerals and King Abdul-Aziz City for Science and Technology-Technology Innovation Centre on Carbon Capture and Sequestration (KACST-TIC-CCS) for funding this research work under project number KACST-TIC-CCS-6.

My appreciations also goes to the Centre of petroleum and minerals (CPM) of the Research institute of the King Fahd University of Petroleum & minerals for giving me access to its numerous and valuable laboratory facilities. Special thanks to Dr. Abdullah Sultan, the chairman of the petroleum engineering department and director of CPM of the research institute of the University for his relentless support, encouragement, and advices. I thank Dr. Abdulaziz Al-Majed of the department of Petroleum Engineering for his motivation and advices. Special thanks also to Dr. Taha Okasha of Saudi Aramco for his support in the NMR spectroscopy experiments. I appreciate the support of Mr Ahmad Adeniran of the systems engineering department for the design of the data acquisition software. The support of the following is very much appreciated: Mr. Abdulrahim

Muhammadain, Mr. Abdulsamad Iddrisu, Mr. Mosa Ali Mosa, and the entire faculty and staff of the petroleum engineering department. Similarly, I appreciate the assistance of the following: Mr. Abdulrashid I. Mohamed of the Centre for Engineering Research (XRF) in the research institute of the university; Mr. Mansoor Al-Marhoon (MICP measurements), Mr. Abdulmalek Al-Sanounah (porosity and permeability), Abdulrahman Al-Ghamdi (core cleaning), and Syed Rizwanullah (NMR) - all of the centre of petroleum and minerals of the research institute of the university.

I also thank Abubakar Tafawa Balewa University, Bauchi, Nigeria for her support.

To the Nigerian community at KFUPM, life would have been boring without you. Thanks for making another home far from home.

My lovely wife, Mrs Shakirat Ilufoye, my son, Abdullah, my twins Uwais & Umamah, and my new son Abdulshakur, your company, patience, encouragement, and prayers made this great achievement a reality. What more can I say than I love you all.

Finally and most importantly, all praises and gratitude belong to Allah.

TABLE OF CONTENTS

LIST OF TABLES

LIST OF FIGURES

LIST OF ABBREVIATIONS AND SYMBOLS

BV	:	Core bulk volume
CBRI	:	CO_2 – brine – rock interaction
COBRI	:	Carbon dioxide oil brine rock interaction
D	:	Diameter of core sample
EDTA	:	Ethylene di-amine tetra-acetic acid
EOR	:	Enhanced Oil Recovery
$\mathbf{I_R}$	:	Resistivity Index
k	:	Sample permeability
L	:	Length of core sample
LCR	:	Inductance capacitance resistivity
M	:	Molality of component salts in brine
MICP	:	Mercury injection capillary pressure
NMR	:	Nuclear magnetic resonance
P	:	System total pressure, bar
R	:	Universal gas constant
ROS	:	Remaining oil saturation
SV	:	Specific volume of CO_2 in cc/moles
T	:	Absolute temperature, Kelvin
TDS	:	Total dissolved solids
XRF	:	X-ray fluorescence
$\boldsymbol{CO_2}$	:	Carbon dioxide
$\boldsymbol{n}$	:	Saturation exponent
$\boldsymbol{R_o}$	:	Resistivity of sample at 100% brine saturation
$\boldsymbol{R_t}$	:	True formation resistivity
$\boldsymbol{S_{irw}}$	:	Irreducible water saturation

S_{or}	:	Residual oil saturation
S_w	:	Water/Brine saturation
$Q_{CO2\ inj}$	:	Volumetric storage
$Q_{CO2\ solubility}$	:	Solubility storage
yCO_2	:	Mole fraction of CO_2 in vapor phase
ζ_{CO2-Na}	:	Interaction parameter between CO_2 and Na^+
$\zeta_{CO2-Na-Cl}$	:	Interaction parameter between CO_2, Na^+ and Cl
$\mu_{CO2}^{1(0)}$	:	Standard chemical potential of CO_2 in liquid phase
ρ_{CO2}	:	CO_2 density, g/cc
ρ_{brine}	:	Brine density in g/cc
φ	:	Core sample porosity

ABSTRACT

Full Name : [Abdulrauf Rasheed Adebayo]

Thesis Title : [An Experimental Study of The Effects of CO2 Sequestration on Electrical Properties of Carbonate Rocks]

Major Field : [Petroleum Engineering]

Date of Degree : [March 2015]

This study investigates the fate of carbonate rocks marked for long term storage of Carbon dioxide (CO_2) and for CO_2-EOR projects. Previous works focused on the applicability of electrical resistivity measurements to track CO_2 migration by way of resistivity change as a function of CO_2 saturation changes during CO_2 sequestration. Many others also studied the effect of CO_2 injection on the petrophysical and electrical resistivity of rocks. Previous works of these types used continuous flow experiments of fluid in and out of rock samples and such flow lasted only few hours. The fate of formation resistivity under static condition and at longer storage period was not considered. In this study, a full suite of experiments was designed to characterize and study the effect of CO_2 storage on rock samples under flow and static conditions. They include Mercury injection capillary pressure (MICP), nuclear magnetic resonance (NMR), CO_2 sequestration, resistivity index, drainage, aging in crude oil, water flooding, CO_2 flooding, and post CO_2 sequestration NMR and MICP measurements. Other supporting experiments were computed tomography (CT) scan, X-ray fluorescence (XRF), and gas/ionic chromatography. MICP and NMR measurements showed that all core samples are of bimodal pore type and are very homogeneous. CT scan was used to confirm that fractures and vugs were not present in the samples while XRF spectroscopy

was used to study rock precipitates. Chromatography was used for pre- and post- storage brine analysis. The results of this study have established that the electrical behaviour of carbonate rocks under long term CO_2 storage is dynamic under a static condition. It stretches the scope of reservoir evaluation and surveillance using resistivity logging technique. It has been observed from an extensive laboratory study that: saturation exponent changed significantly with time during CO_2 storage and that the extent of change is dependent on the extent of CO_2/brine/rock interaction (CBRI); that a change in formation resistivity does not necessarily translate to a change in fluid saturation or fluid migration but can be an indication of CBRI; that the combination of resistivity log and temperature log have been observed and proposed for monitoring rock/fluid interaction and scale formation in-situ and in real-time; and that CO_2/oil/brine/rock interaction (COBRI) during CO_2-EOR cause hysteresis effect on saturation exponent. Post CO_2 storage analyses confirmed rock grain dissolution, scale formation, and altered rock pore geometry.

ملخص الرسالة

الاسم الكامل: عبد الرؤوف رشيد أديبايو

عنوان الرسالة: دراسة معملية لتأثير تخزين ثاني أكسيد الكربون علي الخواص البتروفيزيائية و الكهربائية للضخور الكربونية.

التخصص: هندسة البترول

تاريخ الدرجة العلمية: جمادى الأولى، 1436

تتناول هذه الدراسة مصير الصخور الكربونية التي يتم تخزين ثاني أكسيد الكربون (CO_2) فيها لمدة طويلة ومشاريع الاستخلاص المعزز للنفط باستخدام CO_2 ثاني أكسيد الكربون. ركزت الأعمال السابقة على قابلية تطبيق قياسات المقاومة الكهربية لتتبع هجرة CO_2 عن طريق تغيير المقاومة بوصفها تتأثر بمدي ب ثاني أكسيد الكربون خلال تخزينه. درس العديد من الآخرين أيضا تأثير حقن CO_2 على المقاومة البتروفيزيائية والكهربائية للصخور . الأعمال السابقة إعتمدت علي استخدام تجارب يتم فيها ضخ الغاز بشكل مستمر داخل وخارج عينات الصخور وهذا التدفق يستمر لساعات معدودة فقط. لم تضع في الإعتبار هذه الدراسات تغير المقاومة عند التعرض لفترات أطول. في هذه الدراسة ، تم تصميم مجموعة كاملة من التجارب لتوصيف و دراسة تأثير تخزين CO_2 على عينات الصخور تحت تدفق وظروف ساكنة. وتشمل خاصية الضغط الشعرية باستخدام الزئبق (MICP) ، الرنين المغناطيسي النووي (NMR) ، تخزين CO_2 ، ومؤشر المقاومة ، والصرف ، والشيخوخة في النفط الخام ، وضخ المياه وضخ CO_2، وقياسات NMR وMICP بعد تخزين ثاني أكسيد الكربون. تم استخدام تجارب أخري إضافية داعمة للدراسة مثل التصوير المقطعي (CT) وومضان الأشعة السينية (XRF) ، والتمييز اللوني بين أيونات المائع باستخدام الغاز . أظهرت قياسات MICP و NMR أن جميع العينات فيها النظام المسامي ذو نسقين ومتجانسة للغاية. واستخدمت الاشعة المقطعية للتأكد من أن الكسور و الفجوات لم تكن موجودة في العينات في حين تم استخدام XRF لدراسة رواسب الصخور. تم استخدام التحليل اللوني لتحليل الماء المالح قبل وبعد التخزين.

أظهرت نتائج هذه الدراسة أن السلوك الكهربائي للصخور الكربونية تحت تأثير التخزين طويل المدى لثاني أكسيد الكربون يتغير تحت ظرف ثابتة. ويمتد نطاق تقييم الخزان و المراقبة باستخدام تقنية تسجيل المقاومة . وقد لوحظ من الدراسة المختبرية المكثفة ما يلي: تغير معامل التشبع بشكل ملحوظ مع مرور الوقت أثناء تخزين CO_2 و يعتمد

مدى التغيير على مدى تفاعل CO_2 مع المحلول الملحي والصخر (CBRI)؛ حيث إن أي تغيير في المقاومة الكهربائية للصخر لا تحتم بالضرورة تغيير في تشبع السائل أو هجرة السوائل ولكن يمكن أن يكون مؤشرا للتفاعل بين CO_2 مع المحلول الملحي والصخر حيث أن الجمع بين سجل المقاومة و سجل درجة الحرارة يقترح لرصد التفاعل بين الصخور والسوائل و تشكيل الترسبات في الموقع وفي الوقت الحقيقي . كذلك يسبب تفاعل CO_2 مع الزيت الخام والمحلول الملحي والصخر أثناء عمليات الاستخلاص المعزز للنفط (COBRI) تبطئ على معامل التشبع. أكدت القياسات بعد تخزين CO_2 علي ذوبان حبيبات الصخر وترسب البعض الأخر وتغيير البنية المسامية للصخر

CHAPTER 1

INTRODUCTION

1.1 CO_2— Environmental Effect, Storage, and Monitoring

Greenhouse gases are gases in the atmosphere that are believed to be responsible for the rising temperature of the earth; a phenomenon known as global warming. Primary greenhouse gases are Water vapour, Carbon dioxide, Methane, Nitrous oxide, and Ozone. Water vapour and Carbon dioxide constitute the greatest percentage of greenhouse gases while Methane and Ozone are relatively small according to the statistics provided in Table 1-1[1, 2]. Over several decades since the beginning of industrial revolution, Carbon dioxide (CO_2) concentration in the atmosphere has continued to increase significantly due to the increase in burning of fossil fuels such as oil, natural gas, coal, and wood (Figure 1-1). Global temperature has also been found to increase in the same trend. Different efforts have been deployed to reduce the atmospheric quantity of greenhouse gases particularly CO_2. One of such options which is globally accepted is Carbon Dioxide Capture and Storage/Sequestration (CCS) in geological formations. Potential geological formations according to the Intergovernmental Panel on Climate Change (IPTC) [3] are depleted hydrocarbon reservoirs, un-depleted hydrocarbon reservoirs (during enhanced oil recovery), saline water saturated aquifers, un-mineable coal seams and cavities (Figure 1-2). According to the IPCC report, CCS is expected to contribute about 20% of the total CO_2 reduction in the coming century. Geological (Sedimentary) formations are good candidates because: they can provide the pore volumes needed to store large amount of CO_2; they have adequate permeability required for efficient injection; and they are widely distributed geographically

[4]. They also possess the seal (Cap rock) needed to keep the stored CO_2 in place [2]. Of all the sedimentary formations, saline aquifers have the largest global sequestration capacity [2] but they are limited by uncertainty in seal integrity. Depleted oil or gas reservoirs on the other hand are known to have high seal/cap rock integrity but they are also limited by scarce geographical distribution [5]. In any case, all sedimentary formations have potentials for CCS and are already being used for CCS projects either in saline aquifer (e.g. [6]), or in depleted reservoir, or they are stored in sedimentary formations after they have been used to displace oil during enhanced oil recovery projects [7-9].

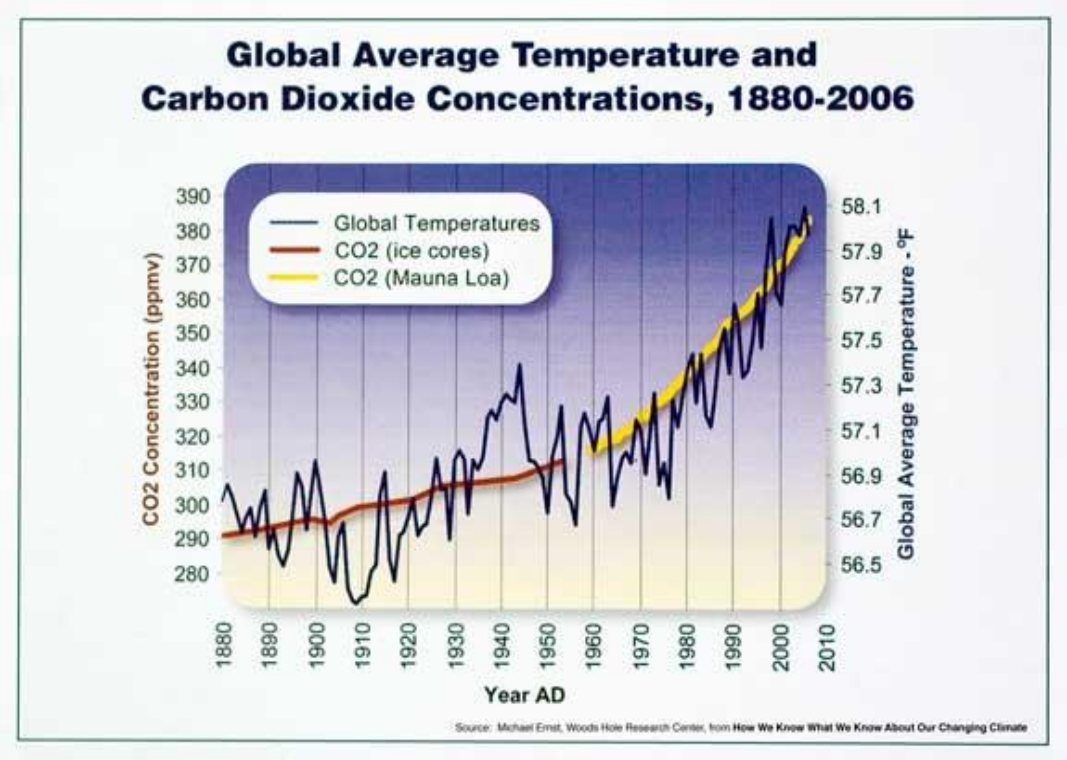

Figure 1-1 Global temperature and CO_2 concentration

Figure 1-2 Potential geological formations for CO_2 sequestration

CO_2 is normally injected into underground formations at high pressure and temperature such that the CO_2 exists in a supercritical state. The supercritical state will reduce the volume of rock space occupied by injected CO_2 per unit volume of CO_2 existing at atmospheric condition. The pressure and temperature at which CO_2 exists in this state can be found in aquifers at depths of about 800 meters or more. Hence candidates for CCS formations must be at this depth [2]. While CO_2 is injected into a subsurface formation, four major trapping mechanisms ensue namely: (i) Physical/Structural trapping – a process whereby impermeable cap rock at the top of the formation prevent the CO_2 from escaping out of the formation, keeping it in place [2, 5], (ii) Solubility trapping – a process whereby injected CO_2 dissolves in formation pore water, (iii) Mineral trapping – occurs when aqueous CO_2 reacts with formation rock minerals producing precipitates of carbonate minerals, and (iv) Residual or Capillary trapping which occurs after CO_2 injection stops and water begins to

imbibe into the aquifer displacing the CO_2 already in the aquifer. Not all the CO_2 is displaced but some are left behind as residual CO_2 (residual trapping).

Table 1-1 Contribution of greenhouse gases to total Greenhouse gas in the atmosphere [2]

Greenhouse Gas	**Contribution, %**
Water Vapour (H_2O)	36-72
Carbon Dioxide (CO_2)	9-26
Methane (CH_4)	4-9
Nitrous Oxide (O_3)	3-7

Dissolution of CO_2 in water will form carbonic acid which can lead to dissolution of rock minerals and precipitation of other minerals depending on the mineralogy of the formation. Dissolved CO_2 can acidify formation water and subsequently mobilize and transport trace metals as it migrates in the formation [10]. Dissolution of minerals like iron oxy-hydroxides is capable of mobilizing toxic trace metals. In the case of depleted oil reservoirs where residual oil is present, CO_2 injection can mobilize toxic compounds like benzene, toluene and others [2]. Since CO_2–Brine —Rock (CBR) and CO_2–Oil-Brine —Rock (COBR) interaction can result in the dissolution, precipitation, and mobilization of some minerals which may include toxic minerals, a storage formation with strong cap rock is crucial to avoid leakages of toxic metals and compounds into overlying portable aquifers. There is also the need for proper monitoring of CO_2 migration so as to observe its behaviour, distribution and possible leakages. Hence, evaluation of the reliability of CO_2 monitoring techniques should be first step in risk assessment of any CCS project [11].

Techniques required for monitoring CO_2 migration can be borrowed from a variety of other applications such as those used in the oil and gas industry, and those used in ground water monitoring [2]. There are various geophysical monitoring techniques such as acoustics/seismic, gravity, and resistivity measurements. Seismic is the most extensively used

technique but it becomes insensitive at CO_2 saturation above 20% given resistivity an edge (Figure 1-3). The use of resistivity measurements is also promising. Wire line or logging while drilling resistivity measurements is an old and effective petrophysical technique used in the industry to monitor and evaluate oil and gas reserves. Resistivity technique is applicable because rocks contain saline water and are thus conductive. Resistivity is a measure of how much a material resists flow of current. It is the same for a given material regardless of the shape, length, and area in a similar way density is the same irrespective of size and geometry [12]. Just like density, resistivity can only change if the material composition changes. Formation resistivity changes spatially because rock bulk composition changes in any or all of the following ways: changes in type of fluid present in rock pores; changes in fluid saturation; changes in rock mineral composition; and changes in rock's geo-mechanical, geothermal, and petrophysical properties. The use of resistivity measurements to monitor and quantify CO_2 in underground geological formation depends on the fact that formation resistivity is higher at locations occupied by CO_2 compared to locations un-invaded by CO_2, and the resistivity increases as CO_2 saturation increases. The amount of resistivity changes depend on the volume of CO_2 present. With the use of Archie's equation, CO_2 saturation distribution, migration, and volume can be estimated. Many experimental and field studies have successfully used resistivity measurements to monitor CO_2 migration e.g. [5, 12-15].

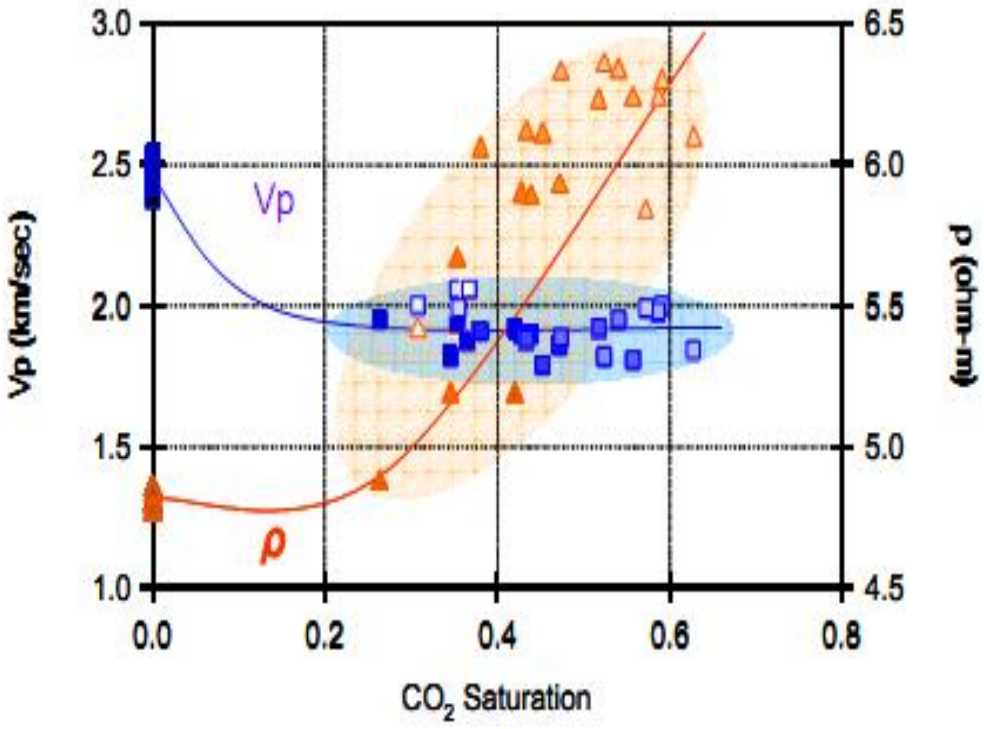

Figure 1-3 Comparison between seismic and resistivity monitoring techniques

1.2 CO_2 Evaluation and Monitoring using Resistivity logs

Archie's water saturation model is the basis for resistivity measurements [16]. Archie related three laboratory electrical measurements of core sample with water saturation and derived the popular Archie equation (**1-1**).

$$S_w^n = \frac{FR_w}{R_t} \qquad 1\text{-}1$$

Where: F = formation factor, R_w= formation water resistivity, R_t= true resistivity of a formation containing water and other fluids, and n = saturation exponent. The formation factor is the ratio of rock resistivity at 100% brine saturation given by equation **1-2** and can also be written as given by equation **1-3**.

$$F = \frac{R_o}{R_w} \qquad 1\text{-}2$$

$$F = \frac{a}{\emptyset^m} \quad \text{1-3}$$

Where: 'a' = consolidation factor, and 'm' = cementation factor. Resistivity index, I_R is the ratio of true formation resistivity to resistivity of formation with 100% brine saturation.

$$I_R = \frac{R_t}{R_0} \quad \text{1-4}$$

$$S_w^n = \frac{1}{I_R} \quad \text{1-5}$$

Equations **1-2**, **1-3**, **1-4** and **1-5** can be combined to form Archie's water saturation model (equation **1-6**)

$$S_w = \left(\frac{aR_w}{\emptyset^m R_t}\right)^{1/n} \quad \text{1-6}$$

Values of 'a', 'm', and 'n' also called electrical parameters or Archie's constants are obtained from laboratory resistivity measurements of core samples in the laboratory.

If values of porosity and resistivity are obtained at different locations in a given saline formation used for CO_2 storage, water saturation can be estimated at the different locations using equation (1-6) while CO_2 saturation distribution can also be estimated using equation 1-7 and equation 1-8.

$$S_{CO2} = (1 - S_w) \quad \text{1-7}$$

$$Vol_{CO2} = 7758Ah\emptyset(1 - S_w) \quad \text{1-8}$$

Where: Vol_{CO2} = Volume of CO_2 in place, in barrels; A = area of reservoir, acres; h = thickness of reservoir, ft, and $\emptyset$ = reservoir porosity, fraction.

Archie's equation has been widely used for a long time up till today with few changes [17]. Archie plotted $\frac{R_o}{R_t}$ versus log (S_w) to get a slope of 'n', and also plotted log (F) versus log (∅) to get a straight line with a slope of 'm' and an intercept of 'a' at 100% porosity. Archie's values of 'n' and 'm' were 2 while the value of 'a' was 1. The constant 'n' is called saturation exponent because it describes the change in electrical tortuosity with changes in water content while 'm' describes the change of electrical tortuosity with porosity [18].

1.3 Non-Archie Rocks

Herrick [18] pointed out that only a rock with a uni-modal pore geometry will have a straight line plot of formation factor versus porosity like that described by Archie. Worthington and Pallat [19] also argues that Archie's linear plot is due to the fact that the rock has uni-modal pore structure whereby desaturation of pore space occurs in a uniform manner such that tortuosity increases as saturation decreases at a rate in accordance with equation **1-5** making 'n' value constant. Archie also assumed that saturation exponent, 'n' is constant for all sedimentary rocks. Wyllie and Rose [20] disagree with the theory that 'n' is constant for all porous rock and their point was confirmed by the work of Carter and Power [21] which showed that 'n' varied from core to core they studied. They attributed the varying values of 'n' to the differences in textural properties of their cores. Similarly, Archie's value of 'n' and 'm' were 2 while value of 'a' was 1. However, values of 'n' in the range of less than 1 to 20 have been reported in the literature [17]. It is therefore generally agreed then that Archie's equation is ideal and only holds when a formation has all of the following properties [18, 21, 22]: (i) homogenous, (ii) simple and uni-modal pore geometry, (iii) strong water wetness, (iv) absence of clay content, (vi) all of the water contribute to current flow, and (v) the rock grains are non-conductive. Only then, will the plots of log (F) versus log (∅), and that of $\frac{R_o}{R_t}$ versus log (S_w) be perfectly straight. Hence, Archie's equation (equation **1-4**) is

limited to clean sandstones with the characteristics described above. Rocks that do not exhibit one or all of the properties of Archie type of rock have been commonly referred to as 'non-Archie rocks' and they tend to exhibit non-linear resistivity versus water saturation plots and also non-linear formation factor versus porosity plots [18]. Non-Archie rocks are therefore rocks that have any or all of the following properties: heterogeneity, oil wetness, complex pore size distribution and pore geometry, and shalyness. The validity of Archie's equation on such rocks has been the subject of many researches. According to Herrick [18], most non-Archie rocks will have 'm' less than 2 or sometimes less than 1 while 'a' will always have values greater than 1.

Another source of concern in Archie's equation is the ability to accurately determine the Archie constants 'a', 'm', and 'n' since Archie saturation equation 1-6 is highly sensitive to these values. Errors in the constants can translate into over estimation or underestimation of S_w and subsequently erroneous hydrocarbon/CO_2 saturation distribution. Carbonate rocks and shaly sandstones are non-Archie rocks and they have exhibited electrical responses that could not be adequately described by Archie's model.

CHAPTER 2

LITERATURE REVIEW

Non-Archie behaviour can manifest through non-linear resistivity index plot. A number of cases where values of 'n' changes as water saturation decreases within a given rock have been reported in the literature [23-25]. Non-linear plots of log (*F*) versus log (∅), have also been observed in many experimental studies. The non-linearity has been ascribed to several factors such as: presence of clay mineral formations; rough grains surfaces; non-uniform distribution of conductive phase saturation (brine) caused by heterogeneous pore networks as desaturation/drainage progresses; and wettability effect [19].

2.1 Effect of Clay on Saturation Exponent

Deviation from Archie's equation was first noticed in the resistivity index curve of shaly formations [26]. Clays present in rocks as laminated, dispersed, or structural shale have been proven to conduct electricity through Cation Exchange Capacity (CEC). Clay conductivity was first identified by Waxman and Smits [27] to be responsible for the non-linear relationship in resistivity index versus water saturation plots. Different researchers proposed different saturation models to account for this shale effect. Waxman and Smits [27] developed a modified I^*_R-S_w relationship that gives a straight line whose slope is called modified saturation exponent, n* corrected for clay effect. Their saturation equation (modified Archie's equation) is given below (equations 2-1, **2-2**, and **2-3**)

$$I_R\left[\frac{1+\ R_w BQ_v/S_w}{1+\ R_w BQ_v}\right] = \ S_w^{-n*} \qquad 2\text{-}1$$

$$I_R^* = I_R \left[\frac{1 + R_w B Q_v / S_w}{1 + R_w B Q_v} \right] \qquad 2\text{-}2$$

$$S_w^{n*} = \frac{1}{I_R^*} \qquad 2\text{-}3$$

Where,

I* = clay corrected resistivity index

n* = clay corrected saturation exponent

Qv = Cation Exchange Capacity per unit volume, (meq/ml)

B = clay counter ion equivalent conductance, (cm^2 meq^{-1} ohm^{-1})

Diederix [28] showed that even, after clay effect was accounted for (using Waxman and Smits model) in the plots of I^*_R vs S_w, non-linear trends were still seen in three of the twelve cores he investigated. Further investigation of those cores by SEM revealed rough clay coatings on their grains' surfaces which were not present in the nine cores that exhibited linear trends. Han et al. [29] also reported a non-linear relationship between resistivity and brine saturation at water saturation below 20% which they also attributed to clay coatings. Herrick and Diederix [18, 28] pointed out that rough surfaces (caused by clay minerals coatings such as Kaolinites and Illites, or chlorites) have continuous micro pores (containing water at high capillary pressure) which exhibit dominant surface conductance effects at low S_w which lower 'n' values at lower S_w resulting in non-linear plots. Hence the observed non-linear plots even after clay effects have been accounted for were as a result of surface conductance effect caused by rough clay coatings on pore surfaces. The same grain surface effect was also observed in Rotliegend sandstone which was coated with clay minerals [24]. Swanson [23] also attributed the low value of 'n' at low water saturation to microporosity in

cherts and clay coatings after the use of Wax-man-Smits model could not adequately describe the non-linear resistivity index behaviour. Herrick [18] is of the opinion that in addition to the water in grain micropores, CEC on the clay coatings can also contribute to the conductivity of the grains.

2.2 Effect of Pore Geometry on Saturation Exponent

Non-uniform distribution of conductive phase saturation (brine) during desaturation is agreed to be due to complex pore geometry and pore size distribution present in most non-Archie rocks such as rocks with poly-modal pore system [19]. Non-uniform saturation distribution means that, at a given bulk S_w less than 1, individual pores exhibit a range of S_w with some pores having S_w lower than the bulk S_w value. The pores with S_w lesser than the bulk value tend to increase the overall tortuosity/resistivity of the bulk rock above what is appropriate for the bulk S_w. This effect is more pronounced as water saturation further decreases. Since water distribution is non-uniform across all pores at a given partial water saturation, tortuosity and resistivity may not increase linearly with decrease in water saturation. On the resistivity index plot, the effect can be seen as points not all falling on a straight line. In other words, 'n' values tend to be high at some water saturations and low at some other water saturations.

Also, Worthington [19] explains that when micro pores are present in a poly-modal pore system, they dominate the conductivity of the rock at lower S_w and they tend to reduce the effect of the tortuosity because of the high surface conductivity associated with micropores. The overall effect is the reduction in 'n' values at low S_w. The reason why micropores dominate conductivity at low saturation seems to be in accordance with the electrical model suggested by Swanson [23] which states that poly-modal pore system containing micro-pores behaves like electric circuits containing resistors in series. So the

macropores (inter granular pores) act like the big and first resistor through which current passes (at high S_w). They are big resistors because of the increasing tortuosity effect as conductive phase saturation decreases. They are the first resistors because they dominate flow and electric conductivity at high S_w values while the micro pores are the last pores to be drained because brines exist inside them at high capillary pressure [18, 29, 30]. As S_w decreases, tortuosity increases and resistivity increases leading to high slope or 'n' values [19]. As the brine saturation in the macro pores further reduces, the influence of the micro-pores increases. When the large (macro) pores have been drained, such that S_w becomes small and most of the formation water exists in the micro-pores, the micro pores take over or dominate the conductive role. Because of the surface conductance effect of micropores, R_t is lowered than what is commensurate with the S_w values and its associated tortuosity. Hence, 'n' values are low at low S_w values [19, 26]. In essence, 'n' can either drop or rise as S_w decreases depending on which of tortuosity and surface conductance effect dominate, or it can remain constant if the two factors counterbalance each other [25]. Tortuosity seems to take dominance when the micro pores are not connected or when they are dissolved to form macro pores thereby reducing the surface conductance effect and increasing R_t. Micro porosity exists in different forms and in all the forms they exhibit the same effect as described above. Examples of micro pores are: rock grains with internal effective pores caused by partial dissolution of grains (e.g. micro-porous cherts, fossil fragments, and oolites) which may be continuous or discontinuous. Because they are conductive, they act like resistors in series with inter-granular pores and tend to reduce tortuosity caused by decreasing S_w in inter-granular pores [18, 19, 23]. Moldic porosity normally present in carbonate rocks have also been reported to show non-Archie trend [18]. Resistivity is insensitive to vugs whether they contain oil or water. Whereas, resistivity is sensitive to fractures resulting in low 'n' [24].

It is understood how ‘n’ values or resistivity index slope can significantly change at low water saturation. The important lesson from the above explanations is to ensure that a large range of S_w ranging from 1 to very low S_w should be covered during a resistivity test so that estimated ‘n’ can be a representative value that can be used to predict S_w. Otherwise, the ‘n’ derived will result in a significant error in S_w calculations [25]. Worthington [19] also demonstrated how the use of incomplete S_w data range can cause an error of S_w calculation to the tune of 10%.

2.3 Effect of Conductive Minerals on Saturation Exponent

The presence of conductive rock minerals like pyrites have also been reported to cause low ‘n’ values at lower S_w in some cores and the value varies with the amount of conductive minerals present [21].

2.4 Effect of Wettability on Saturation Exponent

The effect of wettability change on ‘n’ appears to be the most significant and dominant factor affecting ‘n’ in a partially saturated core [31]. Many experimental works [32-35] have shown wide variation of ‘n’ values for different wettability on a given rock. Some of these works are summarized in Table **2-1**. Mungan and Moore [22] noted that since fluid distribution in a rock is dependent on the rock wettability, ‘n’ should also depend on the wettability, hence, the reason for the varying values of ‘n’ at different wettability condition. Anderson paper [36] is an excellent review paper on the effect of wettability on electrical properties of rock.

Brine preferentially fills small pores in water wet rocks and preferentially fills large pores in oil wet rock when the water saturation is less than unity [36]. During drainage in water wet rocks, the displacing fluid (hydrocarbon or CO_2) first enters and displaces large volume of brine in the large pores since lesser capillary pressure is required to drain water in

the large pores. The displacing fluid then occupies the centre of the large pores whose pores' surfaces are coated by thin water films that are stable at high capillary pressure [37]. Because the water films allow the continuous passage of current even after large displacement of water from the big pores, only a small change in resistivity can be noticed for large change in S_w [37], i.e. high slope. This is also because, at any saturation in a water wet rock, the number of pores occupied by water is always higher than that occupied by oil resulting in increased connectivity between different pockets of water inside the pore network [31]. As the small pores are drained, small changes in resistivity are still noticed but now for smaller changes in water saturation, i.e. lower slope. The increased connectivity between different pockets of water inside a pore network even at low S_w has been found to be responsible for the low resistivity measurements at low saturation resulting in the I_R-S_w plot concaving down at lower values of S_w [38]. The thicker the water film, the more the concaveness [37]. As the applied displacement pressure (capillary pressure) increases, S_w decreases as well until S_w drops below a critical water saturation when thin water films begin to break into non-continuous droplets which causes further rise in resistivity measurements at much lower S_w values [34, 35]. The thickness of water film can be affected by the type of non-wetting phase used which in turn can affect measurements of 'n' [37]. Keller [34] observed breakage of water globules in water wet sandstones (air-water system) after reduction of water saturation to below 30%. Mungan and Moore [22] observed from their studies that in the case of strongly water wet rock, saturation exponent, 'n' does not change with decrease in S_w even at value lower than 15% , though they worked with a synthetic homogeneous core without the complexity present in carbonates and shaly sands. Anderson [36] also noted that all of the water in water wet rock remain continuous and conductive even as water is reduced to irreducible water saturation making 'n' to be constant and that the increasing resistivity is due

to the reduction in cross sectional area of conducting brine and not by increase in path length (tortuosity).

For oil wet system, large change in resistivity is expected for small change in S_w (i.e. low slope) at high S_w values because hydrocarbon/CO_2 enters the small pores first at lower capillary pressure [37]. As displacement continues, water in the large pores begin to drain and as the water saturation decreases, discontinuous water globules begin to form in the centre of large pores which cannot conduct electric current [22, 34]. In essence, resistivity measurements are high right from the time saturation decreases resulting in higher slope (saturation exponent). Mungan and Moore [22] noted that discontinuous water globules started to form at water saturation of about 35% in oil wet Teflon cores. At the point when discontinuous water globules begin to form, resistivity begins to increase but not as rapidly as in the case of water wet core since the water that remains is mainly in the large pores where its effect on resistivity is minimal [35]. Sweeney [39] also noted that sealing of pore throats of pores containing water can also cause discontinuity of water droplets. Anderson [36] also noted that resistivity may be too high to be measured if the interstitial water saturation is so low such that most of the water is discontinuous.

Fractional and/or mixed wettability also affect saturation exponent. It is evident from the work of Morgan and Pirson [40] that saturation exponent of a fractionally wetted rock is dependent on the ratio of the oil wet fraction to the water wet fraction and that the higher the fraction of oil wet portion, the higher the saturation exponent. According to Anderson [36], mixed wettability can occur when oil displaces brine in the large pores of a water wet rock such that the small pores still contain water while the surfaces of large pores become oil wet due to the deposition of organic materials from the invading oil. Anderson is therefore of the opinion that the resistivity response in such case will not be like that of an oil wet system

because of the water in small pores which will continue to conduct electric current at low water saturation. Instead, the response will be similar to that of a water wet system but the saturation exponent will differ from the water wet situation.

Table 2-1 Saturation exponent range from water wet to oil wet conditions

Authors	'n' ranges	Lithology
[32]	1.6 – 2.7	Sandstone
[33]	1.5 – 25	Sandstones
[34]	1.5 – 11.7	Carbonates
[39]	1.6 – 5.7	Sandstones
[39]	1.7 – 13.5	Glass beads
[41]	2.5 – 25	Sand packs
[40]	1.8 – 2.4	Teflon
[42]	2.3 – 9	Sandstone
[22]	1.96 – 4.41(Drainage)	Glass beads
[22, 37]	1.53 – 4.80 (Imbibition)	Glass beads
[37]	2.22 – 4.86(Drainage)	Glass beads
	1.69 – 5.84 (Imbibition)	Glass beads

Table 2-2 Effect of Toluene Cleaning on Saturation Exponent [32]

Core ID	'n' for Uncleaned	'n' for Cleaned
1	2.37	2.03
2	2.68	2.29
3	2.48	2.07
4	2.71	1.91
5	2.82	2.44
6	2.21	1.91
Average	2.55	2.11

The lesson from the information above on wettability is that all cores must be of the same wettability when carrying out research studies on many rock samples if the influence of

wettability must be ruled out. Since many reservoir cores do not always have uniform wettability due to different surface chemistry caused by differences in minerals on rock surface [36], making a core have uniform wettability will be necessary for some kind of research studies where wettability differences can hamper research objectives.

2.5 Changing Wettability of Cores

Wettability can be changed in various ways. The use of chemical reactions such as hot solvent extraction, oxidation, or chemical coating of grain surfaces have been reported in the literature [16, 34, 43]. However, Mungan and Moore, [22] observed that chemical treatment method can result in the following: non-uniform wettability in cores; ions exchange from the minerals in the cores can influence the electrolyte resistivity; and core porosity and pore structure can change. However, cool solvent cleaning using flow through or Soxhlet extraction can help preserve clay mineral and micro pores [44].

Treatment of cores with toluene during cleaning have been reported to cause water wet conditions in cores [36]. Moore's [32] experimental studies of the effect of cleaning with toluene on saturation exponents of some oil wet cores showed that cleaning lowered the saturation exponent for all the cores as seen in Table **2-2.** It was believed that treatment with toluene changed the cleaned cores' wettability to water wet thereby reducing the saturation exponent. However, Anderson [36] pointed out that it is possible that not all of the organic coatings on the cleaned cores may have been extracted which suggests that they may not be strongly water wet. Lasswell [44] on the other hand pointed out that the use of soxhlet extraction or solvents like chloroform-methanol azeotrope and tetrahydrofoam can result in a strongly water wet rock. Richardson et al.'s [45] laboratory study on mix wettability cores showed that the resistivity of the cores at interstitial water saturation continued to drop after repeated cleaning that rendered the oil wet portion of the cores more water wet. Sharma et al.

[37] also changed his glass beads to strongly water condition by treating them with Sodium Hydroxide (NaOH) solution (with pH 11), then flushed with distilled water followed by oven heating at 80^{o}C overnight. In order to change the wettability of the water wet beads to oil wet condition, they soaked the water wet glass beads in asphaltic crude oil for 2 hours and then flushed the beads with pentane in order to remove the nonpolar fraction of the crude. The beads were then dried in oven for 4 hours at 80^{o}C. Sharma et al. Sharma et al. [37] also made some sandstone cores water wet by flushing with isopropyl alcohol followed by heating at 95^{o}C for 24 hours. Polar compounds in oil components such as naphtanes and paraffin when deposited on rock surfaces can change rock surface to oil wetness [46]. Sweeney and Jenings [35] used silicone material to coat sandstone cores in order to change the wettability to strongly oil wet. The method was not successful for carbonate rocks. Instead, they used 10% solution of organic acid (naphtanic acid) in benzene to saturate the carbonate cores. Trantham and Clampitt [47] have also reported that chamosite clay was responsible for the oil wetness in their cores taken from North Burbank reservoir. Morgan and Pirson [40] used organo chlorosilane solution to render water wet beads to oil wetness.

Because of the complications in changing wettability, some researchers [22, 33, 37] have resorted to using synthetic cores materials which have uniform wettability, inert, homogeneous, and free of contaminants, making it easy to study the effect of wettability alone. Examples of such synthetic core material include polytetrafluoroethylene (TFE or teflon) and glass beads.

2.6 Effect of Saturation Cycle on Saturation Exponent

Saturation cycle (drainage or imbibition) can also affect resistivity measurement as seen by the differences in saturation exponents obtained from a given core when resistivity index measurements were plotted against saturation during drainage and imbibition (a

phenomenon known as hysteresis) [37]. Wettability also has an influence on hysteresis. Hysteresis in water wet rock is either low or absent while it is higher in oil wet rock [31].

2.7 Effect of Pore Structure on Archie's Cementation ('m') and Tortuosity ('a')

Archie found an empirical correlation between formation factor and porosity as follows.

$$F = \frac{1}{\emptyset^m} \qquad 2\text{-}4$$

Where, 'm' is defined as cementation exponent which is widely believed to represent pore tortuosity to electric current [24].

Winn [48] developed a similar equation for formation factor (equation **2-5**)

$$F = \frac{L_w^2}{L_t^2}\frac{1}{\emptyset} \qquad 2\text{-}5$$

$$\tau^2 = F\emptyset \qquad 2\text{-}6$$

Where,

L_t= Length of a cubic porous material containing saline water

L_w = length of conducting water volume in the porous media

$\tau = \frac{L_w^2}{L_t^2}$ = tortuosity 2-7

Tortuosity can also be written as ratio of length of the conducting volume to the length of the cubic porous media, $\frac{L_w}{L_t}$= tortuosity

Rasmus [24] noted that if in the equation above, porosity equals unity (i.e. no rock grains present in the cube), then L_t will equal L_w and formation factor of a hollow cube of water will be unity. Similarly, Archie formation factor will be unity under the same condition. This confirms that both 'm' and L_w/L_t describe the tortuosity created by the porous grains.

Equation 2-4 and **2-5** can be re-written as

$$\log F = -\log \emptyset + \log \tau_o^2 \qquad 2\text{-}8$$

$$\log F = -m \log \emptyset + \log 1 \qquad 2\text{-}9$$

The plot of formation factor versus porosity on a log scale will give a slope of -1 with an intercept of $\log \tau^2$ for Win's cubic model (equation 2-8) while for Archie model (equation **2-9**), the slope is 'm' and intercept is 1. Herrick [18] noted that cores having equal tortuosity will fall on the straight line slope of -1. The same applies to Archie empirical equation meaning that all 'Archie' cores will fall on the 'm' slope with an intercept of 1 passing through the origin in accordance with Archie equation (Figure **2-1**). Hence, 'm' can be defined as a constant that describes the change of electrical tortuosity with porosity just as 'n' describes change of electrical tortuosity with brine saturation [18].

All points falling on the straight line slope could mean that all the cores have uniform and the same pore character (resulting in uniform change in tortuosity as porosity changes from core to core, or porosity change with time for a given core). Hence, all the cores are on a single tortuosity slope). However, it has been observed in some plots that not all points fall on a single straight line in many non-Archie rocks. This phenomenon tends to support Verwer et al.'s [49] assertion that flow of electric current is dependent not only on porosity but on combined effect of micro porosity, pore network complexity, and sizes of macro pores. In

other words, the reason for the scatter could be due to variation in pore character from core to core as opposed to the previous case. The presence of poly-modal pore system (such as presence of micro-pores) and conductive minerals which may be present in some cores and absent in others could be responsible for the non-uniform change in tortuosity. A line of best fit drawn in such cases would reflect the rate of change in tortuosity with changing porosity and pore character for such heterogeneous core while the intercept would represent a measure of the combined tortuosity. A plot of formation factor versus porosity for a set of cores can therefore be a diagnostic plot to compare the rate of change of tortuosity between heterogeneous cores. A complete scatter or very low coefficient of regression will mean that the cores have completely different pore structure and size distribution. Specifically, Archie found 'm' to be 2 and intercept to be 1 for his cores and all of his points fall on the slope meaning that his cores have similar pore geometry. Other researchers working on sandstone have reported 'm' values other than 2 and intercept greater or lesser than 1. Winsauer [50] laboratory studies on some sandstones showed that the sandstones have a characteristic 'm' value of 2.15 and an intercept of 0.62. Values of 'a' of as low as 0.62 [51] to as high as 9.55 [52] have been reported while 'm' value of 1[53] and above 4 [54] have also been reported.

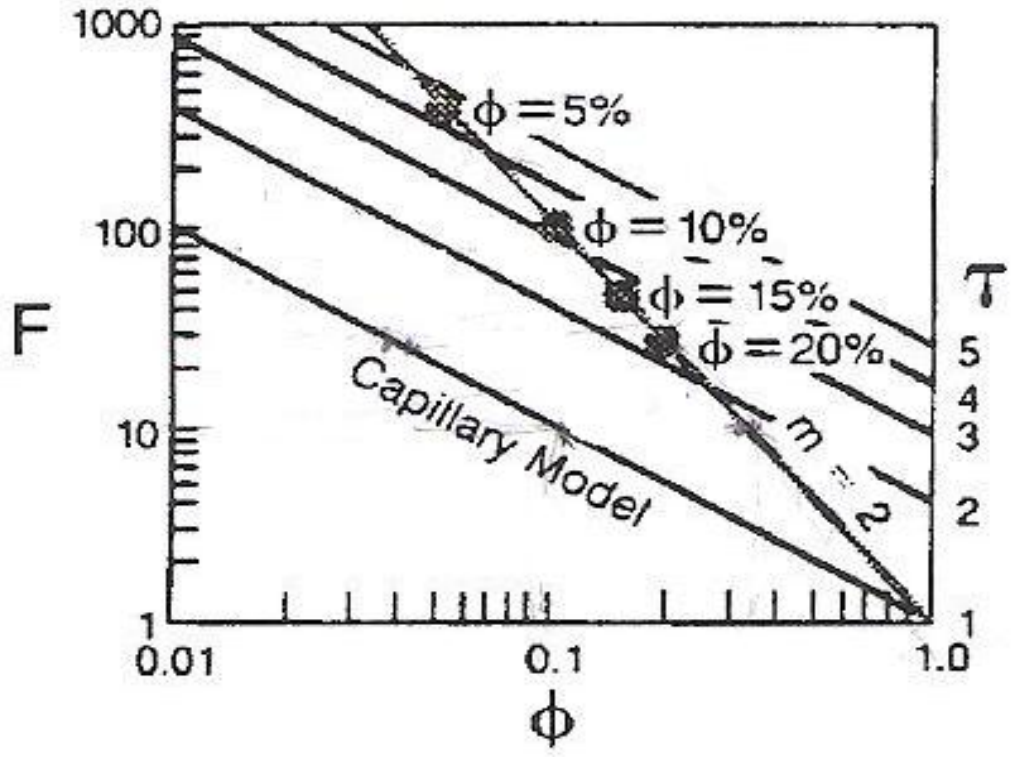

Figure 2-1 Plot of formation factor versus porosity for uni-modal rock [18]

It therefore follows that a rock that deviates from Archie type of rock will have a slope ‘m’ other than 2 and an intercept ‘a’ other than 1. So, changing ‘a’ and ‘m’ for a given rock can be an indication of changing pore character. Cementation factor ‘m’ vary greatly in carbonate rocks [37] primarily due to the heterogeneity of the pore structures in carbonate rocks. Verwer et al. experimental work [49] showed that cores with small pores and complex pore structure exhibited low ‘m’ values while those with large and simple pore structure exhibited large value of ‘m’ and those with vugs have the highest value. Ragland [55] studies of large number of carbonate cores (98 cores) from 10 wells that cut across different geographical locations showed that cores dominated by moldic porosity have the highest value of ‘m’ (2.46) followed by those cores that were dominated by inter particle porosity (larger pores) with ‘m’ value of 1.9, and then those cores dominated with inter crystalline porosity showed ‘m’ value of 2.03. Ragland [55] observed that presence of micro porosity in

core samples lowered the cementation exponent and that the greater the proportion of micro-pores in a rock samples, the lower the cementation factor which is in accordance with Verwer et al.'s results [49]. Cementation exponent, 'm' changes with confining stress [56]. Little work has been done on the effect of wettability on formation factor. Some of the works reported no change in formation factor while few others reported some changes [36]. In summary, cementation exponent, 'm' depends on type and shape of grains, pore types and geometry, tortuosity, anisotropy, and compaction [57]. It appears that pore structure have the most influence on cementation factor.

2.8 Effect of Electrodes Geometry on 'a' and 'm'

Sharma et al. [37] showed that the use of two electrodes to measure resistivity usually results in measurement error due to electrode contact resistance at the interface between brine and electrodes. They showed how the use of four or more electrodes will minimize or eliminate the error. Two electrodes usually lead to high values of 'a' and 'm'. Sweeney and Jennings [39] explained that polarization at the electrodes causes contact resistance and contact capacitance, and that the degree of polarization depends on the type of electrodes, the electrolyte and the current frequency. They therefore observed that gold-plated or Monel-metal electrodes used with a 1000-cycle current produced negligible contact resistance. However, recently, Lasswell [44] pointed out that the use of two electrodes can be very accurate if the measured phase angle is kept as low as 2 degrees or less. He compared measurements by two electrodes with measurements by 4 electrodes for thousands of core samples and observed that 'm' and 'n' values for both cases do not differ by more than 0.01 and that the differences were due to round off errors.

2.9 CO_2-Brine-Rock-Interaction and its Effect on Archie's Constants

CBR interaction has been the subject of many researches because of the corrosive nature of CO_2 [10]. Also the performance of a CO_2 flooding project is dependent on the interaction of CO_2 with the rock and rock fluids [58]. A proper understanding of the geochemical interaction between CO_2, rocks, and brine/oil is important for effective application of resistivity measurements in monitoring CO_2 migration and saturation distribution.

2.9.1 Super Critical CO_2

Carbon dioxide is usually injected into underground formations at high temperature and pressure such that the injected CO_2 exists underground as super critical CO_2 (S-CO_2) [59]. It exists in such state at a formation depth of 800 meters or more [5]. Super critical CO_2 is a fluid state CO_2 held at or above its critical temperature and pressure. Critical state of CO_2 occurs at a temperature of 31.1^oC (88^oF) and at a pressure of 72.9 atm (7.39MPa or 1,072 psi). In supercritical state CO_2 behaves half way like liquid and halfway like gas. It expands to fill its container (like gas) but with density like liquid. Because S-CO_2 can diffuse through solids and dissolve solid materials, it is commercially used as a solvent. S-CO_2 is very sensitive to temperature and pressure change such that any small change in this condition can change its physical properties [5].

2.9.2 S-CO_2 Solubility in Brine, Acidity, and Reactivity

S-CO_2 is soluble in brine and its solubility depends on pressure, temperature, and brine salinity. Solubility increases as pressure increases and decreases with increase in salinity and temperature as described in Figure 2 2. Formation and aquifer water normally contain the following ions [60]: H^+, Ca^{2+}, Na^+, Mg^{2+}, Cl^-, HCO^-_3, and SO^{2-}_4. When CO_2

dissolves in water (Solution trapping), carbonic acid is formed which further dissociates to release hydrogen ions thereby increasing the acidity of the water [10]. When reactive metals (such as Ca, Mg, and Fe bearing minerals) are present in a rock, dissolved CO_2 and water can react with these metals to form stable carbonate compounds (Mineral trapping) such as Calcium Carbonates and Magnesium Carbonates as represented by the following chemical reaction (Equations **2-10** to 2-18) in a CO_2-Brine-Rock system [3]. Some of the carbonates can precipitate out of solution [61]. The reactivity of the CBR system depends on the concentration of CO_2 in solution which is also a function of temperature, pressure and brine salinity. Hence, temperature, pressure and salinity determine the reactivity of the system [10]. The dissolution of CO_2 in brine is rapid while reaction of carbonic acid with metal ions (mineral trapping) is relatively slower [62].

$$CO_2(g) \leftrightarrow CO_2(aq) \quad \text{2-10}$$

$$CO_2(aq) + H_2O \leftrightarrow H_2CO_3 \quad \text{2-11}$$

$$H_2CO_3 \leftrightarrow H^+ + HCO_3^- \quad \text{2-12}$$

$$HCO_3^- \leftrightarrow H^+ + CO_3^{2-} \quad \text{2-13}$$

$$C_a^{2+} + CO_3^{2-} \leftrightarrow C_aCO_3(aq) \quad \text{2-14}$$

$$C_aCO_3(aq) \leftrightarrow C_aCO_3(s) \quad \text{2-15}$$

Carbonic acid can also dissolve rock minerals such as iron oxyhydroxides or calcites rocks according to the following (2-16 to 2-18) chemical reactions (Mark Raistrick 2009).

$$CO_2 + H_2O \leftrightarrow H_2CO_3 \quad \textbf{2-16}$$

$$H_2CO_3 + CaCO_3 \leftrightarrow Ca^{2+} + 2HCO_3^- \quad \textbf{2-17}$$

$$2H_2CO_3 + CaMg(CO_3)_2 \leftrightarrow Ca^{2+} + Mg^{2+} + 4HCO_3^- \qquad \textbf{2-18}$$

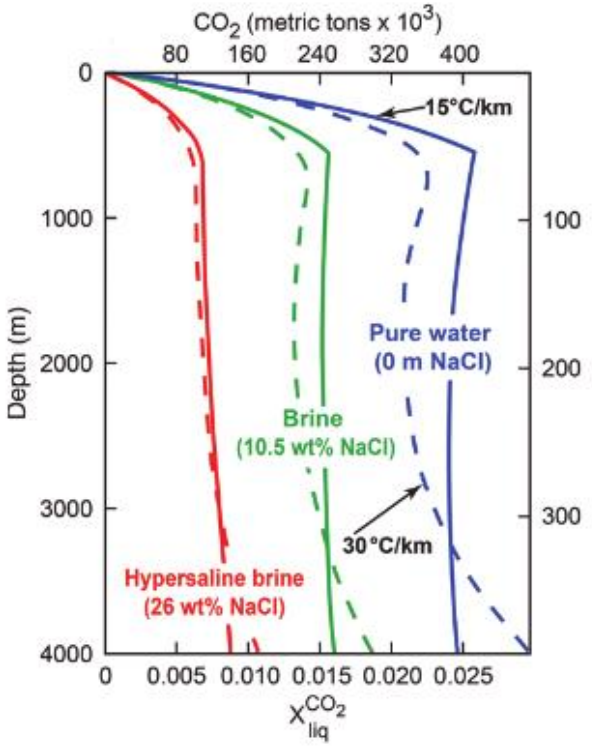

Figure 2-2 Solubility of CO_2 as a function of depth and salinity for two geothermal gradients. X_liq^(CO_2) means solubility of CO_2 in liquid. Modified from [1]

Dissolution of rock minerals (carbonate and iron oxyhydroxides) by carbonic acid will lower the acidity of the acid system (increase in pH) [62]. Under this condition, precipitation of gypsum can occur [10]. The acid solution can also attack alumina-silicate minerals (such as clay and feldspars) but at a very slow rate. The dissolution and precipitation kinetic-rates of most carbonates and some sulphates are generally known to be high and takes several hours to complete (at ambient temperature) while kinetic rates for alumina-silicate minerals is very slow and can take thousands of years for a complete reaction at ambient temperature [10]. However, Wildenborg and Van de Meer [63] noted that experiments at higher temperature can accelerate reaction kinetics of carbonic acid with silicates to an

observable level in the laboratory. Evidence of CBR interaction include reaction textures on rock minerals, precipitates of carbonate minerals, and change in brine chemistry [64].

2.9.3 Effect of CO_2 – Rock Interaction on Resistivity and Archie's Constants

When Archie's equation is to be applied to carbon dioxide sequestration projects for monitoring and evaluating CO_2 distribution, a new factor comes into play which has an influence on saturation exponent and cementation factor and that is rock fluid interaction. It becomes imperative then to consider the effect of CO_2 – brine – rock interaction (CBRI) since carbonic acid formed after dissolution of CO_2 in formation brine will dissolve some soluble carbonate grains and thereby alter rock pore structure and possibly change saturation exponent as CO_2 sequestration last. Many previous works focused on the applicability of electrical resistivity measurements to track CO_2 migration by way of resistivity change as a function of CO_2 saturation changes during CO_2 sequestration (e.g. [65] and [66]) shown in Figure 2-3 (A) and Figure 2-3 (B) respectively). Many others also studied the effect of CO_2 injection on the petro-physical and electrical properties of rocks. Previous works of these types use continuous flow of fluid in and out of the sample and such flow experiments lasted only few hours. The fate of formation resistivity under static condition and at longer storage period was not considered.

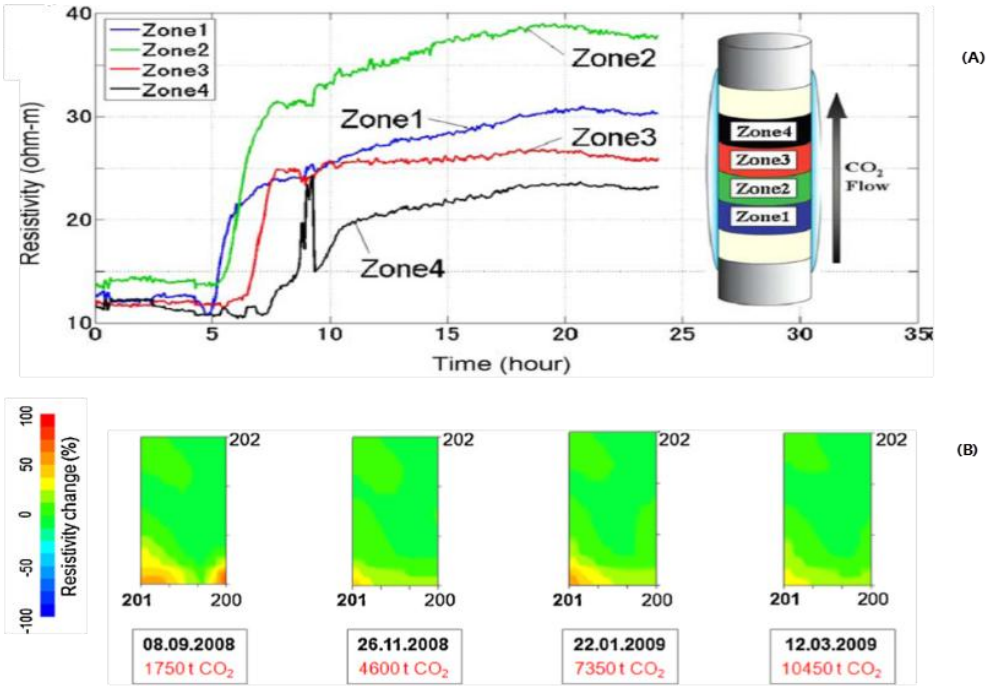

Figure 2-3 Resistivity log for monitoring CO_2 in dynamic state [65 and 66]

Following the literature review, it is apparent that pore character and wettability are the dominant factors amongst other factors affecting resistivity measurements in non-Archie rocks. These two properties and others have complex behaviour in carbonate rocks which makes carbonate rock the most challenging non-Archie rocks. Carbonate rocks are more complex than sili-clastic rocks in terms of heterogeneity of pore character (i.e. pore size distribution, connectivity of pores, fractures and dolomitization) [67, 68]. Vugs and fractures are also usually present in carbonate rocks [24] because of their solubility and brittleness [69]. Different pore types can co-exist in carbonate rocks such as macro-, micro-, and meso-pores [69, 70]. Carbonate rocks can also contain clay minerals, evaporites, and conductive minerals like pyrites [69]. In heterogeneous reservoirs like carbonate rocks, petrophysical properties such as permeability can change by several orders of magnitude between points few centimetres away on a core sample [69]. Whole core measurements are therefore crucial

in heterogeneous reservoirs so that small scale heterogeneity can be captured [69]. Well connected intra-particle micro porosity exists in almost all carbonate rock grains and tend to be conductive at even low S_w [30]. Carbonate rocks are also more inclined to oil wetness than water wetness [46, 69]. All the properties discussed above make petrophysical studies on carbonates a very complicated task. Nearly all the factors affecting resistivity measurements are present in carbonate rocks.

2.9.4 Applicability of Archie Equation for CO_2 Monitoring in Carbonate Rocks

Mungan and Moore [22] argued that Archie's equation may still be applicable in non-Archie rocks if the proper 'n' value is used and then suggested that the best approach to obtain a representative saturation exponent is through laboratory core analysis on well preserved cores and reservoir fluids (so as to have representative wettability), and at saturation range representative of what is believed to exist in the reservoir.

2.9.5 Challenges of Resistivity Measurements as a Monitoring Technique for CO_2 Sequestration in Carbonate Rocks

Carbonate rocks hold more than 50% of world hydrocarbon reserves [39] which makes them good prospects for CO_2 sequestration (after oil depletion). Although, electrical resistivity logs for CO_2 monitoring purpose can be a powerful tool for monitoring and quantifying CO_2 distribution in geological targets. However, the dissolution of CO_2 in pore saline water plus the possible geochemical reactions between resulting carbonic acid and rock minerals is opening a new dimension of difficulty in measuring and interpreting electrical resistivity of carbonate rocks. Since rock electrical properties 'a', 'm', and 'n' have already been shown to have a complex relation with pore geometry, the CBR and COBR reaction is expected to further complicate measurements since carbonate pore structures are expected to change after reaction by dissolution of cement bonds and/or soluble grains, or blockage of

some pore throats by produced precipitates. Not only will CBR and COBR interaction change pore geometry, other petrophysical properties such as wettability and permeability will also be affected at a rate and location that will be hardly predictable. Wettability change strongly influences resistivity. Change in wettability can come from change in pore surface mineralogy and deposition of reaction products like polar compounds on pore surfaces. Thus, at a given point in time and space, resistivity and Archie parameters are all controlled by many factors mostly uncontrollable making it difficult to accurately estimate CO_2 saturation using resistivity measurements. Hence, it is important to understand CBR and COBR interaction and how it affects resistivity, electrical parameters, and petrophysical properties of carbonate rocks. Many papers have appeared in the literature studying the impact of CO_2 on rock petrophysical properties but to the best of our knowledge, none has studied the impact of CBR and COBR interaction on electrical parameters of rocks either sandstone or carbonates.

2.9.6 Impact of CBRI and CBORI on Petrophysical Properties of Rocks

Kaszuba et al. [64] carried out studies on rock samples at higher reservoir condition of 200^{o}C and 200 bars. A brine-rock system (sand and shale) that is representative of a saline aquifer formation was allowed to stay in the test apparatus for 59 days so as to attain steady state after which CO_2 was injected for another 80 days all at 200^{o}C and 200 bars. They periodically collected brine samples for analysis. Inductively coupled plasma-optical emission spectroscopy (ICP-ES) and ICP-MS were used to determine dissolved Cations while ion chromatography (IC) was used to determine anions. Their results showed that carbonate precipitated and silicate minerals also showed signs of strong reaction all due to the low pH caused by the introduction of CO_2. Kharaka et al. [62] carried out field study on the impact of CBR on the Frio sandstone formation in an oil field in Texas, USA. They continuously injected CO_2 at the bottom of the formation about 30 meter down dip and

monitored the CO_2 migration to the top of the formation which was overlain by a thick marine shale bed that served as a seal or cap rock. Continuous sampling of gas and water at the top of the formation were used to monitor arrival of CO_2. After 3 days of injection, comparison of the chemical analysis of the water samples obtained from the injection and observation wells prior to and after injection showed that there was small increase in electrical conductance and major chemical changes occurred in the brine taken from the observation well namely – a sharp drop in pH (from 6.5 to 5.7), significant increase in alkalinity, and major increase in dissolved Fe, Mn, and Ca. This confirms that low pH brine (acid) can rapidly dissolve calcite and iron oxyhydroxides. Zemke et al. [71] studied the effect of CBR interaction on petrophysical properties of Stuttgart sandstone samples (outcrops and well cores) at 40^oC and 6MPa for a period of 15 months. Pore throat and pore size distribution were measured prior to and after CO_2 exposure (using mercury injection and NMR respectively). At the end of the 15^{th} month, only a slight increase in porosity was noted while the pore size distribution shifted from a larger proportion of small pores to larger proportion of big pores suggesting a change in pore structure and geometry. There were however few cores that showed increase in proportion of small pores in which reason was attributed to possible plugging of pore space by salt precipitates. In general, the porosity and permeability increased in most of the cores. They further studied the effect of changed pore geometry on electrical, mechanical, and acoustic properties of the rock by comparing these rock properties prior to CO_2- brine exposure with those after CO_2 exposure. Results showed that there was no significant change in the compressional wave whereas, the shear wave showed sign of being affected which in turn slightly affected the Poisson's ratio. For the outcrop samples they studied, a decrease of resistivity and permeability was observed while small change in ultrasonic wave velocity was observed. Kjoller et al. [72] also carried out experiments on core samples from five different sandstones with wide variety of mineralogy.

The core samples were allowed to react with brine and CO_2 for 13 months at reservoir conditions of 70^oC and 20 MPa. Fluid samples were then taken from each core monthly while core samples were studied at the end of the 7th and 13th month. Geochemical and petrographic analysis of the samples revealed that dissolution of carbonates, dolomites and siderites present in the host cores were the dominant dissolution that took place. Dissolution of other rock minerals such as silicates and alumina silicates were slower and difficult to detect within the period covered by the experiment. They used ICP-OES to detect cations present in the brine while ion chromatography (IC) was used to detect anions present. Lu et al. [73] carried out similar experimental studies on Navajo Sandstone at reservoir condition. They studied the interaction of sandstone grains with CO_2 and Brine in a batch reactor at 200^oC and 25-30MPa. Geochemical and petrographic analysis of the fluid samples collected at regular interval produced the following results: secondary clay particles such as Allophane and illite were seen after 552 hours (23 days); few carbonate precipitates emerged; SiO_2 concentration increased with time suggesting silicate dissolution; smectite coatings on grain surfaces were intact; secondary precipitates filled rock pore spaces; pH value reduced shortly after the start of the experiment and later began to increase and finally stabilized; and dissolution of silicates was faster at low pH. They also noted that porosity increased because of dissolution of silicate while permeability decreased because of clogging of pore throats by precipitates. Other similar works on the dissolution of silicate and precipitation of carbonates as a result of CBR have been reported [74-76].

Mathis and Sears [77] studied the effect of CO_2 and brine flooding on dolomite rock. They took cores from 5 closely spaced wells before the start of CO_2 injection and another set of cores were taken from another 5 wells in the same CO_2 injected area 2 years later. Analysis of the reservoir core properties before and after the CO_2 injection showed only a minor

change in porosity. The change in porosity was concluded to be from the dissolution of anhydrites (by pre-flood brine) as noticed in thin section and chemical analysis of pilot flood water (which showed high concentration of Ca^{+} and SO_4^{-} above normal level). Thin section did not show any evidence of dolomite dissolution. They tried to give reasons why dissolution of dolomites did not occur. They believed that most of the pore volumes during CO_2 flood may probably contain only CO_2 instead of carbonic acid since some un-displaced water will be trapped in the small pores as immobile wetting phase and the Ca^{+}, Mg^{2+}, and HCO_3^{-} ions formed as a result of carbonic acid reaction cannot be transported out because the un-displaced water is immobile. Post flooding produced water in the studies of the effect of CO_2-brine flooding on dolomites rock (with 95% dolomites and 5% anhydrites) in Permian basin San Andres reservoir showed increase in the concentration of calcium bicarbonates and calcium sulphate [78]. Permeability and porosity increased significantly after CO_2 flooding of a carbonate core (with 67% dolomites and 20% anhydrites) at 38^{o}C and back pressure of 13.79MPa [79]. Mohamed and Nasr-El-Din [80] studied the effect of temperature, injection rate, brine composition, and injection scheme on the dissolution and permeability of dolomite rocks when exposed to CO_2-brine. CO_2 was injected at supercritical condition at pressure of 1,300 psig and temperature in the range of 70-200^{o}F at different rates. Their results showed that temperature, injection rates, and injection scheme have no impact on rock permeability. However, calcium carbonates precipitates and other precipitates (from reaction of silicates with carbonic acid) were responsible for formation damage. Study on Indiana limestone and dolomites showed that CO_2-brine flooding caused dissolution of anhydrites, limestone and dolomites. Alam et al. [81] studied the impact of Supercritical CO_2 on petrophysical and mechanical properties of chalk formation during EOR using supercritical CO_2. Results showed increase in porosity and permeability. However, no significant change in wettability was observed from the NMR T_2 relaxation time. Change in smoothening of grain surfaces

was also observed. Results of rock mechanical test also showed that injected CO_2 has no effect on rock shear strength and compaction properties; though slight reduction in rock stiffness and elastic deformation parameters occurred.

Several other works on the effects of CBRI on rock porosity and permeability have also been reported in quite a number of papers. Precipitation of minerals can plug rock pores and reduce permeability [9, 73, 82, 83]. Dissolution of rock minerals can increase porosity [9, 83, 84]. Dissolution of rock carbonate cements can increase permeability [85-87]. Observed small increase porosity in some experimental works may be due to the fact that porosity increase via dissolution of rock minerals is accompanied by porosity reduction via precipitation of secondary minerals [71]. Xiao [88] found porosity increase near the CO_2 injection well (due to mineral dissolution) and a decrease in porosity at points far from the injection point (due to mineral precipitation).

It is clear from the forgone discussions that CBRI dissolves rock minerals and also affect rock petrophysical properties. However, the effect of CBRI on resistivity is yet to be fully understood. Also, the effect of CO_2-Brine-Oil-Rock interaction (CBORI) in the case of CO_2 storage in depleted reservoir or during enhanced oil recovery, on rock wettability and resistivity has not been studied. Furthermore, the effects of CBRI and CBORI on petrophysical and electrical properties of carbonate rocks have not been reported in the literature.

2.9.7 How CBRI and CBORI is Expected to Affect Resistivity in Carbonates

Carbonic acid reaction with carbonate minerals may cause dissolution and/or precipitation of solids leading to changes in pore geometry, porosity, permeability, wettability, and other rock properties [79, 81, 89]. Since electrical conductivity depends on the connectivity of pore spaces and their micro geometry [90], brine composition, and also on

wettability, effect of CBRI and CBORI on electrical conductivity is expected to be great as we expect change in pore geometry, pore connectivity, brine composition, and wettability.

From basic chemistry, it is known that strong acids and bases dissociate more readily into their respective ions than weak acids resulting in higher conductivity. The higher the solute concentration of a strong acid, the higher the conductivity while the higher the solute concentration of the weaker acid, the lower the conductivity. Carbonic acid is a weak acid and its acidity can further be reduced by its reactions with carbonate minerals. Chemical reaction between carbonic acid and rock minerals can result in ions exchange between electrolyte and rock minerals which can change the conductivity of the brine in pores. However, Gaus [10] noted that CO_2 induce changes in composition of brine is small compared to the high salinity of the brine in deep saline aquifer.

Also, because of the solubility of carbonate rocks [69], complete or partial dissolution of some carbonate grains can be expected when carbonic acids are formed during CBRI. The interconnectivity of dissolution pores will determine the kind of electrical response of carbonate rocks. Ragland [55] found the following carbonate grains as the most abundant grains in his carbonate samples taken from widely scattered geographical locations. They are fossil fragments, ooids, and peloids. Herrick [18] earlier noted that partial dissolution of such types of grains can result in formation of micro porous grains such as micro porous cherts, micro porous fossil fragments, and micro porous oolites. Complete dissolution of fossil fragments can result in moldic porosity which is a common pore type in carbonate rocks [55]. The effects of this type of porosity on resistivity measurements will depend on the interconnectivity of the micro pores in the micro porous grains as have already been discussed earlier. It then follows logically to say that CBRI can result in continuous change in carbonate pore structure as long as CBRI progresses. Digenesis can cause cementation,

compaction, dissolution and dolomitization [49]. The implication of CBRI can be likened to the effects of diagenesis since CBRI can cause dissolution of carbonate grains, enlargement of moldic pores, cementation, and dolomitization. Dolomitization often results in enlarged pore throats. So the higher the concentration of dolomites in a carbonate rock, the higher the porosity, permeability and ease of ions' movement [46]. CBRI can also change the pore distribution of carbonates in similar way digenesis can reverse the pore distribution of carbonate rocks whereby original grains are dissolved to form new pores and original pores are filled with cement to form new rock grains [91]. Furthermore, since constricted pore throats can hinder ions' transport and result in increased resistivity [46, 92], we can expect lower conductivity caused by precipitates from CBRI that plug some pore throats and ions path. Carbonate mineral precipitates are common in CBRI [64]. Interparticle pore sizes in carbonates studied by Ragland [55] have diameters in the range of 0.06mm to 0.50mm. If the size range of the pores in a carbonate rock can be ascertained and that of the precipitates from CBRI can also be measured, then one can tell if precipitates can plug ions' path ways and cause high resistivity measurements.

Wettability is another significant factor that affects electrical property of rocks. It has already been observed that CO_2 reaction with hydrocarbon can result in deposition of asphaltene [89, 93, 94]. Hence CBROI during storage in depleted reservoir can result in deposition of some polar compounds on rock surfaces. Wettability is also expected to change during storage in saline aquifer after carbonic acids react with rock surface minerals. We also suspect wettability change to either fractional or mixed wettability because of the heterogeneous nature of the carbonate rock.

Also, resistivity measurements of saline aquifer or depleted reservoir can be affected by not only CO_2 presence but also by the change in composition of formation brine and

change in permeability (which can influence ions' movement) brought about by ion exchange and by mineral precipitates respectively during CBRI.

In summary, since saturation exponent, 'n', cementation factor, 'm' have been shown to depend not only on saturation but also on pore structures, wettability, permeability, and also because CBRI and COBRI change pore structure, permeability, wettability, and conductivity of brine in pore spaces, it will be logical then to expect 'n', 'm', and 'a' to be sensitive to CBRI and COBRI during CO_2 sequestration. For these reasons, electrical parameters of carbonate rocks are expected to change from time to time and as a function of CBRI and COBRI. Hence, understanding and prediction of the effect of CBRI and COBRI on resistivity of carbonate rock as well as on wettability, permeability, porosity, pore geometry, and brine composition is crucial and challenging.

2.10 Pore Sizes and Pore Size Distribution

Considering the role of pore geometry in electrical properties of rocks and the complexity of pore character in carbonate rocks, a basic understanding of the types and description of pores in carbonate rock becomes crucial in this research. In order to understand what sizes constitute micro-pores, macro, and mesopores, Nelson [95] defined high quality reservoirs as those having macro pores generally greater than 30 micrometres and pore throat size greater than 10 micrometres. He then classified any pore size less than 10 micrometres as micro pores and any pore throat less than 1 micrometre as micro throat, while pore sizes between macro and micro pore size were classified as meso pores. Several other definitions of micro pores exist such as: pores with an average diameter of either 1/66 mm (15.5μm); or not more than 1 μm; or those that cannot be recognized at magnifications less than 50x [25]. Micro-pores can be found within grains of porous cherts and between crystals of clay [23]. Micro-pores can be identified in a Pc-S_w plot [19, 29]. Swanson, [23] defined micro pores as

pores with entry pressures greater than the pressure at the inflection point of the capillary curve while macro pores are those entered by mercury at pressure below the inflection pressure. Pores and pore throat sizes can also be identified and measured from thin section, Nuclear Magnetic Resonance (NMR)- Relaxometry, High pressure mercury porosimetry, Scanning Electron Microscope (SEM), and X-Ray Computer Tomography (CT) scan [96]. The proportion of micro-porosity to macro-pores can be determined with high pressure mercury porosimetry [23] or capillary pressure measurements combined with Scanning Electron Microscope [26]. Dixon and Marek [30] also showed equations that are useful in using capillary pressure curve to determine the ratio of small pores to large pores. Different equations/models can be used to convert mercury injection pressure to pore throat sizes. Washburn equation is one of such equations. Washburn model assumes capillaries to be cylindrical in shape while other models assume different shapes [95].

2.11 Oil Reservoir Surveillances using Resistivity Logs

Occasional downhole measurements miss some important production trends. In addition, the cost of intervention and the cost of production loss during periodic reservoir measurements can be extremely high. Simple intervention in a single well can be as high as $2 million and more than $5 million for wireline logging in subsea wells of water depth in excess of 1500 meters [97]. Recently, permanent monitoring sensors are installed down hole near sandface during well completion for constant reservoir surveillance. Data can be delivered continuously or on demand thereby avoiding intervention cost. Data acquisition frequency can be as high as per fraction of a second and at every meter. Examples of data measured include pressure, temperature, flow rate, fluid phase, and resistivity. Also permanent sensors have been used to monitor working environment of downhole pumps such as motor temperature, vibration, and current leakage. Constant reservoir and well surveillance

can help detect potential problems, predict future reservoir and well performance, and also in timely decisions and corrective actions such as adjusting production parameters and scheduling workover operations. Many decades of experience with downhole sensors have brought about innovative methods and technologies that ensure effective data transmission and handling, and longer sensors life. One service company [97] recorded 75 years of continuous measurement of permanent down hole sensors with only one recorded failure. Furthermore, combined-tech base reservoir monitoring techniques such as combined resistivity and time lapse (4D) seismic have been utilized to observe changes in reservoirs around injection and production wells which is helpful in detecting and mitigating potential production problems. The following subsection takes a closer look at temperature and resistivity logs for reservoir surveillance.

2.11.1 Temperature and Resistivity Logs

The use of temperature log for monitoring fluid entry or production from oil and gas wells is an old practice. As fluid is injected or produced from a well, the temperature profile changes from the geothermal gradient. Cooling effect (joule Thomson effect) occurs due to formation gas expansion as they enter the well bore from the reservoir while warming effect occurs during oil and water entry into wells. Temperature log is therefore used to detect location and time of premature fluid entry, early water breakthrough, leakages in completion, and other production problems. In artificial lift operations, downhole pumps environment (temperature, vibration and current leakages) are continuously monitored and adjusted for optimal performance. Pump optimization will ensure longer pump life, reduced intervention and pump replacement cost.

Improve practice include advance technology that allow safe deployment and efficient transmission of quality data such that very small change in temperature can be accounted for.

Advance use of temperature log for well surveillance is reported in a field in Oman [97]. A distributed temperature system (DTS) installed down hole transmits temperature profile of the production interval of a horizontal well. The DTS data taken at two different times - July and August (Figure 2-4) distinguished between flow zones and no flow zones. Temperature profile in the high flow zones is lower than the well geothermal profile (blue line) while in the no flow zone, the temperature curves overlay. The temperature profile is above the geothermal gradient at low flow interval. It was clear that only 2/3 instead of the entire completed interval was contributing to flow. A new stimulation strategy was then employed to improve production. An important feature of this log is the sensitivity to small temperature change as low as $\pm$ 0.4^{o}C

In the same field, temperature profile was run in another horizontal well shut in after 39 hours of water injection for the purpose of identifying high and low injectivity zones (Figure 2-5). Low injectivity zones were characterized by fast warm up rate after well shut in. The high injectivity zone (7000-8000ft) absorbs the cold injected water resulting in slow warm up rate (front to back) while warm up was slow in low injectivity zone.

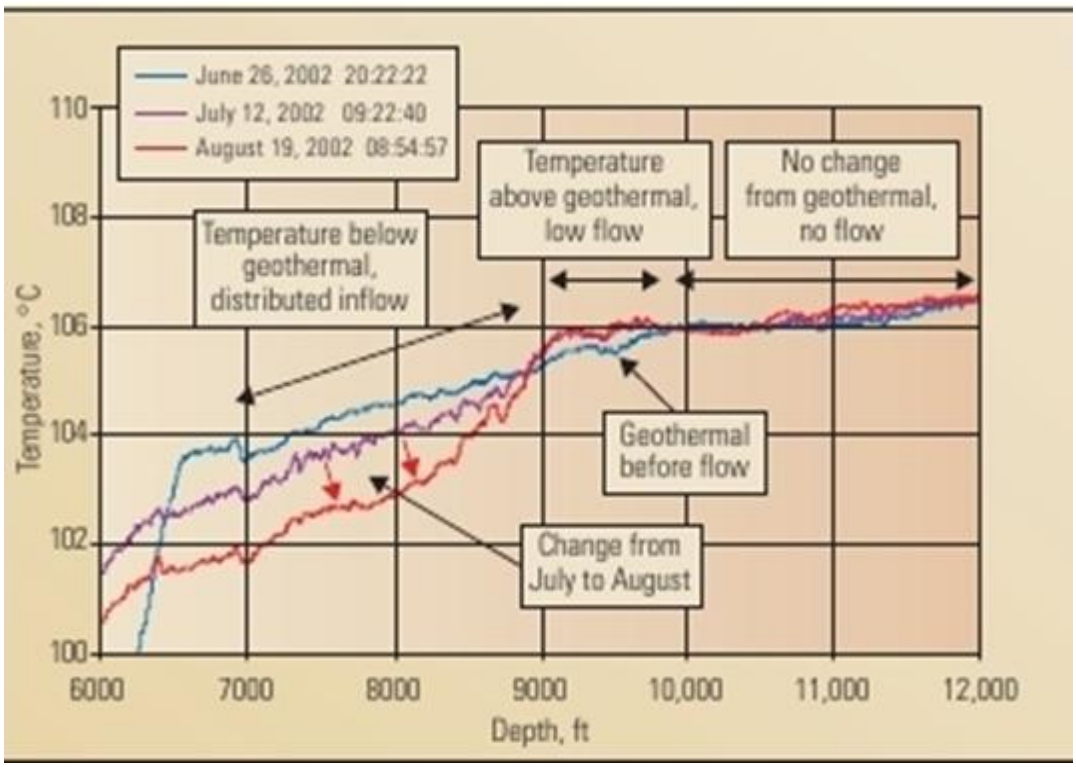

Figure 2-4 Temperature log taking from a production well at two different times. It shows interval contributing to flow and no flow intervals [97]

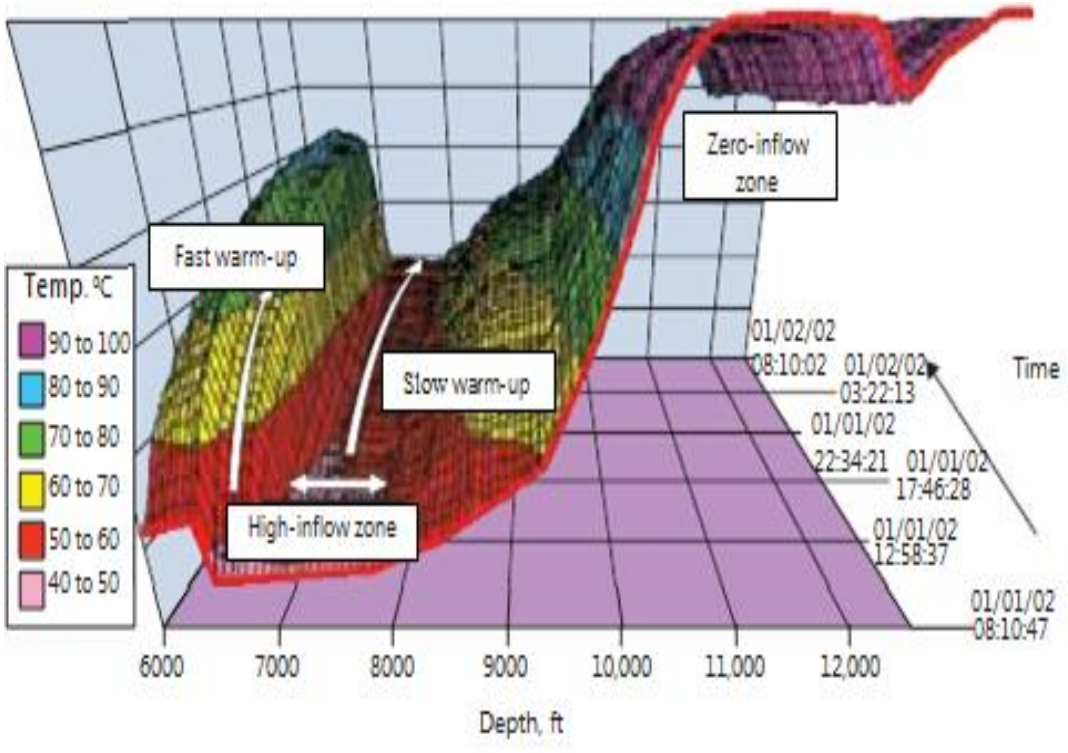

Figure 2-5 Temperature log taking after water injection in a horizontal well showing low and high injectivity zones [97]

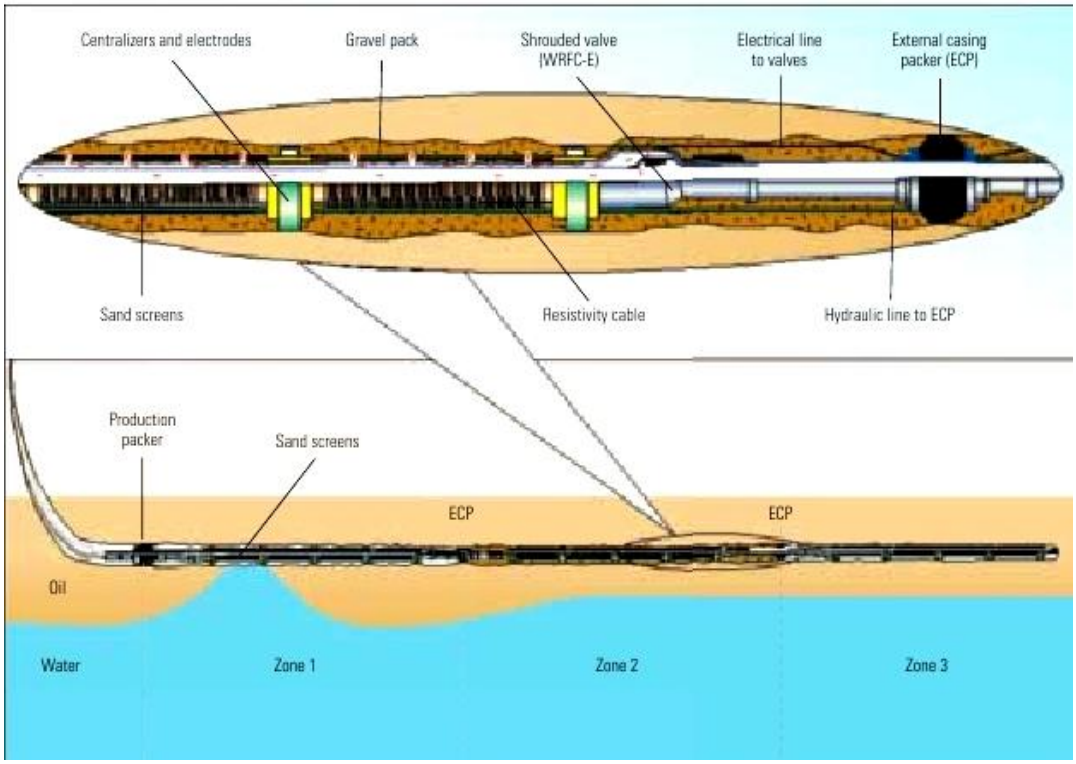

Figure 2-6 Well completion comprising of 21-electrode resistivity array together with other sensors [97]

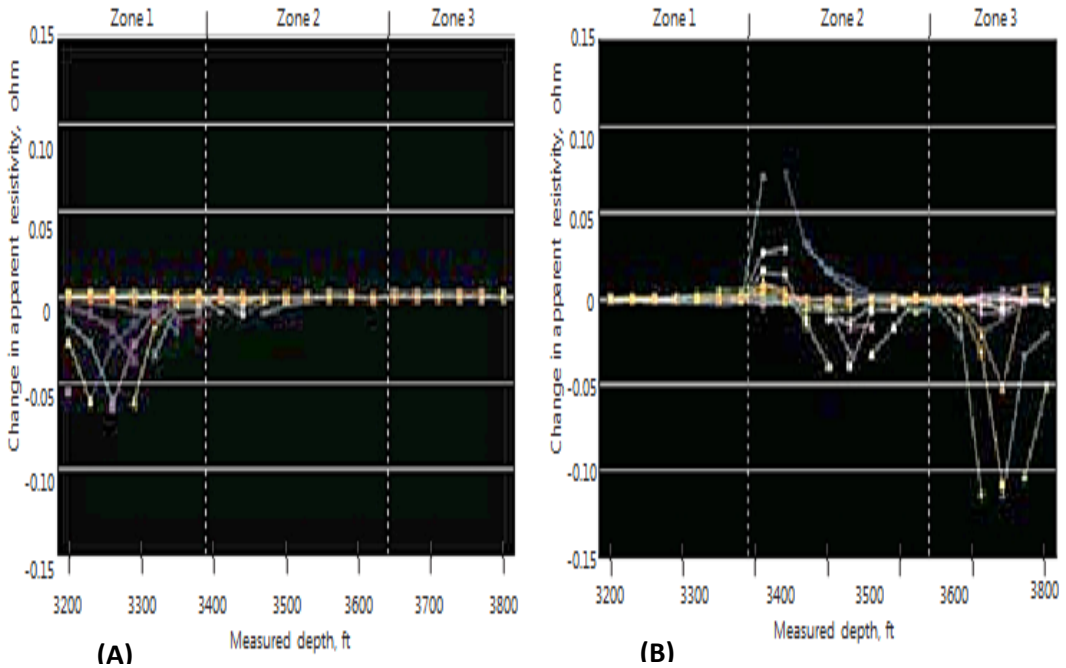

Figure 2-7 Resistivity array used to identified water migration between zones. (a) Production from zone 1 (b) production from zone 3 [97]

Resistivity log was also used in the horizontal section of a well in another field (Lamott field in Indiana, USA) to monitor fluid movement in a reservoir [97]. The well completion comprises of 21-electrode resistivity array together with other sensors as shown in the completion schematic (Figure 2-6). Centralizers spaced 20 ft apart were used as the electrodes. Current was applied at one end of the electrode and received at the surface. The voltage drop across each electrode divided by the current through it is a measure of the formation resistance at the corresponding electrode location. The depth of investigation of each electrode is 300 ft. The voltage difference per cycle (i.e. from one data acquisition to the other) is plotted on the y-axis while electrode location is on the x-axis, hence, points on the log represent change in rock resistance from one cycle to the other (3 hours interval between cycle) (Figure 2-7). The resistivity array identified water migration due to production from zone 1. Formation resistance was seen to change per cycle as water migrates from the zone (Figure 2-7(A)). The log also showed that zones 2 and 3 were not communicating with zone 1 as resistivity remained unchanged in these zones. When zone 2 was produced for 4 days, resistivity log (Figure 2-7(B)) showed water migration in zone 2 and 3 confirming communication between these two zones while zone 1 showed no change in resistance. Again resistivity changes as low as 0.05 ohm-meters were captured by the sensors and they provided meaningful information about reservoir fluid migration.

2.12 Scale Problems during CO_2 sequestration in carbonate formations

A common production or injection problem in CO_2 sequestration project is scale formation in reservoirs and around injection and production wells. Uncontrolled scale formation ultimately hampers formation injectivity and productivity. Scales plug formation pore throats and well perforations. They also deposit on downhole pumps, tubings, casing, flowlines, valves, separators, and many other production facilities. Scales form as a result

depressurization, or commingling of formation fluids [98]. Common oil field scales include Calcium Carbonate, Calcium Sulphate, Barium Sulphates, and Strontium Sulphate.

Temperature, pressure, and pH variation, and contact with incompatible water are the driving force for oil field scale formation. Several scale management techniques exist. Chemical treatment involves injection of scale inhibitors such as chelating agents, inorganic phosphates, and phosphonates into formation water either continuously or the injected agents are allowed to return to the surface with produced fluid at concentration high enough to prevent scale formation. Frequent and continuous geochemical analysis of produced formation water and petrographic analysis of cuttings for the purpose of monitoring the presence of scaling ions is another key part of scale management. Such analyses allow the surface engineers to detect when and where scale inhibitor placement is not optimal. Immediate injection of more concentration of scale inhibitor will then be needed to avoid production or injection problem. The use of computer models to predict scaling tendency is also common but do not overwrite the need for monitoring. Sources of concern with these methods include high cost, possible unsuccessful inhibition strategy, and susceptibility of surface analysis to error. Other problems include compositional change with time of produced fluid caused by evolution of dissolved gases (e.g. CO_2), scale precipitation, co-precipitation of scaling ions with suspended solids, and microbial actions. Hence, offline fluid analyses do not capture the dynamics of produced water chemistry [98]. Other field tested online techniques have been reported in the literature namely: ultrasonic [99], pulsed spectral gamma logs [100], dual energy venture multiphase flow measurements [101], gamma ray attenuation [102], and attenuated total reflectance [98]. Some real time monitoring techniques have also been tested in the laboratory such as rotating disc electrode [103], tapered optical fibre [104], and near real time sensors [105]. Online monitoring from

resistivity and temperature logging is different from the aforementioned methods because monitoring is done at the pore scale and does not wait for or depend on produced fluid before it can detect scale formation. It is also cost effective because it does not require any supporting equipment as it uses the same permanent sensors normally used for reservoir surveillance. Rugged, calibrated, and complex permanent downhole surveillance technology have been successfully used for well and reservoir surveillance in the oil and gas production operations with high accuracy, reliability, and cost reduction. The prospect of using permanent downhole sensors for scale monitoring is therefore an important possibility that deserves exploring and it is the subject of this study.

CHAPTER 3

STATEMENTS OF PROBLEM AND RESEARCH OBJECTIVES

Following the literature review, it is apparent that pore character and wettability are the dominant factors amongst other factors affecting resistivity measurements in non-Archie rocks. These two properties and others have complex behaviour in carbonate rocks which makes carbonate rock the most challenging non-Archie rocks. Carbonate rocks are more complex than sili-clastic rocks in terms of heterogeneity of pore character (i.e. pore size distribution, connectivity of pores, fractures and dolomitization) [67, 68]. Vugs and fractures are also usually present in carbonate rocks [24] because of their solubility and brittleness [69]. Different pore types can co-exist in carbonate rocks such as macro-, micro-, and meso-pores [69, 70]. Carbonate rocks can also contain clay minerals, evaporites, and conductive minerals like pyrites [69]. In heterogeneous reservoirs like carbonate rocks, petrophysical properties such as permeability can change by several orders of magnitude between points few centimetres away on a core sample [69]. Whole core measurements are therefore crucial in heterogeneous reservoirs so that small scale heterogeneity can be captured [69]. Well connected intra-particle micro porosity exists in almost all carbonate rock grains and tend to be conductive at even low S_w [30]. Carbonate rocks are also more inclined to oil wetness than water wetness [46, 69]. All the properties discussed above make petrophysical studies on carbonates a very complicated task. Nearly all the factors affecting resistivity measurements are present in carbonate rocks.

3.1 Problem Statements

Water saturation determination is often required during CO_2 EOR in order to ascertain unrecovered oil saturation. Also during CO_2 sequestration in saline aquifer, estimation of water saturation can help determine CO_2 saturation distribution in aquifers. Water saturation can be obtained from resistivity measurements using Archie or modified Archie equations. However, the use of resistivity measurements and Archie model is complicated by the fact that rock electrical parameters (also called Archie constants i.e. 'a', 'm', and 'n') during CO_2 storage or EOR in Carbonate rocks are affected by multiple factors that are dynamic in nature-because they are also affected by CBR interactions. The factors are:

i. changing wettability
ii. changing pore geometry caused by precipitation and dissolution of rock minerals
iii. changing composition of formation brine brought about by ion exchange
iv. changing permeability by mineral precipitates during CBRI (which can influence ions' movement)

These factors tend to change with time as CBRI and CBORI progress throughout EOR or storage period, and because Archie constants are significantly affected by them, Archie constants are expected to change with changes in wettability, pore geometry, and rock mineralogy. It then becomes incorrect to use constant values of 'a', 'm', and 'n' when estimating water saturation and hydrocarbon/CO_2 saturation distribution throughout the life of CO_2 storage and during CO_2 EOR in carbonate formations. The use of constant values for 'a', 'm', and 'n' can mask hydrocarbon/CO_2 saturation either by over estimation or underestimation of hydrocarbon/CO_2 saturation. There is therefore the need to study the effect of CBRI and COBRI on electrical properties, wettability, permeability, porosity, pore geometry, and brine composition of carbonate rocks. There is also the need to be able to

develop a method of determining new values of ‘a’, ‘m’, and ‘n’ as time of storage and CBRI and COBRI advance. Such techniques should be able to utilize regular log measurements to update values of ‘a’, ‘m’, and ‘n’ after regular and considerable time interval necessary for CBRI and CBORI.

3.2 Objectives of Research

The objectives of this research work are as follow:

i. To study the effect of CO_2 sequestration on petrophysical properties of carbonate rocks such as wettability, permeability, porosity, pore geometry, and mineralogy
ii. To study the effect of CO_2–Brine–Rock interaction and CO_2–Brine–Oil-Rock interaction during CO_2 sequestration in saline aquifer and during CO_2EOR on electrical properties (‘a’, ‘m’, ‘n’, R_t) of carbonate rocks
iii. Since, dissolution and precipitation process is expected to be dynamic, it is therefore unrealistic to depend on a constant value of ‘a’, ‘m’, and ‘n’ as they are expected to change as well. This research attempt to develop a protocol for predicting the change in these values during CO_2 sequestration.

The proceeding chapters discuss the experimental set up and procedures implemented to achieve the stated research objectives. The experimental procedures are divided into phases. Phase I involves sample collection and preparation while phase II is rock and fluid characterization prior to CO_2 storage. Phase III involves exposure of rock cores to CO_2 in two major ways, namely- storage in saline aquifer and storage during CO_2-EOR. Phase IV involves petrophysical analysis of cores after exposure, geochemical analysis of brine effluents, mineralogical study of precipitates, and resistivity measurements on core samples after CO_2 storage.

Chapter 4

EFFECT OF CBRI ON ARCHIE'S ELECTRICAL PARAMETERS

This section discusses an experimental investigation of the impact of carbon dioxide-brine-rock interaction on saturation exponents and cementation factor in carbonate formations. The challenge in this type of study is the difficulty to ascertain that the difference in the slope of a resistivity index plot of a plug prior to CBRI and after CBRI is not due to hysteresis and measurement errors but due to changed pore structure as a result of CBRI. To overcome this challenge, we avoided measuring resistivity index experiment twice on the same sample in order to avoid cycle dependence hysteresis. Cycle dependent hysteresis means that results are different for successive displacement with the same fluid in the same rock sample [106]. Most similar core plugs were selected from many plugs acquired from an outcrop of Indiana limestone which is a very homogenous carbonate formation. This will allow results to be compared among samples without having to repeat resistivity index experiment after CO_2 storage on the same plug. The proceeding sections describe the procedure,

4.1 Sample Preparation

1.5 inch diameter cylindrical samples were cut from dry Indiana lime stone samples obtained from Indiana outcrops in the US. The carbonates are pure calcite minerals. The use of a precision drill press with water as the lubricant enabled us to cut core plugs that are as perfectly cylindrical as possible (Figure 4-1). Surface grinding of both ends of the cores

resulted in very flat and smooth surfaces required for resistivity measurements. With the aid of a caliper (with resolution of 0.001 inch), five measurements of length and diameter were made for each sample spaced across the core length and circumference, and then averaged to estimate each core's average length and diameter. The averaged length and diameter were used to calculate the cross section area required for resistivity calculations. A total of 12 samples were prepared and their end pieces were preserved (Figure 4-1) for petrographic analysis such as thin section, Scanning Electron Microscopy (SEM), and Mineralogical analysis which was useful in interpretation of experimental results. All the core plugs were then thoroughly cleaned using the solvent reflux method. Each sample was placed over methanol in a soxhlet apparatus (Figure 4-2) and heat applied continuously for 3 days to allow for complete leaching out of all salt deposits in the pore spaces. The use of toluene was not necessary because the samples are outcrops and were never in contact with crude oil. At the end of the third day of cleaning, the samples were placed in a vacuum oven and allowed to dry for 24 hours at oven temperature of 80^{o}C and a vacuum of 15mmHg.

Figure 4-1 Cylindrical cores with end pieces

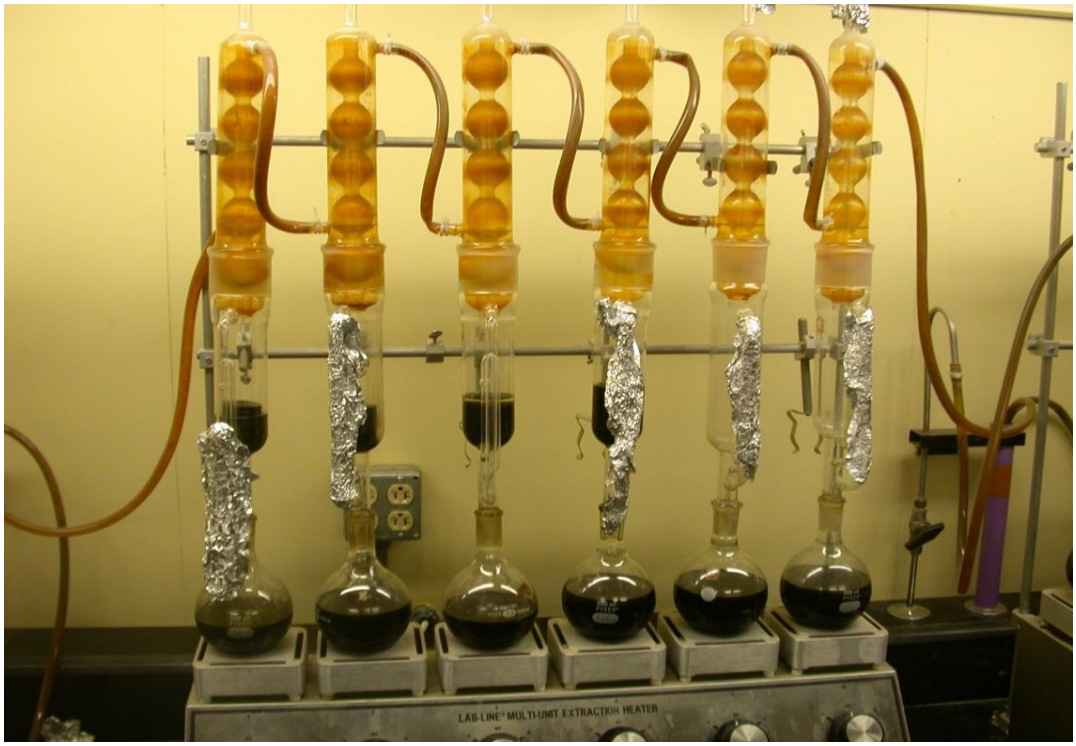

Figure 4-2 Soxhlet apparatus for cleaning samples

4.2 Brine Preparation and Characterization

Synthetic formation brine was prepared using the volumetric method in which desired weights of component salts were dissolved in a given volume of high quality distilled water. A slightly heated magnetic stirrer was used to stir the mixture until all the salts dissolved in water and a clean homogeneous brine solution was formed. The brine solution was then filtered with the '44 Ashless Whatman' filter paper which has a slow filter speed and fine crystal retention capacity (9.0 cm). The filter was allowed to sit on a filter holder tightly sitting on another flask connected to a vacuum pump. The brine solution was then poured onto the filter and a vacuum applied to the receiving flask allows the brine to drain through the filter (Figure 4-3). After filtration, the brine was degassed by applying vacuum of 30 in Hg (100 KPa) for 3 hours (Figure 4-4) to avoid or minimize residual air trapping in the cores. Samples of the degassed brine were taken for brine density and resistivity measurements.

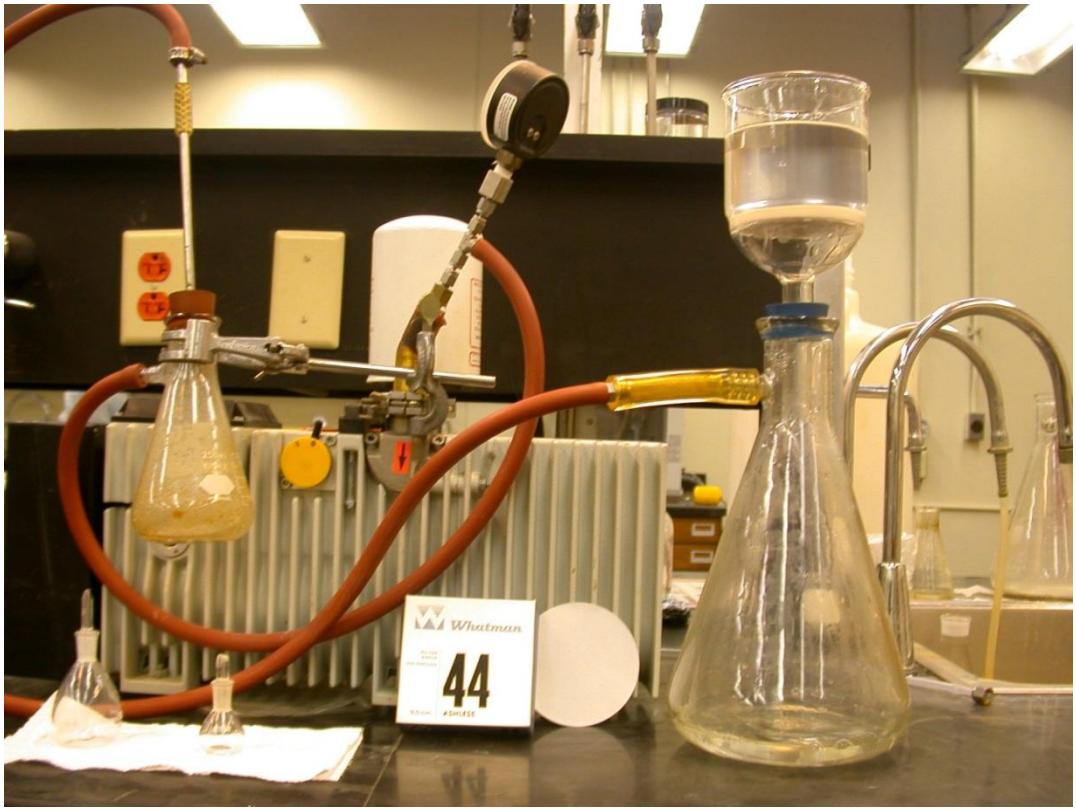

Figure 4-3 Filteration of brine using Whatmann filter paper

Figure 4-4 Degassing brine solution by vacuuming

4.3 Brine density and resistivity

The brine density was measured using the 'Fann' resistivity meter (model 88c). Nine different resistivity measurements were made from nine brine samples at an average temperature of 22.4^{o}C to give an average resistivity measurement of 0.401ohm-meter. A pycnometer was also used to obtain an average brine density of 1.0202 g/cc. Two brine compositions were prepared namely saline aquifer brine and sea water. Their compositions and physical properties are shown in Table 4-1.

Table 4-1 Brine composition and properties

	Saline Aquifer	**Sea Water**
Composition	**Weight (g/l)**	**Weight (g/l)**
Sodium Chloride (NaCl)	44.5	44.5
Calcium Chloride ($CaCl_2.2H_2O$)	9.65	0.28
Magnesium Chloride ($MgCl_2.6H_2O$)	3.41	1.6
Sodium Bicarbonate (NaHCO3)	0.15	0.15
Sodium phosphate (Na_2SO_4)	0.28	9.65
TDS (g/l)	57.99	56.18
Density, g/cc	1.02	
Resistivity @ 22.5 ^{0}C , (ohm-m)	0.201	

4.4 Core Characterization

4.4.1 Pore volume, Porosity and Permeability Measurement

The core samples were removed from the oven, allowed to cool to room temperature, and weighted. We then measured pore volume, porosity, and permeability of the cleaned cores using a well calibrated automated helium porosimeter-permeameter (Figure 4-5)

capable of measuring permeability in the range of 0.001 to 10,000 mD and at a confining pressure of 500 psi. The porosimeter-permeameter utilizes the isothermal ideal gas law (i.e. Boyle's law) to determine pore volume and grain volume. The dimensions, permeability, and porosity values for the cores are provided in Table **4-2.** A CT scan was conducted on the dried samples in order to visualize internal features like fractures and other crystals which may not be visible with the naked eyes.

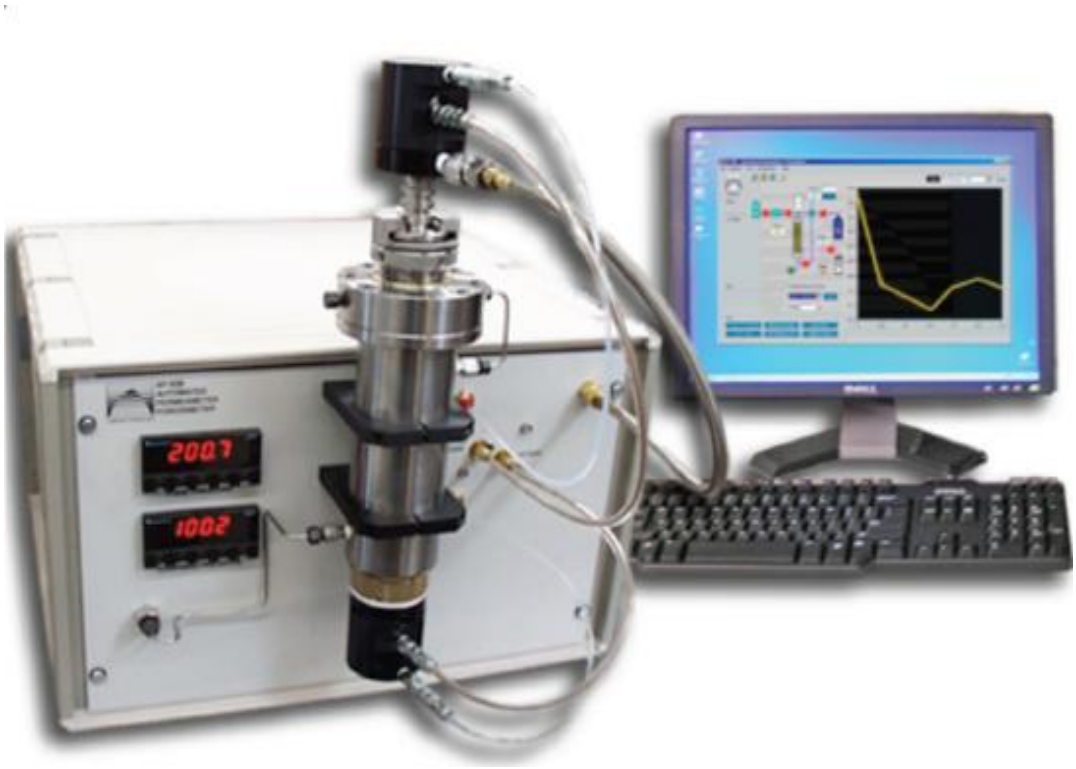

Figure 4-5 High pressure porosimeter-permeameter

Next, we saturated the cores with prepared brine using the vacuum saturation method (Figure 4-6) and the saturated weights in air were measured with an electronic spring balance. The difference in saturated weight and dry weight divided by the brine density gives the liquid pore volume. The brine pore volume and the helium pore volume are in agreement (Table **4-2**). Core samples were then stored in brine under vacuum for about three weeks to allow for electrochemical equilibrium.

Table 4-2 Core Basic Properties

	L	D	Bulk Vol.	He. Pore Vol. (500 psi)	He Porosity (500 psi)	k
ID	**(cm)**	**(cm)**	**(cc)**	**(cc)**	**(%)**	**(mD)**
S-1	6.6	3.735	72.35	14.00	18.312	341
S-2	7.06	3.736	77.43	13.78	17.518	423
S-3	6.8	3.743	74.84	14.70	17.691	599
S-4	7.03	3.741	77.37	14.70	17.69	324
S-5	6.82	3.737	74.76	14.55	18.302	539
S-6	6.82	3.735	74.77	14.47	18.563	528
S-7	7.09	3.743	77.96	14.60	18.079	354

Figure 4-6 Vacuum saturation

4.4.2 Pore Size Distribution using Mercury Injection Capillary Pressure (MICP) and NMR T_2-Relaxometry

The role of pore size distribution in electrical resistivity of reservoir rocks particularly carbonate led us to carrying out an extensive study of samples' pore system using the MICP and NMR technique on 12 samples. NMR spectroscopy was performed on samples while MICP was performed on samples' end pieces since it is a destructive technique. The objective of these analyses is to identify and select plugs of most similar pore character.

MICP test was conducted on the sample using the Micrometrics Auto Pore IV 9500 Series (Figure 4-7). Mercury was injected into the sample at an incremental pressure of 1.5 psi using nitrogen gas as the displacing medium to complete the low pressure stage at 30 psi. The injection pressure was released to the atmosphere and the penetrometer removed and weighed with the sample and mercury in place to determine the assembly weight and sample bulk volume. The sample was then loaded into the high-pressure chamber for the high pressure stage terminating at 60,000 psig injection pressure. The injection pressure was relieved and the penetrometer removed completing the test.

Figure 4-7 MICP - Micromeritics AutoPore IV 9500 Series

NMR experiments were performed using the Oxford Instruments' GeoSpec 2-75 with Green Imaging Technologies' GiT Systems v6.1 software (Figure 4-8).

Thomeer hyperbola was chosen to analyse MICP data because it can handle rock multimodality and can be upscaled to field scale [107]. Thomeer in 1960 observed that MICP data can be represented by a hyperbola when plotted on a log-log graph. He observed that a hyperbola type-curved to a given MICP data can be characterized by three parameters namely pore geometrical factor, G which determines the shape of the hyperbola, the minimum entry pressure, Pd which is the maximum pore throat diameter, and percent bulk volume ($B\infty$) of rock occupied by mercury at infinite applied pressure (see Figure 4-9). Thomeer empirical formula is given as:

$$\log\left(\frac{B_v}{B^{\infty}}\right) \times \log\frac{P_C}{P_d} = K \quad \text{4-1}$$

$$K = \log\left[exp(-G)\right] \quad \text{4-2}$$

$$\frac{B_v}{B^{\infty}} = \exp\left[\frac{-G}{\log\left({}^{P_c}/_{P_d}\right)}\right] \quad \text{4-3}$$

Pc is capillary pressure, psi.

Figure 4-8 NMR - GeoSpec 2-75

Plotting the Thomeer function on a log-log scale will generate the hyperbolas. Figure 4-9 shows the three Thomeer parameters. Various values of G are possible (0.1 < G < 10). In a polymodal pore system, two or three hyperbolas can be used to type fit a given MICP data. Thomeer Swanson excel spread sheet developed by Clerke and Martin [108] was used to type-curve the MICP data in this study (Figure 4-10 and Figure 4-11). When Thomeer function was applied to the study samples, geometric factor, G for macro pores are within the

range of $0.2 < G < 0.6$ for all samples while their micro pores fall in the range $0.3 < G < 0.7$. It is therefore clear that all samples have very similar pore character based on their pore geometric factor since a difference in geometric factor of ± 0.5 is not enough to differentiate between two pore systems ([1]personal discussion). Generally, two pore systems exist- the macro pores with pore size in the range of 10 - 100 microns while the meso/micro pores are between 1 to 10 microns.

Figure 4-12 shows the pore size distribution of a group of samples (S-1. S-2, S-3, S-4, and S-5) called Group 1. They are grouped because of their very similar pore geometry based on NMR (Figure 4-12) and MICP (Figure 4-13) analyses. Figure 4-14 and Figure 4-15 show another group comprising of samples with similar pore character namely S-6 and S-7. Figure 4-16 and Figure 4-17 are the capillary pressure curves for the two groups. It can be seen from the figures that MICP and NMR are in good agreement which confirms that all samples in each group are almost a replica of each other except for sample S-2 which has a slightly different pore character from the rest. Generally, two pore systems exist in all samples- the macro pores with pore size in the range of 1 - 100 microns while the meso/micro pores are between 0.01 to 1 microns (Figure 4-13 and Figure 4-15). The different pore types are well connected as seen in the NMR spectroscopy (Figure 4-12 and Figure 4-14)

[1] Personal communication with Clerke E. A during a course work at KFUPM 2013

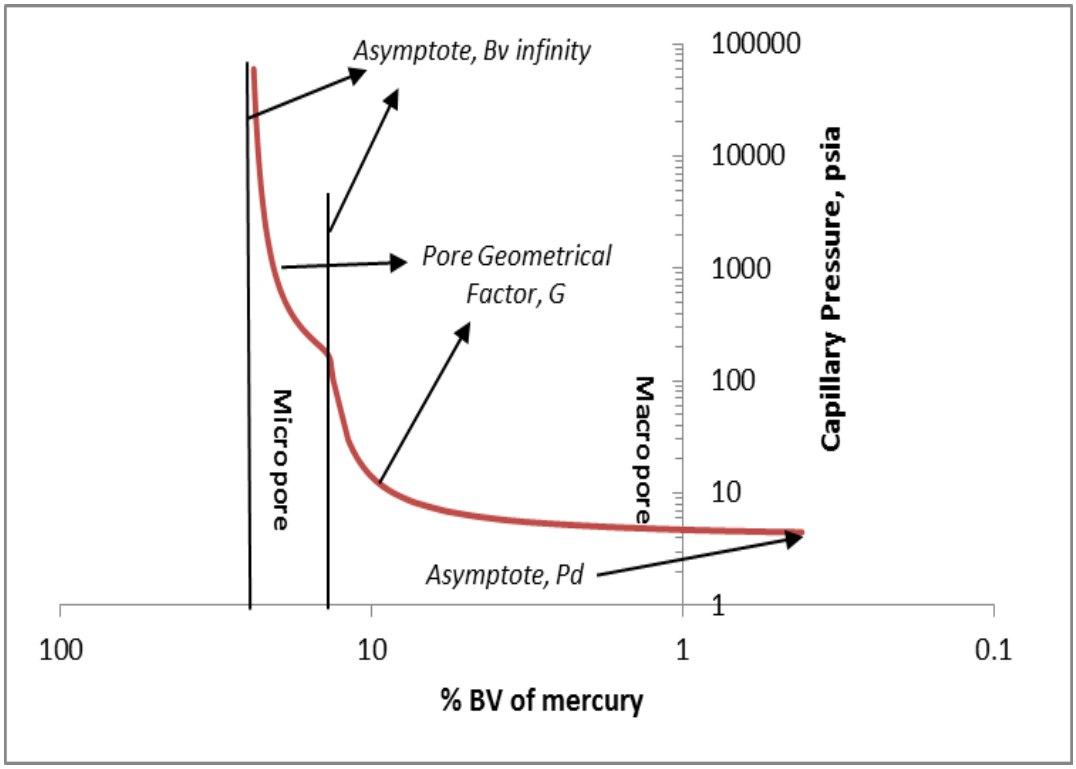

Figure 4-9 Parameters of Thomeer Hyperbola

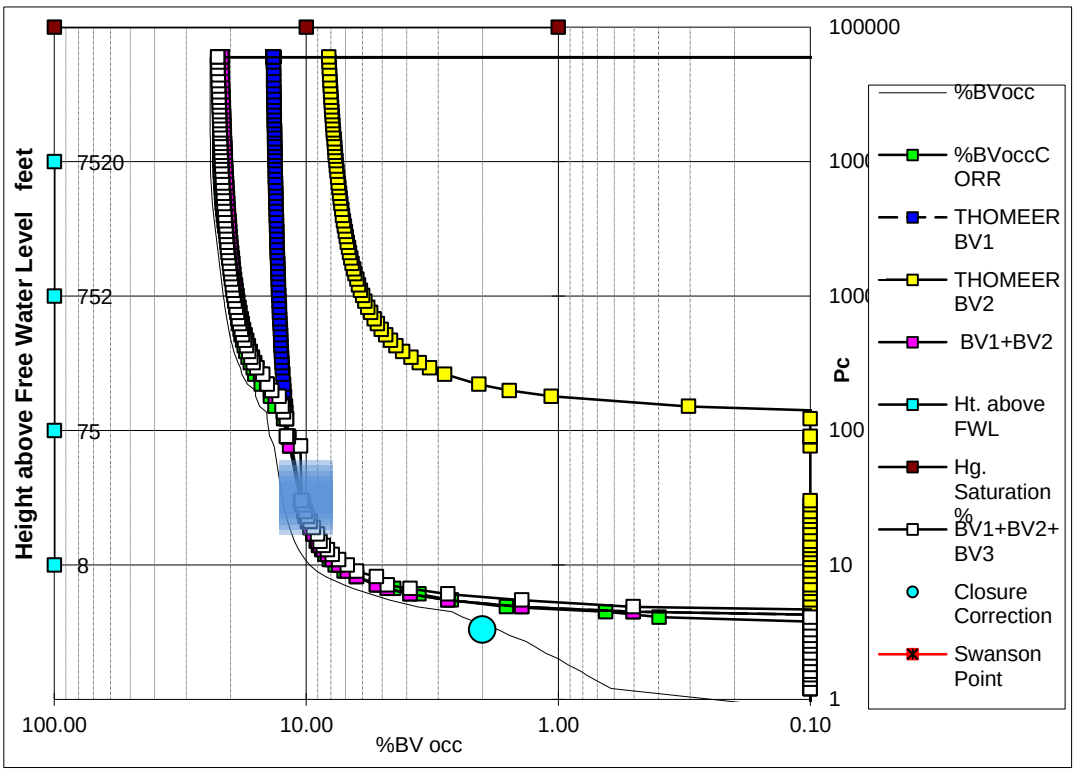

Figure 4-10 Typical Thomeer Hyperbola (Clerke and Martin 2004)

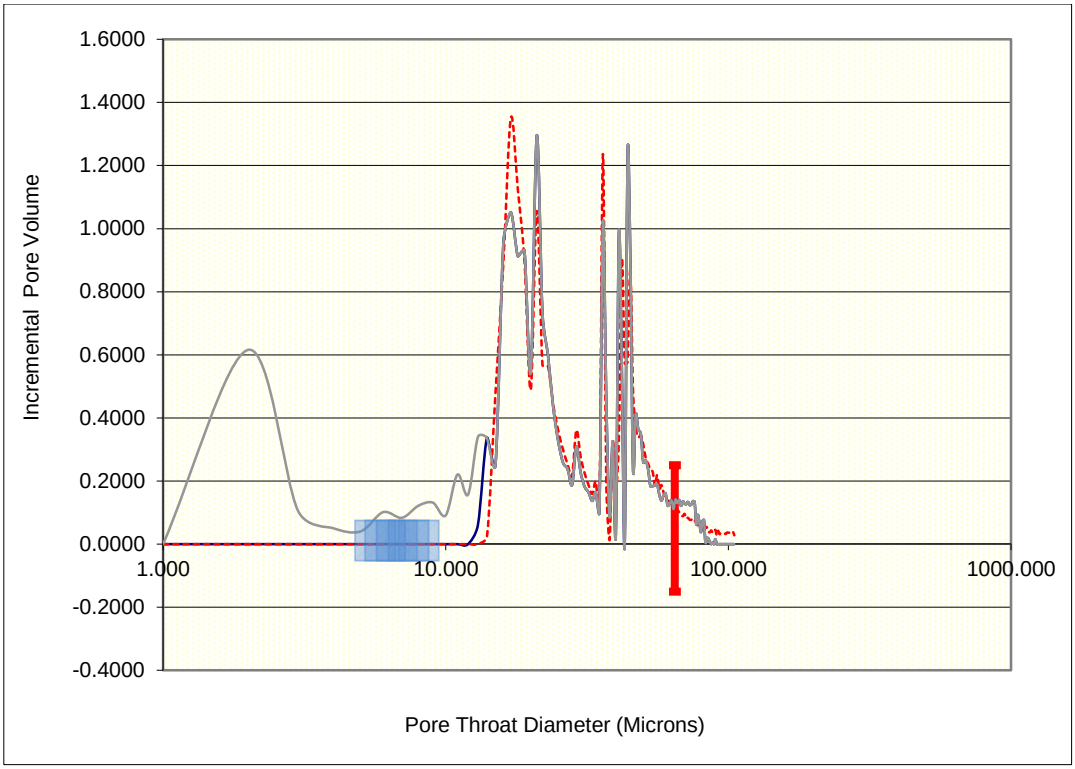

Figure 4-11 Typical pore size distribution after Type curve [108]

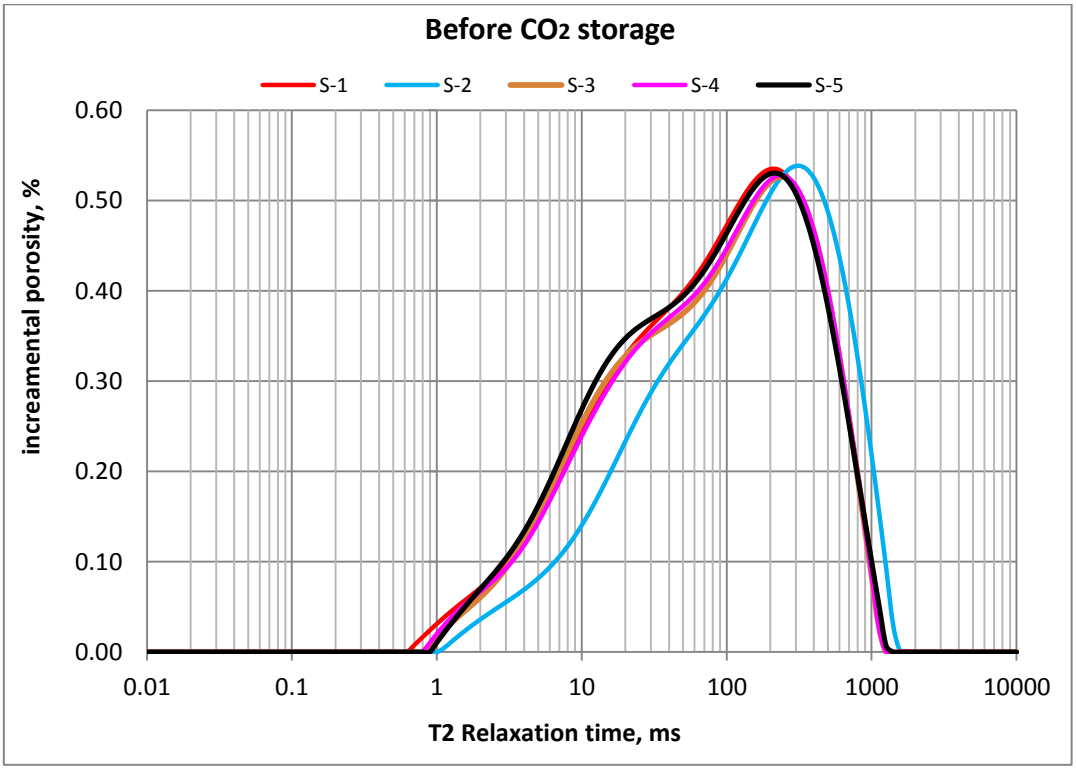

Figure 4-12 Pore size distribution on group 1 samples before CO2 storage. NMR T2 relaxometry performed on whole sample

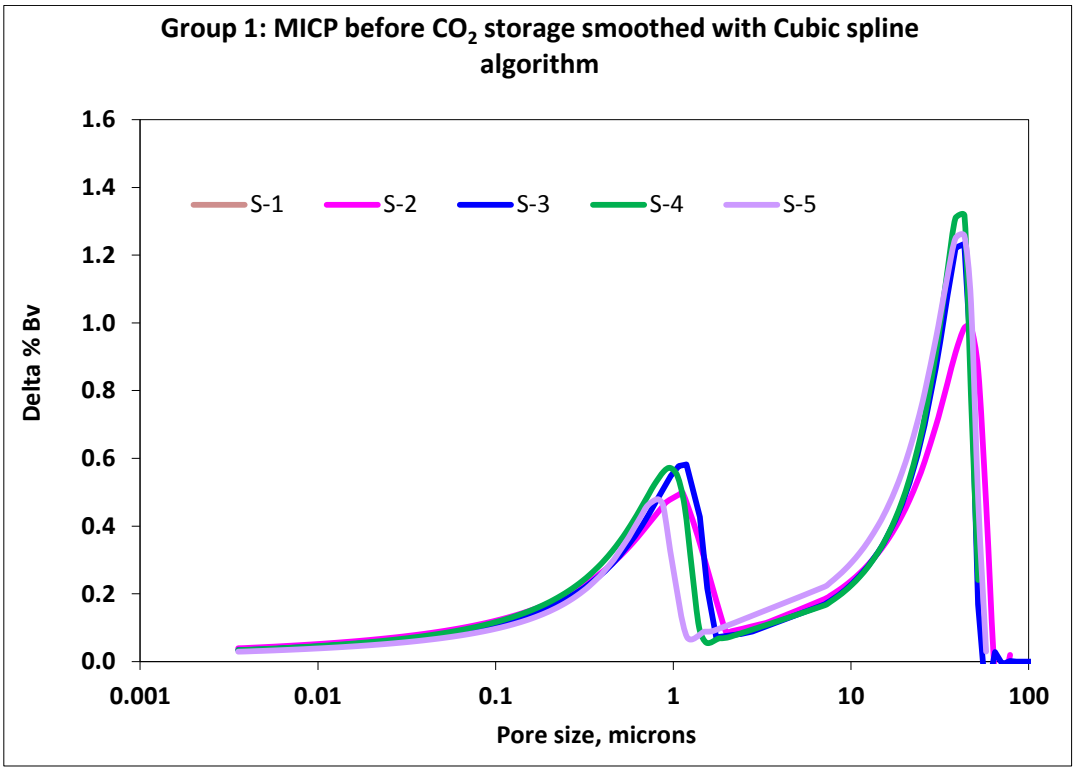

Figure 4-13 Pore size distribution on group 1 samples before CO2 storage. MICP pore throat distribution performed on samples' end pieces

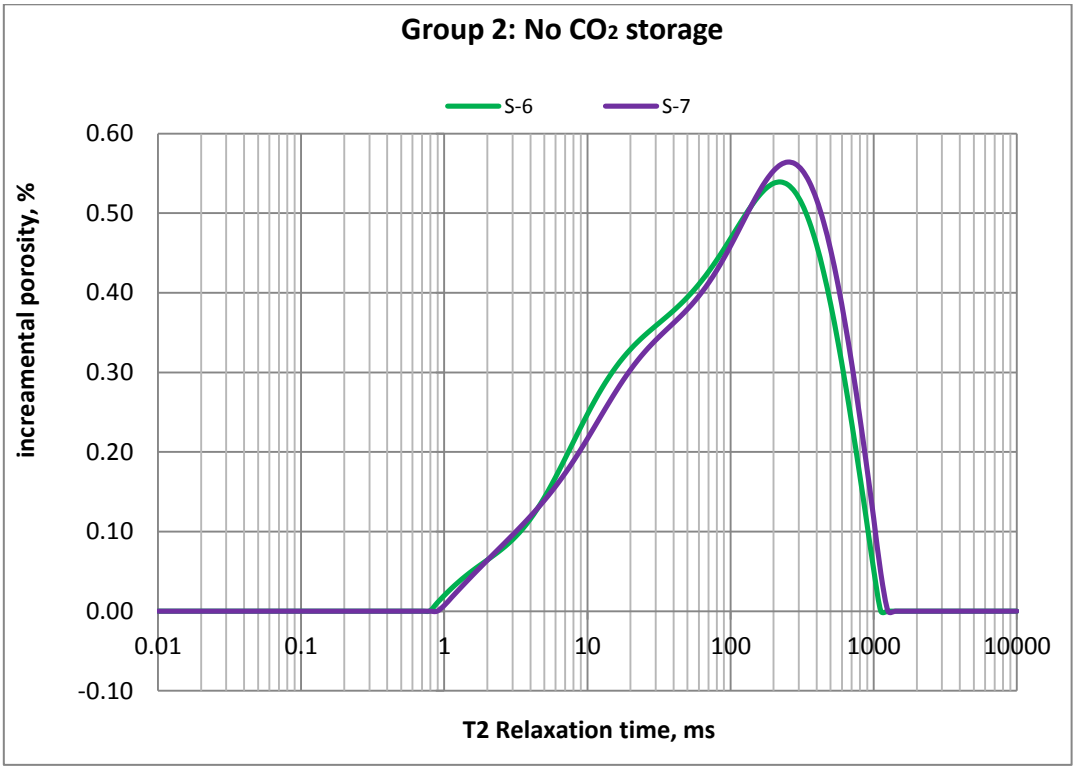

Figure 4-14 Pore size distribution of group 2 samples without CO_2 storage. NMR T2 relaxometry performed on whole sample

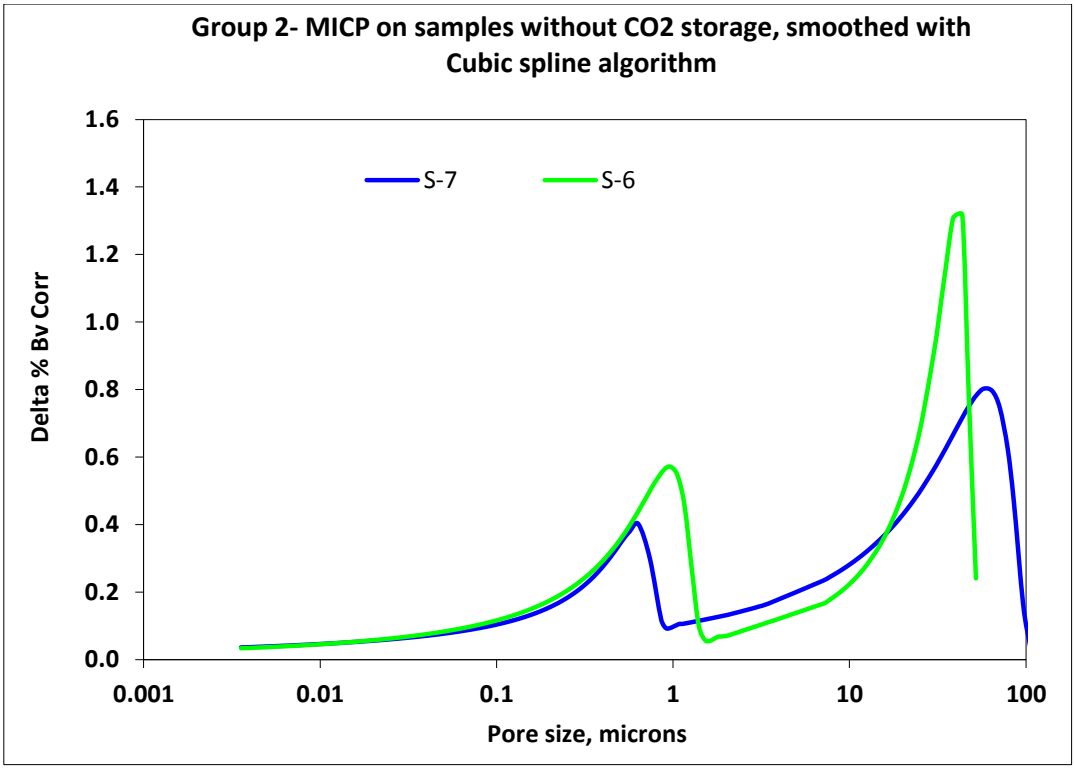

Figure 4-15 Pore size distribution of group 2 samples without CO2 storage. MICP pore throat distribution performed on samples' end pieces

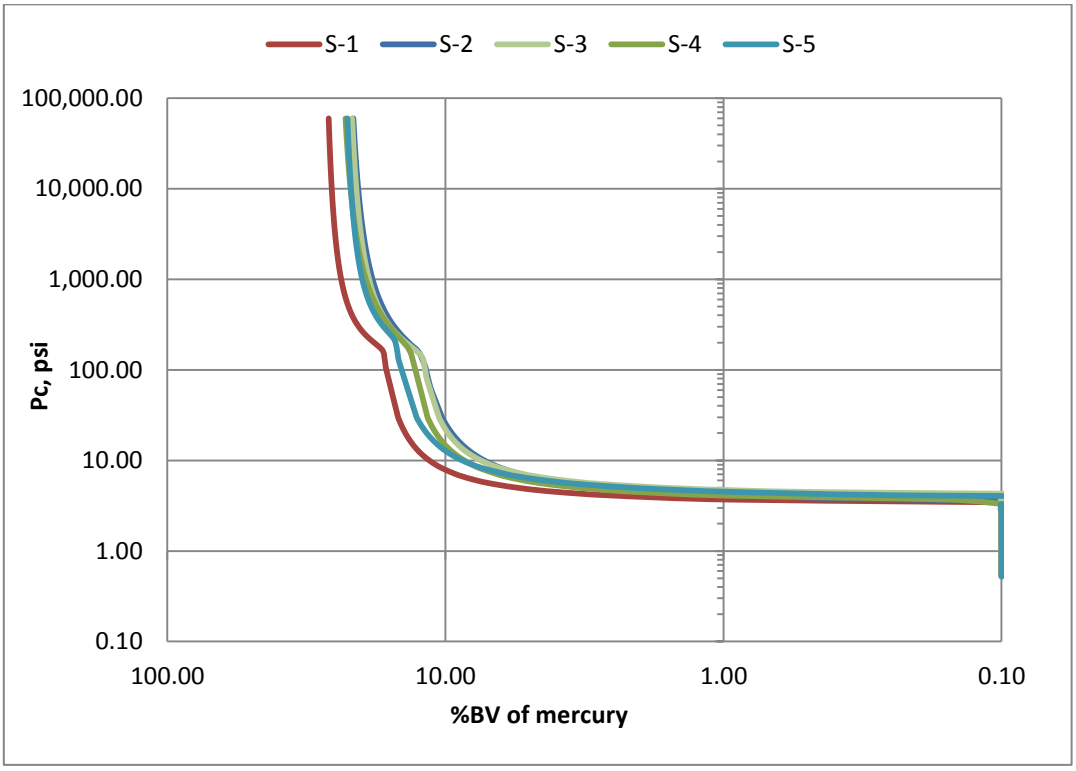

Figure 4-16 Capillary pressure curves for group 1

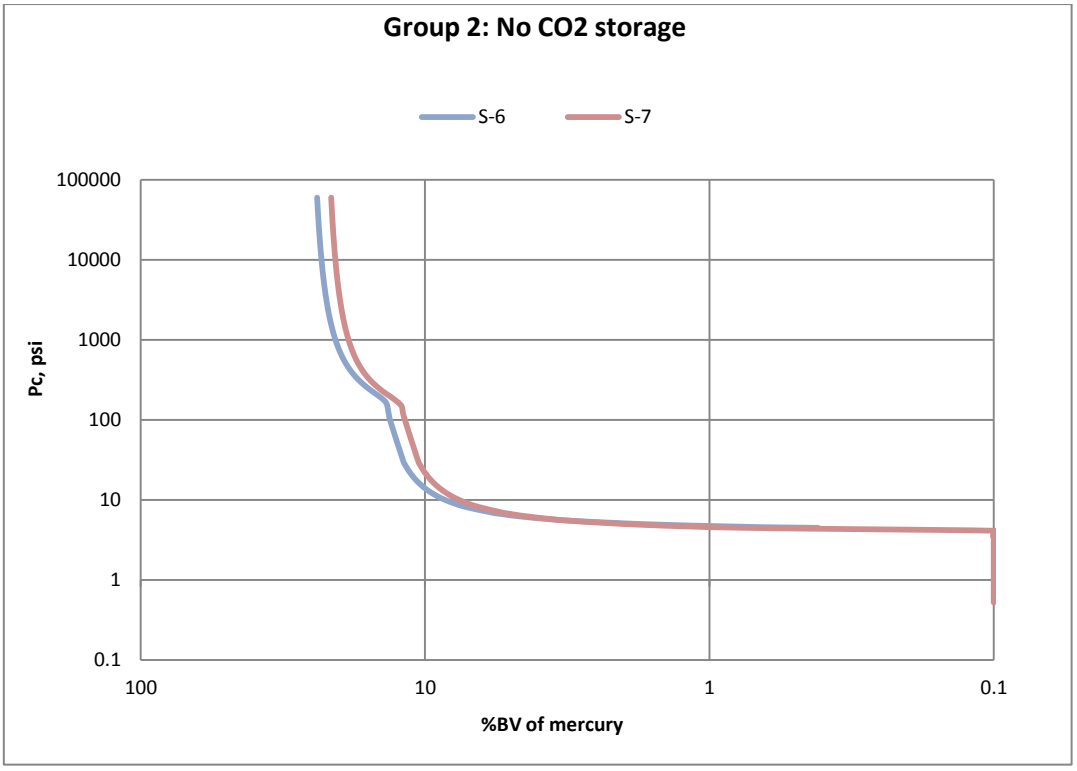

Figure 4-17 Capillary pressure curves for group 2 samples

4.5 Experiment Setup for CO_2 Injection

There are several ways in which CO_2 can be injected into underground formations namely: as a dense CO_2 stream; as supercritical phase; as water alternating gas; and as carbonated brine [109]. Carbonated brine was injected in two dry samples (S-3 and S-5) and supercritical CO_2 was injected into another two brine saturated samples (S-2 and S-4) all from the same group 1 (Figure 4-12 and Figure 4-13).

Figure 4-18 shows the batch system for the CO_2-brine-rock system. It consists of the aging cells (Hastelloy) labelled A, B, and C. Each cell has a volume capacity of about 300 cc of brine at a pressure of 2000 psig. The pore volume of each core sample is also known. Prior to start of aging, cells' seals were replaced with new Viton seals and the cells pressure tested at 3500 psig for 10 days. Although, the pressurized cells were left at slightly varying room temperature, the cells' pressure appeared to be constant except for some fluctuation of ± 60

psi attributable to fluctuating room temperature. Although Viton seals have very good tolerance for CO_2, positioning the test cells horizontally such that the CO_2 cap forms below the cell upper wall as shown in Figure 4-18 reduces their contact with CO_2 plume instead of positioning it vertically in which the seals around the cap will be in full contact with the CO_2. Since the aging cells are made of Hastelloy, corrosion is of less concern.

The cells were connected by stainless steel tubing. Each cell has an inlet valve and a port connected to pressure gauges outside the oven. The outlet of each cell was permanently closed. Each of the cells was loaded with a cleaned and dry core (S-3 and S-5) whose petrophysical properties were previously measured. Also housed in the oven was a 1-litter brine cylinder connected to an outside syringe pump at one end. With an arrangement of valves and tubing, the other end of the brine cylinder was connected to the three aging cells and also to a mixing cylinder where brine and CO_2 were allowed to mix at a given pressure. The other end of the mixing cylinder was connected to a CO_2 floating piston accumulator inside the oven. Outside the oven were the following: a CO_2 source, a syringe pressure pump, pressure gauges, pressure transducers, and a data acquisition system consisting of an analogue to digital converter, data acquisition cables, and a computer. The GUI of the data acquisition software is shown in Figure 4-19 was used to monitor and record resistivity and pressure values during sequestration.

After loading the dry cores in their respective cells, vacuum was applied to the cells through the inlet valve for 3 hours so as to completely remove all trapped air in the cores, cells, and tubing. Inlet valves were then closed before disconnecting the vacuum pump. The syringe pump was used to transfer some volume of brine ($2/3^{rd}$ of the storage cell capacity sufficient to submerge the samples) into the mixing cylinder. Vacuum was then applied to the top of the brine in the mixing cylinder and also in the CO_2 accumulator so as to remove

trapped air. CO_2 gas was then transferred from the CO_2 cylinder outside the oven into the floating piston CO_2 accumulator inside the oven at a pressure of 1000 psig. The oven was then allowed to heat up to 45^oC and left at this temperature for over 24 hours to allow the cores and the fluids to equilibrate with the oven temperature. During this period, CO_2 pressure in the accumulator increased due to temperature increase in the oven. A syringe pump was then used to step up the pressure in the CO_2 accumulator to 2000 psig by applying pressure on the water below the floating piston. In order to generate carbonated brine, the inlet valve of the mixing cylinder connected to the CO_2 accumulator was opened to inject supercritical CO_2 into the mixing cylinder containing brine. CO_2 pressure dropped during CO_2 transfer into the mixing chamber. The syringe pump was then used to boost the pressure in the mixing cylinder. Figure 4-20 depicts the pressure path in the mixing cylinder prior to injection into individual storage cells- A and B. It can be seen in the figure that the starting CO_2 pressure in the mixing cylinder is different for cells A and B. The reason for this was just due to the available CO_2 pressure at the time of injection into the mixing cylinder. The difference in pressure was later accounted for by injecting pure supercritical CO_2 into the individual storage cells (after injection of the prepared carbonated brine into the storage cells) until the cells' pressure reached 2700 psig and the cells' valve closed. Supercritical CO_2 at the top of the carbonated brine was used to drive the carbonated brine through the bottom of the mixing cylinder into the storage cells such that the storage cells were filled 2/3rd of the cell capacity and the supercritical CO_2 driving in the carbonated brine filled the remaining space above the cells to form a gas cap at about 1600 psig. Figure 4-21 shows the pressure path in each storage cell during carbonated brine entry and pressure step up to 2700 psig. Sample S-5 was aged for 5 months while S-3 was aged for 4 months.

For cell A, injection of CO_2 into the mixing cylinder occurred at a pressure of about 1800 psig after which the pressure declined with time until it stabilizes at a pressure of 1550 psig after about 400 minutes. The period of decline represents the dissolution period of CO_2 in brine. CO_2-brine mixing pressure prepared for cell B was 1656 psig and pressure declined and stabilized at 1560 psig after about 280 minutes. In another CO_2 solubility experiment, plot 'Cell AB' (Figure 4-20) shows the beginning of CO_2 dissolution in brine from 2000 psig to 1700 psig (after about 400 minutes). It can be concluded from the three cases of CO_2-brine mixing that an average of 300 minutes is required for brine solubility in CO_2 within the experiment condition of 1700 - 2000 psig CO_2 pressure, 45^{o}C temperature and NaCl equivalent salinity of 54,000 ppm. The pH value of the brine before mixing and after brine-CO_2 mixture (1500 psig equilibrium pressure) was measured to be 7.2 and 4.8 respectively at ambient conditions.

In the supercritical CO_2 injection method, brine saturated samples were placed in Viton sleeves prior to placement in cells A and B. Prior to placing in sleeves, Teflon tape was wrapped along the circumference of each sample (Figure 4-22) so as to delay the diffusion of CO_2 through the sleeve. After placing samples in the sleeve, two end caps with flow connection to inlet and outlet tubing respectively were placed at both ends of the samples (Figure **4-23**). In this case overburden oil was injected in the annular space between the sleeve and the storage cells and at a pressure of 500 psig after which the core was circulated with brine to remove trapped air. Inlet and outlet valves attached to the core assembly served as means of either closing up the core after CO_2 injection or for fluid sampling at the end of storage. At the end of brine circulation, cell temperature was raised to 45^{o}C, the overburden pressure too was raised to 2000 psig and the system left for over 24 hours for the core to equilibrate with the surrounding temperature and pressure. After 24 hours, the outlet valve

was closed and CO_2 was applied at the inlet tubing until a core pressure of 2000 psig was attained making the CO_2 to exist in a supercritical state in the test cell. The CO_2 injection pressure was kept constant for 24 hours after which the inlet valve was closed. The outlet tubing was also connected to a pressure gauge used to monitor CO_2 pressure. The same procedure was applied to the other core sample. S-2 was aged for 2 months while S-4 was aged for 3 months. Pore pressure was monitored during this period.

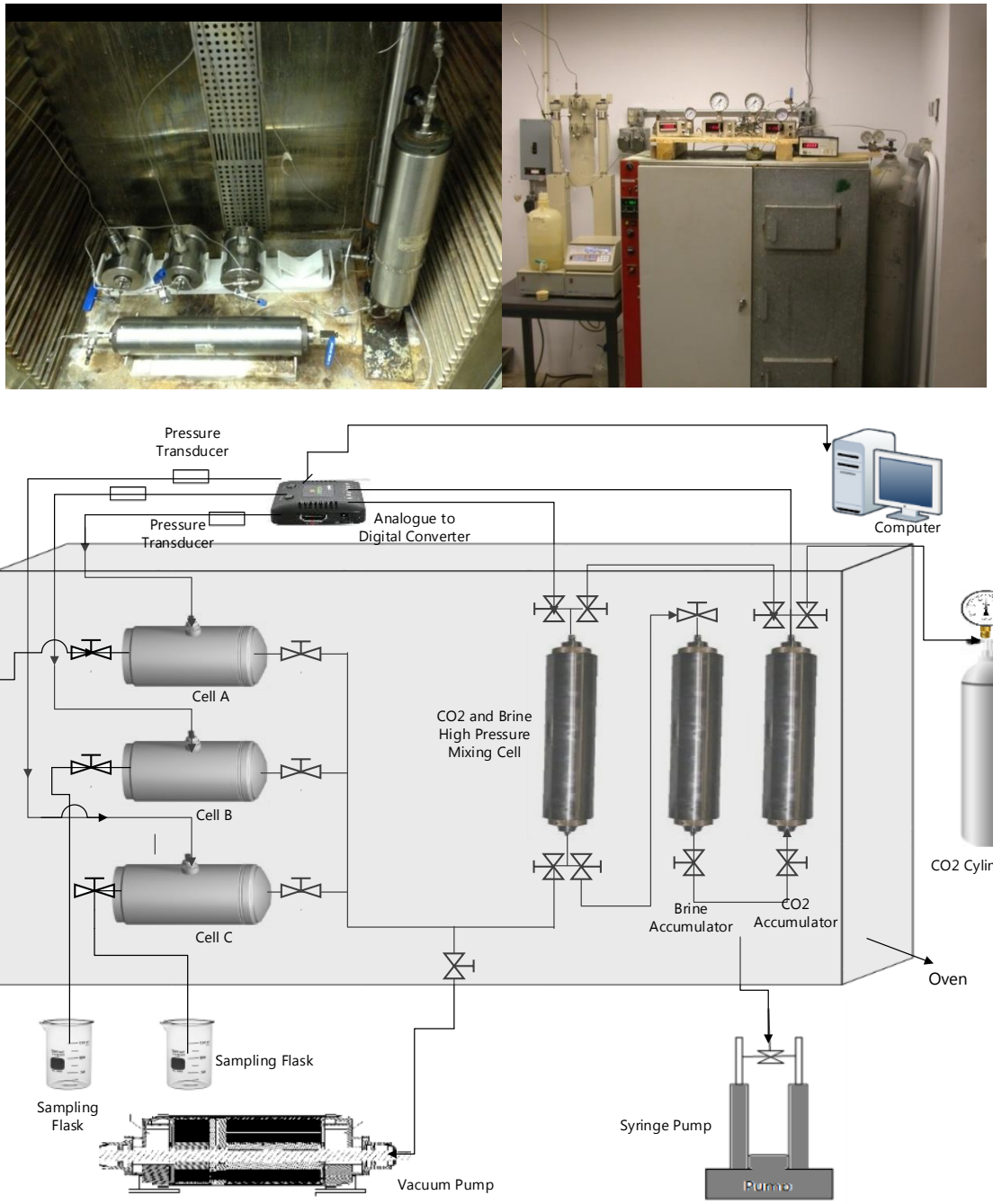

Figure 4-18 Set up for CO2 Sequestration in core samples

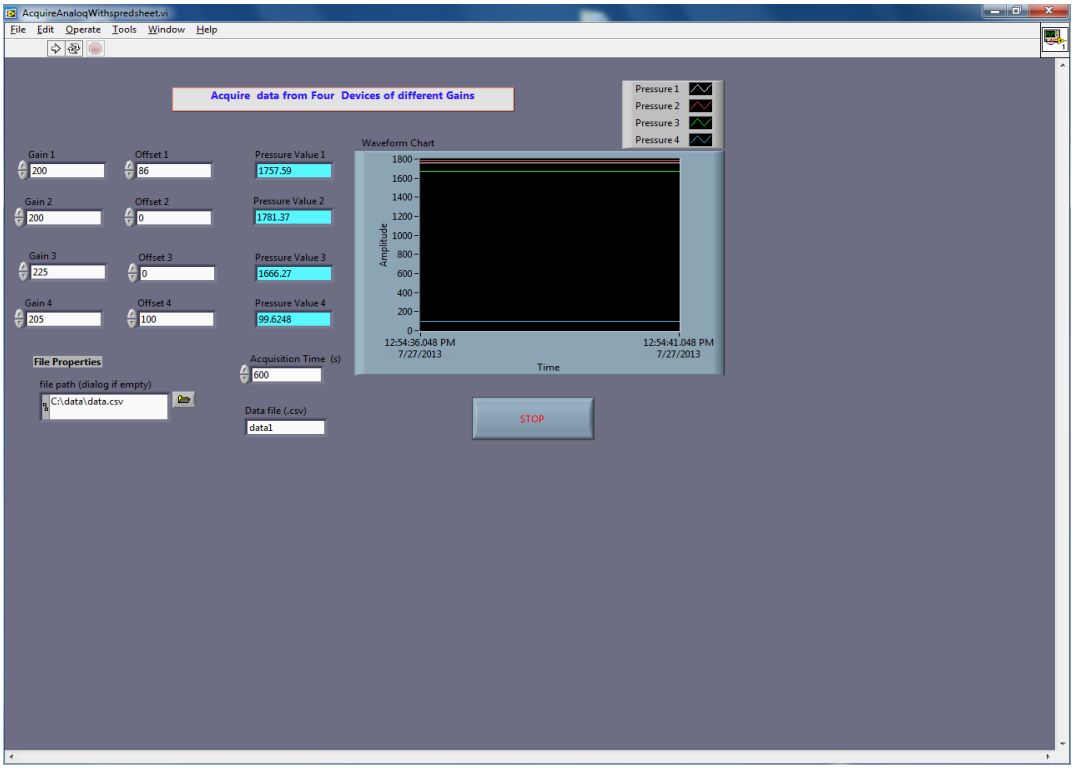

Figure 4-19 GUI for pressure logging

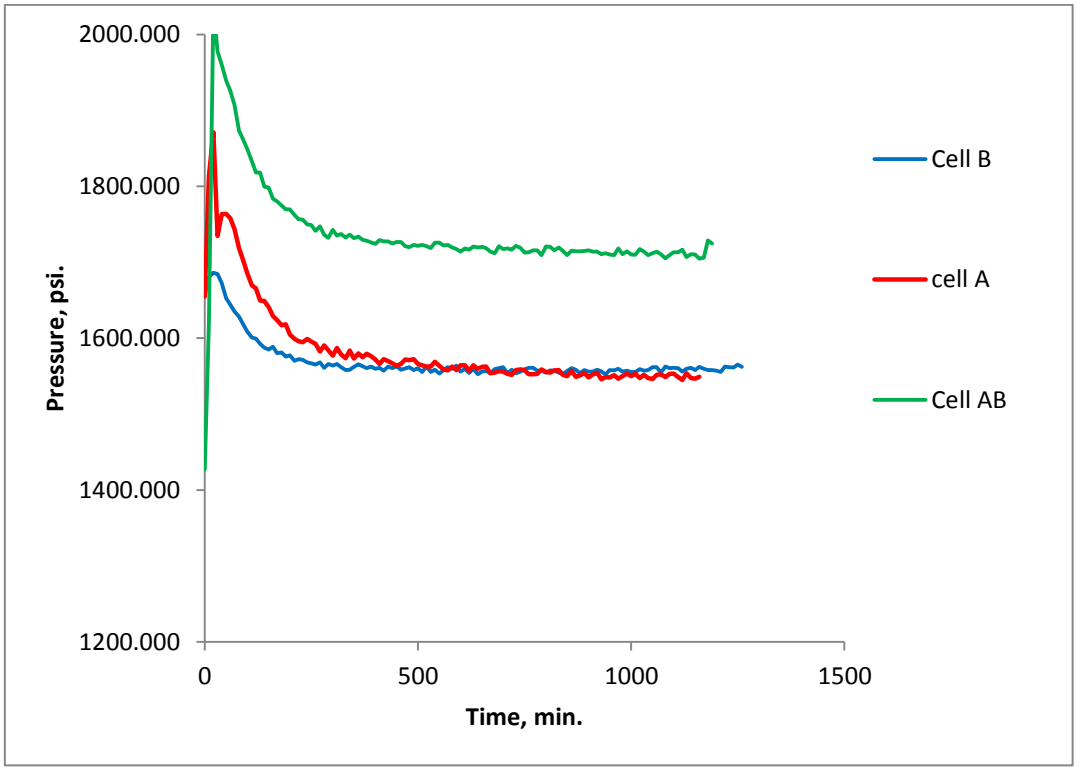

Figure 4-20 Plot of CO_2 pressure versus time in the CO_2-brine mixing chamber prior to injecting into aging cells

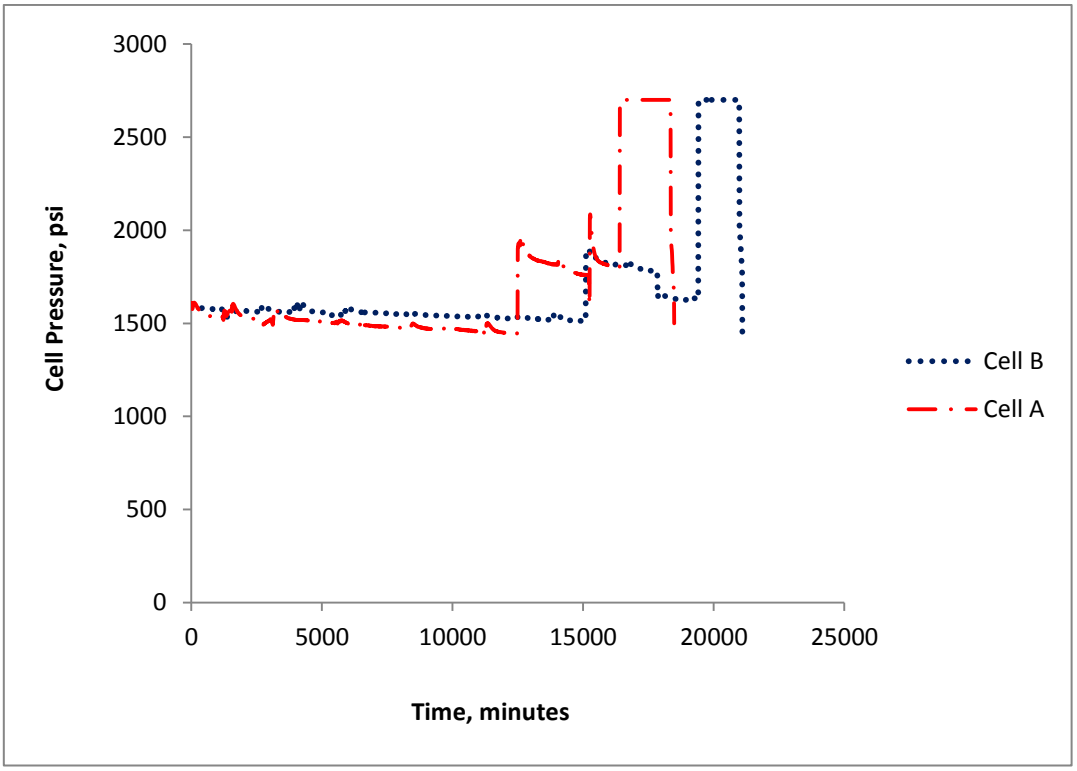

Figure 4-21 Pressure path in individual cells after injecting carbonated brine

Figure 4-22 Sample wrapped with Teflon tape

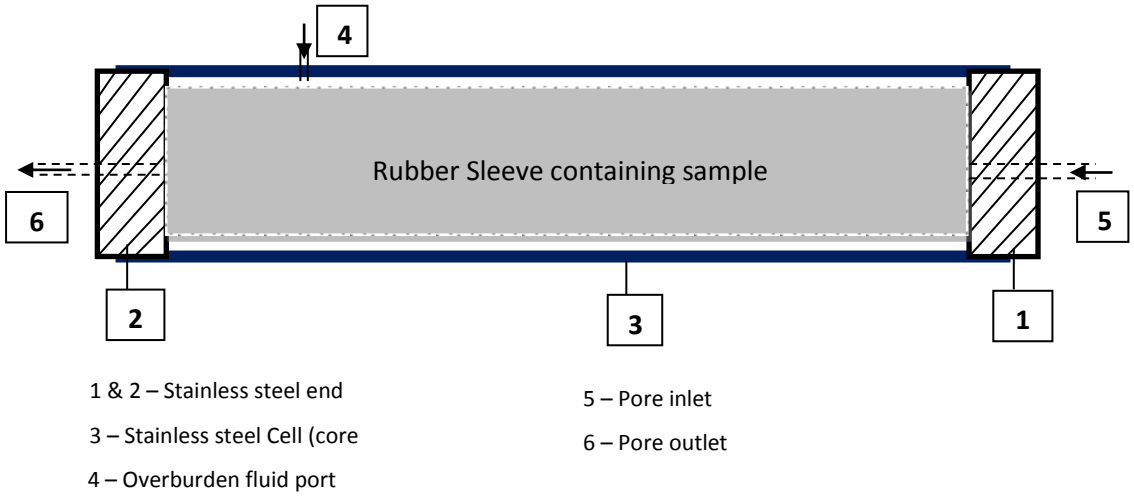

Figure 4-23 Core holder design

4.6 Determination of CO_2 Dissolution Rate in Brine

A record of change in CO_2 pressure with time in the CO_2-brine mixing cell allows for the determination of dissolution rate of CO_2 in brine at experimental temperature of 45^{o}C and

at several equilibrated pressures. The Ideal gas law is a gas law that combines Boyle's law, Charles's law, Gay-Lussac's law, and Avogadro's law. It is described mathematically as in equation 4-4 :

$$PV = uRT \qquad 4\text{-}4$$

Where,

P = gas pressure, Pascal

V = volume of gas, m^3

u = number of gas moles,

T = temperature of gas, Kelvin

R = universal or ideal gas constant which is equal to the product of the Boltzmann constant and the Avogadro constant. The value of R is 8.314 $J.K^{-1}.mol^{-1}$.

Carbon dioxide and brine were mixed in a known and constant volume of gas space above brine, and at a constant temperature of 45^{o}C. A record of changing gas pressure with time obtained from the data acquisition software means that we can calculate using the ideal gas Equation to estimate change of CO_2 moles with time - in other words the dissolution rate of CO_2 in brine. Temperature and gas volume remain constant while the amount of gas (u) changes as pressure changes with time.

4.7 Determination of Sequestered CO_2 Volume in Core Samples

CO_2 storage can be classified into the following stages: *Volumetric storage*: this is the amount of CO_2 trapped or stored in a geological pore spaces by the overlying impermeable cap rock. It is the first stage of CO_2 sequestration; *Solubility storage*: this occurs after

volumetric storage. Part of the CO_2 trapped by volumetric method begins to dissolve into pore brine until no more brine can dissolve at the equilibrated pressure and temperature. CO_2 dissolution in brine is a two way reaction. Some dissolved CO_2 will come out of saturation if pressure decreases and/or temperature increases and vice versa; *Adsorption storage* is the retention of CO_2 molecules on the surface of organic rich rocks like shale and coal; and *Mineral Storage* which is a by-product of the chemical reaction of CO_2 with rock minerals and pore brine. Mineral storage is a long term storage mechanism and depends on the reaction rates of CO_2-brine-rock system. Such reaction is complex and estimating volume of CO_2 sequestered by mineral storage mechanism is clouded by uncertainties in determining the reaction rates. CBR reaction is also a two way reaction and many factors affect the reaction rates and reaction direction.

Solubility of CO_2 in water/brine can be expressed in any of these units of CO_2 volume or mass per brine volume/brine: SCF of CO_2/bbl, lbs/bbl, SCF/Cuft., MCf/acre ft., moles/kg, and tonnes/acre ft. If CO_2 solubility in brine is known at experimental condition, we can estimate how much CO_2 was dissolved in the pore spaces of core samples using equation **4-5** or 4-6.

Sequestered volume by solubility storage:

$$Q_{CO2\ solubility.} = solubility \times \emptyset \times BV \qquad 4\text{-}5$$

$$Q_{CO2\ solubility.} = \frac{SV\ of\ CO2 \times Solubility \times \rho_{brine}}{1000} \times \emptyset \times BV \qquad 4\text{-}6$$

Where,

SV = specific volume of CO_2 in cc/moles

$Q_{CO2\ solubility}$ = number of moles of CO_2 sequestered in pore volume of core

ρ_{brine} = brine density in g/cc

Solubility is in moles of CO_2 per kg of brine i.e. mCO_2/kg

$\emptyset$ = core porosity

BV = core bulk volume

Sequestered volume by volumetric storage is given by equation 4-7 :

$$Q_{CO2\ inj.} = \rho_{CO2} \times \emptyset \times BV \qquad 4\text{-}7$$

Where

ρ_{CO2} = CO_2 density, g/cc

The volume dissolved in the pore brine (solubility storage) was estimated using CO_2 solubility models. Many solubility models are available but that developed by Duan and Sun [110] gained more industry popularity.

Duan and Sun [110, 111] developed a model for the calculation of Carbon dioxide solubility in brine containing Na^+, K^+, Ca^{2+}, Mg^{2+}, Cl^-, and SO_4 under temperature and pressure range of 273^{o}K to 533^{o}K, and 0 to 2000 bars respectively with brine molality in the range of 0 to 4.5. According to Duan et al., [111] the solubility of CO_2 in brine can be calculated using equation 4-8:

$$\ln m_{CO2} = \ln y_{CO2}\emptyset_{CO2}P - {\mu_{CO2}^{1(0)}}/{RT} - 2\zeta_{CO2-Na}(mNa + mK + 2mCa + 2mMg) - \zeta_{CO2-Na-Cl}mCl(mNa + mK + mMg + mCa) + 0.07mSO_4 \qquad 4\text{-}8$$

Where T= absolute temperature, Kelvin

P = system total pressure, bar

R = universal gas constant

M = molality of component salts in brine

yCO_2 = mole fraction of CO_2 in vapour phase

$\emptyset_{CO2}$ = fugacity coefficient of CO_2

$\mu_{CO2}^{1(0)}$ = standard chemical potential of CO2 in liquid phase

ζ_{CO2-Na} = interaction parameter between CO_2 and Na^+

$\zeta_{CO2-Na-Cl}$ = interaction parameter between CO_2, Na^+ and Cl

Fugacity coefficient $\emptyset_{CO2}$ can be calculated as a function of pressure and temperature using equation **4-9**.

$$\emptyset_{CO2} = C_1 + \left[C_2 + C_3T + \frac{C_4}{T} + \frac{C_5}{T-150}\right]P + \left[C_6 + C_7T + \frac{C_8}{T}\right]P^2 + \left[C_9 + C_{10}T + \frac{C_{11}}{T}\right]\ln P + \frac{[C_{12} + C_{13}T]}{P} + \frac{C_{14}}{T} + C_{15}T^2 \quad 4\text{-}9$$

Where $C_1 – C_{15}$ are parametric constants whose values for the pressure and temperature range are presented by Duan et al. [111].

The Duan and Sun CO_2 solubility model (Equation 4-8) was used to compute solubility at different pressures at constant temperature of 45^{o}C and constant brine salinity of 5.8% weight for various experimental pressures (Figure 4-24 and Table 4-3). CO_2 density as a function of pressure was also calculated for various experimental pressures (Figure 4-25).

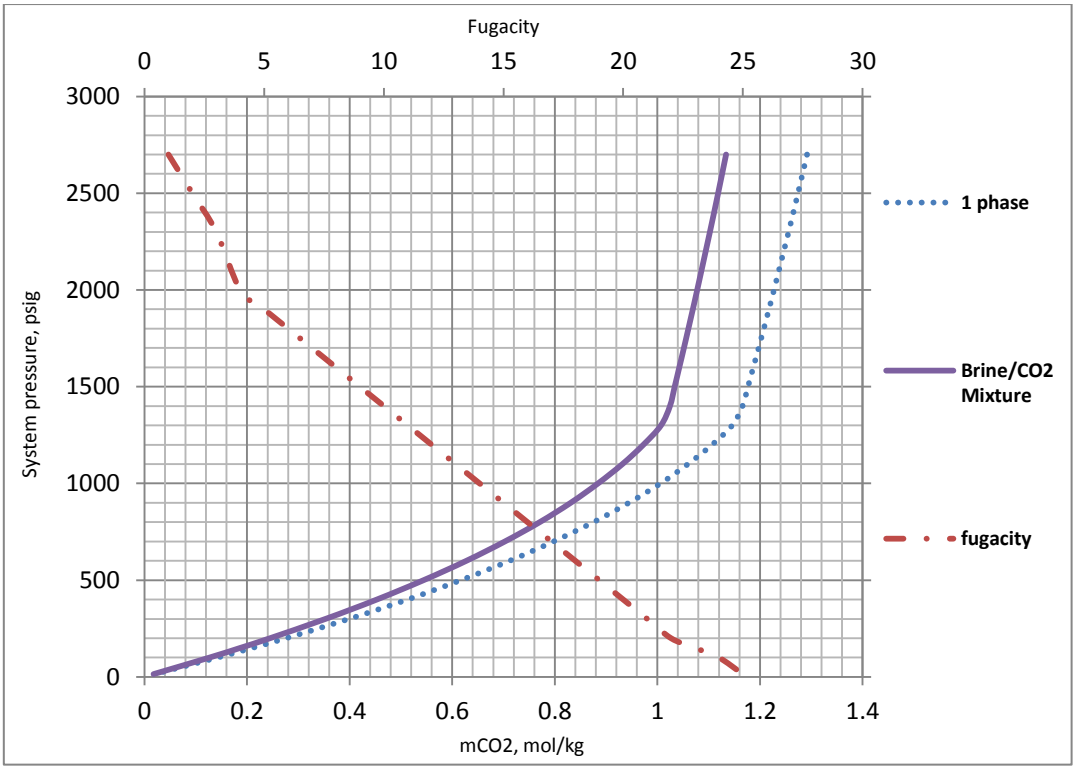

Figure 4-24 Fugacity of CO_2 and solubility of CO_2 & CO_2/Brine mixture at different stages of CO_2 storage

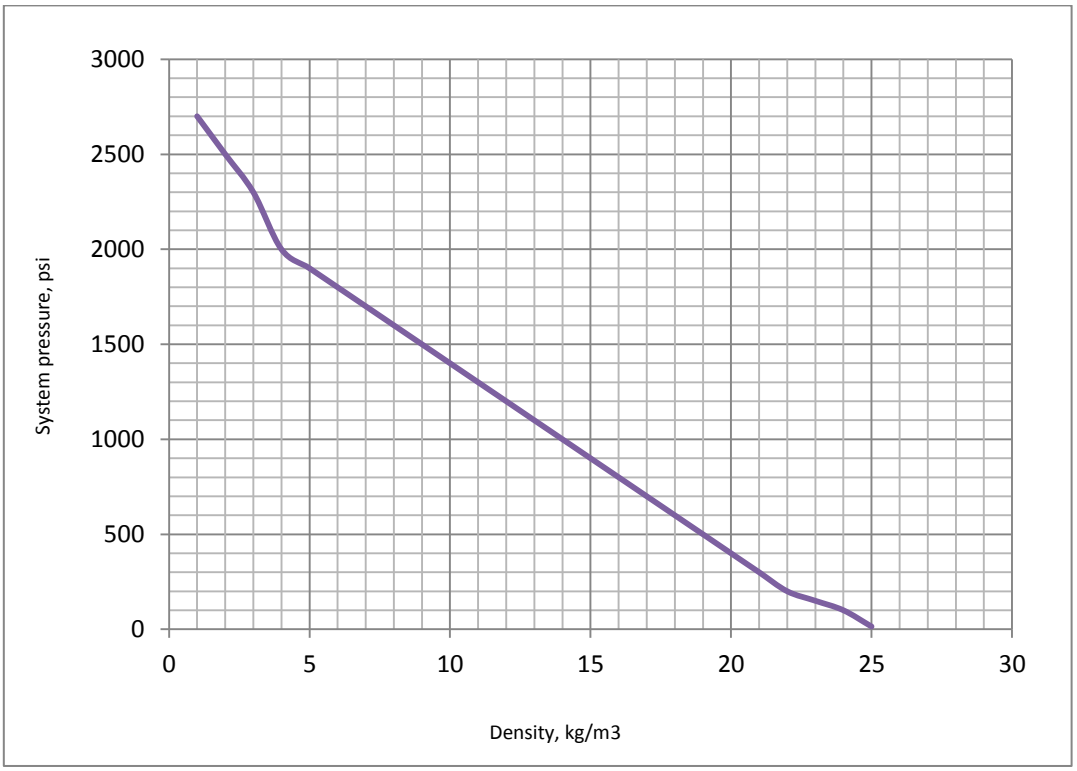

Figure 4-25 Density of CO_2 at different stages of CO_2 storage pressure

Table 4-3 Thermodynamic properties of CO_2 and CO_2-Brine mixture at different stages of CO_2 storage

Temp. 318.15 k		Thermodynamics of CO2 single phase					Brine-CO2 mixture		
Pressure		Solubility mCO2	Density	Specific vol.	Compressi-bility factor	Fugacity Coefficient	Phase Composition		
							mH20	mCO2	mNaCl
(bar)	(psi)	mol/kg	kg/m3	cc/mol			mol/kg	mol/kg	mol/kg
186.2	2700	1.2918	797.08	55.21	0.3887	0.4	55.51	1.1339	0.6844
172.4	2500	1.2741	779.52	56.46	0.3680	0.4196	55.51	1.1184	0.6844
158.6	2300	1.2558	758.95	57.98	0.3477	0.4427	55.51	1.1024	0.6844
137.9	2000	1.2273	719.16	61.20	0.3190	0.4860	55.51	1.0776	0.6844
131	1900	1.2175	701.91	62.70	0.3105	0.5034	55.51	1.0691	0.6844
124.1	1800	1.2075	681.06	64.62	0.3032	0.5227	55.51	1.0604	0.6844
117.2	1700	1.1974	655.48	67.14	0.2976	0.5439	55.51	1.0517	0.6844
110.3	1600	1.187	620.15	70.97	0.2959	0.5677	55.51	1.0427	0.6844
103.4	1500	1.1766	563.65	78.08	0.3054	0.5938	55.51	1.0337	0.6844
96.55	1400	1.166	444.95	98.91	0.3612	0.6219	55.51	1.0245	0.6844
89.66	1300	1.1458	325.74	135.11	0.4579	0.6498	55.51	1.007	0.6844
82.76	1200	1.1065	259.68	169.48	0.5305	0.6763	55.51	0.9727	0.6844
75.86	1100	1.0596	213.99	205.66	0.5898	0.7028	55.51	0.9318	0.6844
68.97	1000	1.0061	179.05	245.80	0.6411	0.7288	55.51	0.8842	0.6844
62.07	900	0.9444	150.08	293.24	0.6881	0.7551	55.51	0.831	0.6844
55.17	800	0.8754	125.71	350.08	0.7305	0.7812	55.51	0.7707	0.6844
48.28	700	0.7976	104.25	422.18	0.7705	0.8077	55.51	0.7026	0.6844
41.38	600	0.7119	85.26	516.19	0.8079	0.8342	55.51	0.6275	0.6844
34.48	500	0.6168	68.02	647.03	0.8435	0.8612	55.51	0.5441	0.6844
27.59	400	0.513	52.35	840.73	0.8772	0.8882	55.51	0.453	0.6844
20.69	300	0.3993	37.84	1162.94	0.9096	0.9157	55.51	0.3531	0.6844
13.79	200	0.276	24.40	1803.46	0.9408	0.9434	55.51	0.2446	0.6844
10.34	150	0.2104	18.00	2444.33	0.9559	0.9575	55.51	0.1867	0.6844
6.897	100	0.1423	11.82	3722.01	0.9709	0.9715	55.51	0.1266	0.6844
1	14.5	0.0196	1.67	26342.71	0.9959	0.9959	55.51	0.0176	0.6844

4.8 Experiment Setup for Resistivity Index Measurements

Samples were removed from batch system after CO_2 storage and then brine samples were collected from each sample for post storage analysis after which the samples were cleaned with methanol in solvent reflux method. Cleaned and dried samples were then saturated again with the same brine and subsequently loaded in a resistivity cell for 4-pole resistivity measurements (Figure 4-26). Nitrogen was used as the displacing fluid using porous plate method. Measurements were done at 45^{o}C, overburden pressure of 2000 psig and frequency of 1 kHz. A water wet ceramic porous plate with 54 bar entry pressure was used to allow desaturation to low water saturation. Desaturation pressure was applied to the test samples in pressure steps. A nitrogen pressure regulator was used to set the desired pressure step. Porous plate desaturation technique was used because of its advantages over other desaturation methods such as: no grain loss during desaturation, elimination of saturation gradient after core saturation is at equilibrium at each capillary pressure, and

eliminated capillary end effect. Few cellulose filters were placed between the core and the porous plates to ensure capillary continuity between the two. An air driven pressure pump was used to pump the overburden fluid into the test cell. A pressure regulator was used to adjust the air supply to the pump. Two pressure sources were used to supply pore pressure. One is a nitrogen cylinder connected to a pressure regulator for air-brine system and the other is a syringe pump that drives the oil for oil brine system.

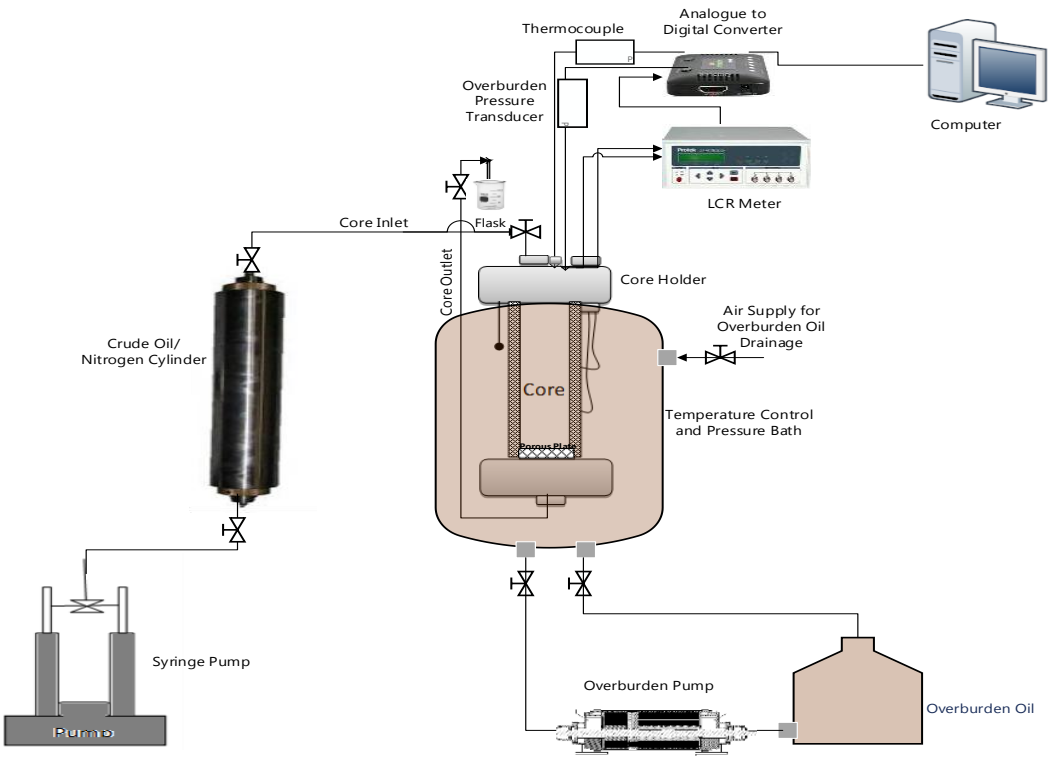

Figure 4-26 Resistivity Measurement Set up

The assembled core holder with the core is loaded into the temperature control bath (Figure 4-26) after which the annulus is filled with the overburden fluid at a pressure of 500 psig sufficient to hold tight the sleeve around the core. Brine was continuously circulated at a very low flow rate through the core from the inlet tubing through the core and collected from the outlet tubing in a flask. This is to expel any trapped air in the core. The circulation was allowed to proceed overnight after which circulation was stopped and the heater was turned

on to heat up the test cell to 45^{o}C. While heating up the overburden fluid, the inlet and outlet valves of the test cell were opened to allow for oil expansion. When temperature equilibrium was attained in the test cell, the overburden pressure was increased to 2000 psig and the cell valves closed. The dead volume of brine collected in the burette attached to the core outlet is recorded. The burette has a resolution of 0.01cc. A sufficient amount of time was allowed for collecting dead volume. Next was the measurement of core resistivity at 100% saturation using the data acquisition system. At each measurement point, the core resistivity values, temperature, pore pressure, overburden pressure, produced brine volume, and time of measurement are all recorded. Desaturation pressure was applied to the test samples in pressure steps. Pressure steps of 1, 2, 4, 7, 10, 20, 40, 60, 100,140, and 200 psig were adopted for the air brine system. Figure 4-27 shows typical measurements at every pressure increment. A nitrogen pressure regulator was used to set the desired pressure step. At each pressure step, the pressure in the test cell was kept constant while pore fluid was being expelled at this constant pressure. During this period, measurements were logged after every 5 hours or as necessary. Pressure was increased to the next pressure step after attaining equilibrium in resistivity and when no more fluid is expelled from the core. Again sufficient time was allowed to elapse to be sure that no more fluid is expelled. At the end of desaturation, measurement data for all the cores were available in a spread sheet for analysis. The desaturation pressure in the core was then bled off through the drain valves. The heater was also turned off and the test cell allowed to cool before draining the overburden fluid back to the reservoir. Finally, the core holder was unloaded and the core removed for further cleaning and further analysis.

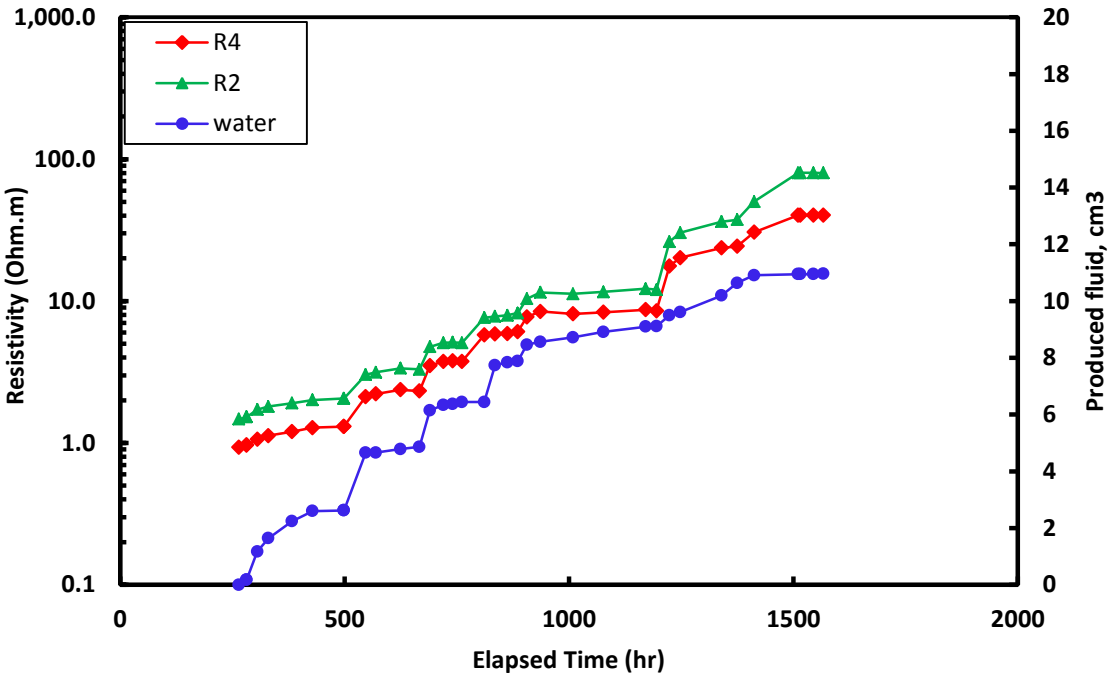

Figure 4-27 Pressure steps during a typical resistivity index experiments

4.9 Results and Discussions

Figure 4-28 and Figure 4-29 compares the pore geometry of identical samples in group 1 prior to CO_2 storage and after CO_2 storage. Prior to storage, NMR (Figure 4-12) and MICP (Figure 4-13) curves of all samples overlap meaning that the pore systems are identical. After CO_2 storage, the NMR curves (Figure 4-29) can be seen separating; an indication of altered pore geometry and redistribution of pore sizes of each core making each core different from the other in a degree dictated by the extent of CBRI in each rock sample. Sample S-1 in the group was not subjected to CBRI and served as the base line prior to and after CO_2 storage for which other samples are compared. The same phenomenon is expected to occur in resistivity index curves for the same samples since resistivity is a very strong function of pore geometry. A closer examination of the effect of CO_2 storage on the rocks' pore structure will be discussed in the next chapter (chapter 5).

The non-power law behaviour of the resistivity plots for all samples as opposed to the power law behaviour in Archie's rocks is due to the presence of micro pores in the study samples- a typical behaviour of carbonate rocks generally known as non-Archie rocks. The water filled micro pores in the samples tend to serve as secondary current path at lower brine saturation resulting in resistivity lower than what is commensurate for a given low brine saturation if the pores were purely macro pores resulting in bending down of the I_R curve (lower saturation exponent, n) at low brine saturation. This means that the observed resistivity index curve cannot be described by Archie's law at low saturation values. Fleury's double porosity conductivity (DPC) model [68] was found to best fit the measured resistivity index for the samples' data set. The DPC model considers the two pore networks to act electrically parallel such that the resistivity index – S_w curve can be fitted with the DPC model derived as follows

Considering,

$$Sw = f_1 S_{w1} + f_2 S_{w2}, \qquad where\ f_1 + f_2 = 1$$

S_{w1}, S_{w2}, f_1, and f_2 are the water saturation and pore volume fraction of macro and micro pores respectively,

$$S_{w1} = \frac{S_w + f_1 - 1}{f_1} S_{w2} = 1, for\ S_{w1} \geq S_c \qquad 4\text{-}10$$

$$S_{w1} = \frac{f_1 + S_c - 1}{f_1 S_c} S_{w2}\ , S_{w2} = \frac{S_w}{S_c}, \text{ for } S_{w1} \geq S_c \qquad 4\text{-}11$$

The conductivity of a rock at 100% brine saturation is the sum of the conductivity of each pore network

$$C_t = C_1 + C_2 = C_1(1+\propto) \text{ where } \propto = \frac{C_2}{C_1}$$

From Archie's law,

$C_t = S_{w1}^{-n1} C_1 + S_{w2}^{-n2} C_2$ at low brine saturation, i.e. $Sw \leq Sc$ 4-12

Introducing α into equation **4-12**, resistivity index at low saturation can be estimated as follows:

$$I_R = \frac{C_t}{C_0} = S_{w1}^{-n1} * \frac{1+\propto}{1+\propto * \frac{S_{w1}^{-n1}}{S_{w2}^{-n2}}} \quad 4\text{-}13$$

For high water saturation, pore network 1(macro pores) dominates such that $S_{w2} = 1$, hence, resistivity index can be estimated as;

$$I_R = S_{w1}^{-n1} * \frac{1+\propto}{1+\propto * S_{w1}^{-n1}} \quad 4\text{-}14$$

Applying equations **4-13** and **4-14** to the entire range of saturation such that one equation can be used to model the type of resistivity index curve observed in this study, the following is noted:

$$S_{w2}^{n2} S_{w1}^{-n1} \approx S_c^{-n2} S_w^{n2-n1} \approx S_w^{n2-n1} \quad 4\text{-}15$$

Where, $S_{w1} \cong S_w$ and $S_c^{-n2} \approx 1$

Hence,

$$I_R = S_w^{-n1} * \frac{1+\propto}{1+\propto * S_w^{n2-n1}} \quad 4\text{-}16$$

Where $\propto$ is the conductivity ratio of the two pore networks 100% brine saturation, n_1 is the saturation exponent of pore network 1 (macro pores), and n_2 is the saturation exponent of pore network 2 (micro pores).

When the resistivity index plots were fitted with Eq. **4-16**, the resistivity index plots were seen to differ significantly for all samples. Figure 4-30 and Figure 4-31 show the resistivity index curves for all samples in group 1. It can be seen

that resistivity index vary for all the samples and all have slopes higher than the base plot (sample S-1). The resistivity index plots for two other samples in group 2 are shown in Figure 4-32. In these samples, crude oil was used as the displacing fluid instead of air for the purpose of resistivity index measurements during CO_2-EOR experiments to be discussed in chapter 6. The pore structure of these samples (S-6 and S-7) was shown in Figure 4-14 and Figure 4-15. It is seen that both samples are identical and it is also expected that the resistivity index plots for both samples should be identical to the extent of the similarity in their pore structure as seen in Figure 4-31 and Figure 4-32. The reference sample, S-1 has the lowest saturation exponent and thus lies at the bottom of the graph while other samples lie above it. Samples S3 and S5 stored CO_2 in a carbonated water form (for 4 and 5 months respectively) while S2 and S4 stored CO_2 in their pore space as a supercritical CO_2 dissolved in water (for 2 and 3 months respectively). Table 4-4 lists the saturation exponents for the storage samples and the reference sample. The saturation exponents of the storage samples can be observed to have increased. Most significant increase were observed in samples in which CO_2 was stored as carbonated brine which means that such method was more effective for storage and rock fluid interaction. The resulting increase in saturation exponent can be ascribed to pore geometrical alteration caused by CBRI. An explanation of why CBRI increased the saturation exponent or the resistivity index slope above the reference sample is necessary. We have tried to explain this phenomenon using post storage pore structure data obtained from MICP, NMR, porosity, and permeability. It was observed from NMR that the pore sizes (porosity) increased while MICP showed decrease in pore throats (permeability). Table 4-5 summarizes the porosity and permeability at pre- and post-CO_2 storage condition for storage samples. A redistribution of pore/pore throat sizes can also be seen from both NMR and MICP plots after CO_2 storage (Figure 5-2 to Figure 5-9 discussed in the next chapter). This was caused by the creation of new pores (micro) due to partial dissolution of

soluble grains and the expansion of some micro pores (to form macro pores), and also by the closure of some small pores and pore throats by precipitates generated according to equations **2-10** to **2-15** discussed earlier. Similar observations were reported in the literature [73-76]. Since precipitates constricted pore throats and also since there is a redistribution of pore sizes and geometry, an increased tortuosity can be said to have occurred in the storage rock samples which resulted in higher saturation exponents reported in Figure 4-30 and Figure 4-31. Saturation exponent have been shown to be directly related to tortuosity in partially saturated rocks. Winn [48] and Amyx [112] defined resistivity index as

$$I_R = \frac{R_t}{R_o} = \frac{L_{w2}}{L_{w1}} \frac{1}{S_w}$$

Where, L_{w1} = total length of water volume that carries the current at 100% water saturation. L_{w2} = total length of water carrying electric current at partial water saturation.

When water saturation is equal to 1.0, L_{w2} equals L_{w1}, and I_R= 1.0. At partial water saturation, R_t increases because L_{w2} increases and that results in higher resistivity index. L_{w1} and L_{w2} are non-measurable quantities and as such researchers reported resistivity of rock as a function of water saturation [24]. Archie [113] then suggested that the resistivity index - water saturation relation can best be fit by the equation

$$I_R = \frac{1}{S_w^n}$$

Where the variable 'n' was introduced as a saturation exponent. The quantity $\frac{L_{w2}}{L_{w1}}$ has been replaced by the exponent, 'n' which can be said to give indication of rock tortuosity at partial brine saturations. With this in mind, the observed increase in saturation exponent observed in Figure 4-30 and Figure 4-31 can be said to be as a result of increased tortuosity which was also caused by pore throats constrictions as evident by the decrease in

permeability of storage samples. It was also observed that the increase in saturation exponents or the extent of departure of the resistivity index plot from the reference sample plot (Figure 4-30 and Figure 4-31) is a function of storage time. This was generally observed in the macro pores (n_1) while the micro pores (n_2) did not show clear relation with storage time (as seen in Table 4-4). However, saturation exponents were also seen to increase compared to the reference samples.

The resistivity index (measured data) for sample S-6 and S-7 in which CO_2 was not stored (group 2) can be seen to be very close (Figure 4-32). The modelled data show slight differences because of the difference in the end saturation (0.3 and 0.45 respectively) while the measured data could be seen overlapping at the same saturation level until 0.3. The difference in end saturation is due to failure of the porous plates during the S-6 experiment at 0.3 water saturation. Although, these samples were drained with crude oil, they are presented here to show that similarity is expected in the resistivity index plots of samples with similar pore character (Figure 4-14 and Figure 4-15).

XRF analysis carried out on precipitates seen at the bottom of brine samples produced from core samples after storage (Figure 4-33) revealed that calcium carbonates dissolved in solution during storage period. This further confirms the shift seen in the NMR T_2 distribution in Figure 4-29. NMR porosity measurements on storage samples also showed increase in porosity while MICP (Thomeer) permeability showed significant decrease in permeability Table 4-5. Detailed pre- and post- CO_2 storage NMR and MICP analyses are discussed in the next chapter (93). Saturation exponent can be plotted as a function of storage time as shown in Figure 4-34 . If sufficient data points are available, an appropriate empirical model can be developed that relates saturation exponent to time such that the saturation

exponent at any time during CO_2 storage can be estimated and used to quantify the amount of CO_2/S_w present at that point in time.

4.10 Effect of CO_2 Sequestration on cementation factor

Assuming 'a' is 1, the cementation factor was calculated using Eq. **1-2** and **1-3**.

Table **4-6** summarizes the cementation factors, 'm' for CO_2 storage samples. Sample S-1 was not treated with CO_2. It only served as a reference sample in the group. It can be seen that the cementation factor reduced slightly in all the storage samples.

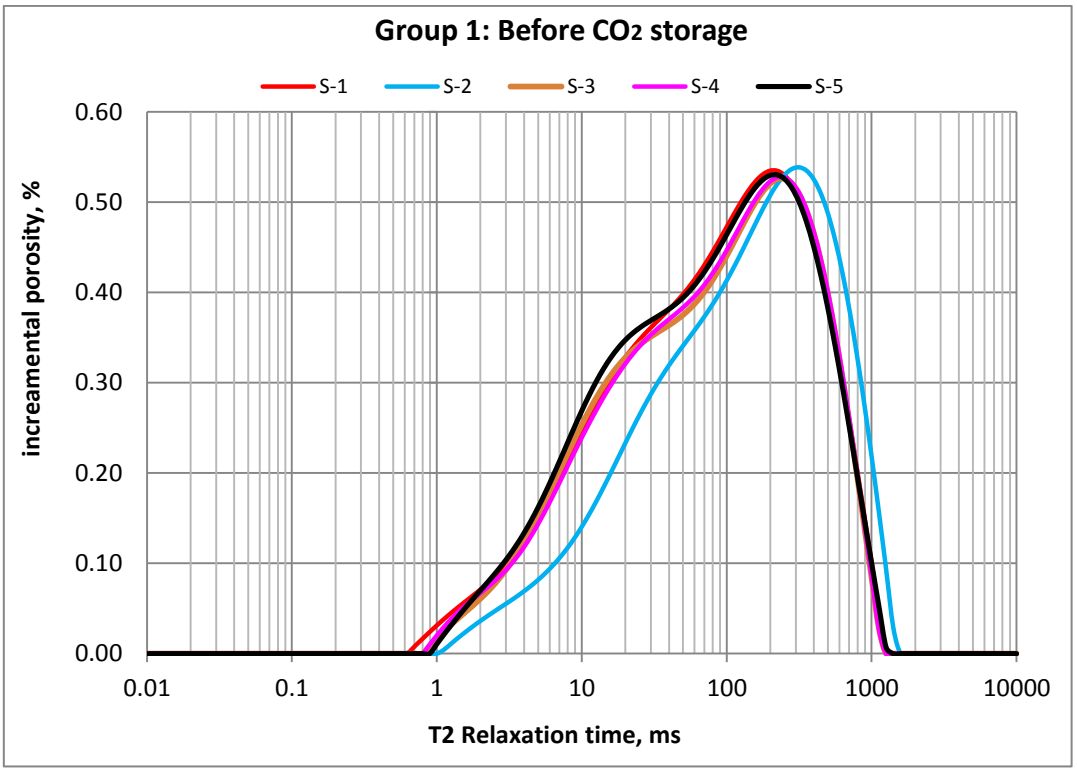

Figure 4-28 Pore size distribution of group 1samples before CO_2 storage. NMR T2 relaxometry performed on core samples

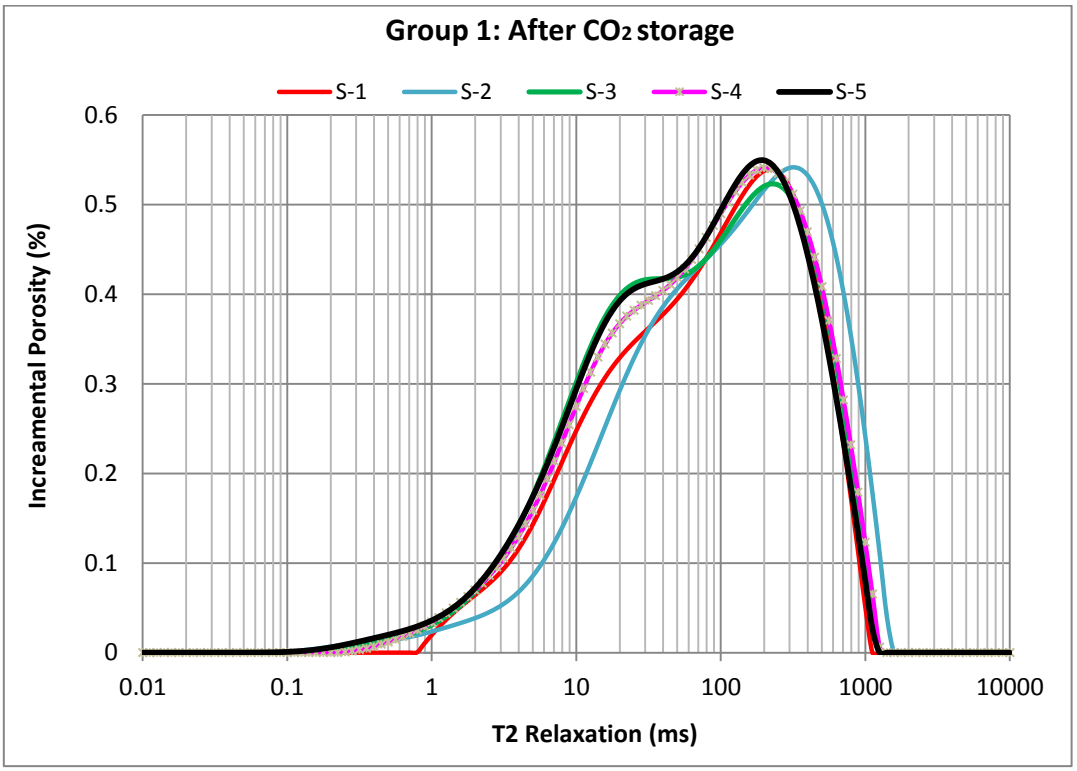

Figure 4-29 Pore size distribution of group 1 samples after CO_2 storage. NMR T2 relaxometry performed on core samples

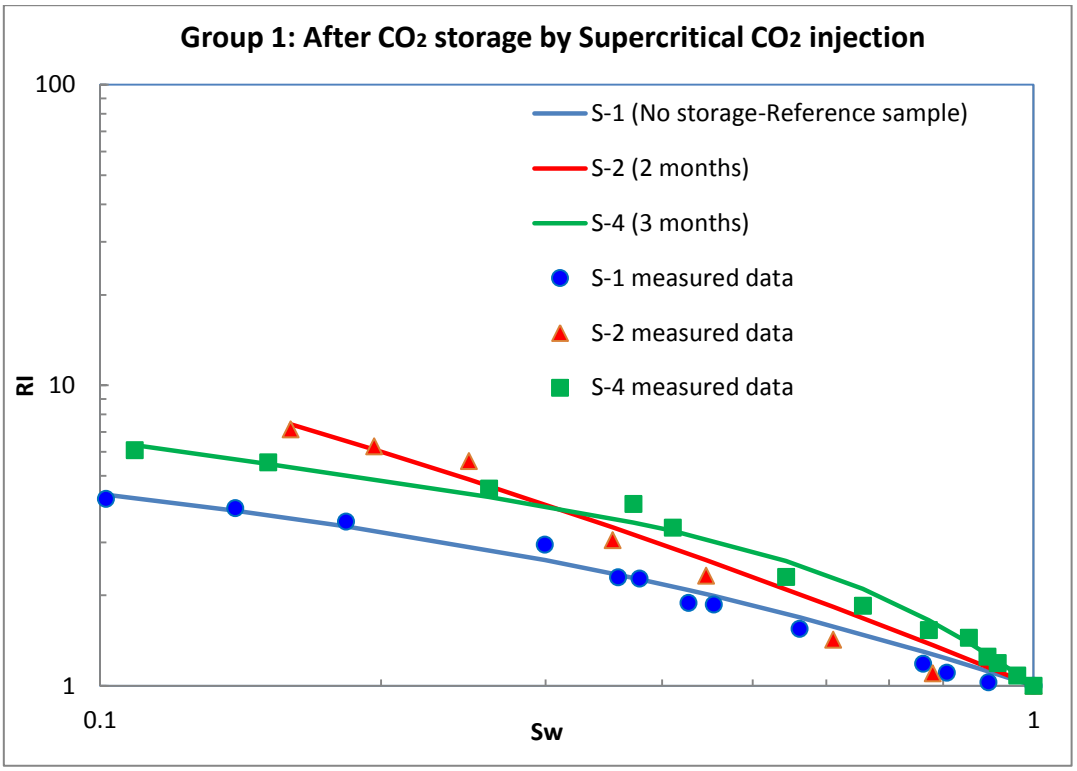

Figure 4-30 Resistivity index - S_w plots for group 1 samples (CO_2 storage by supercritical CO_2 injection)

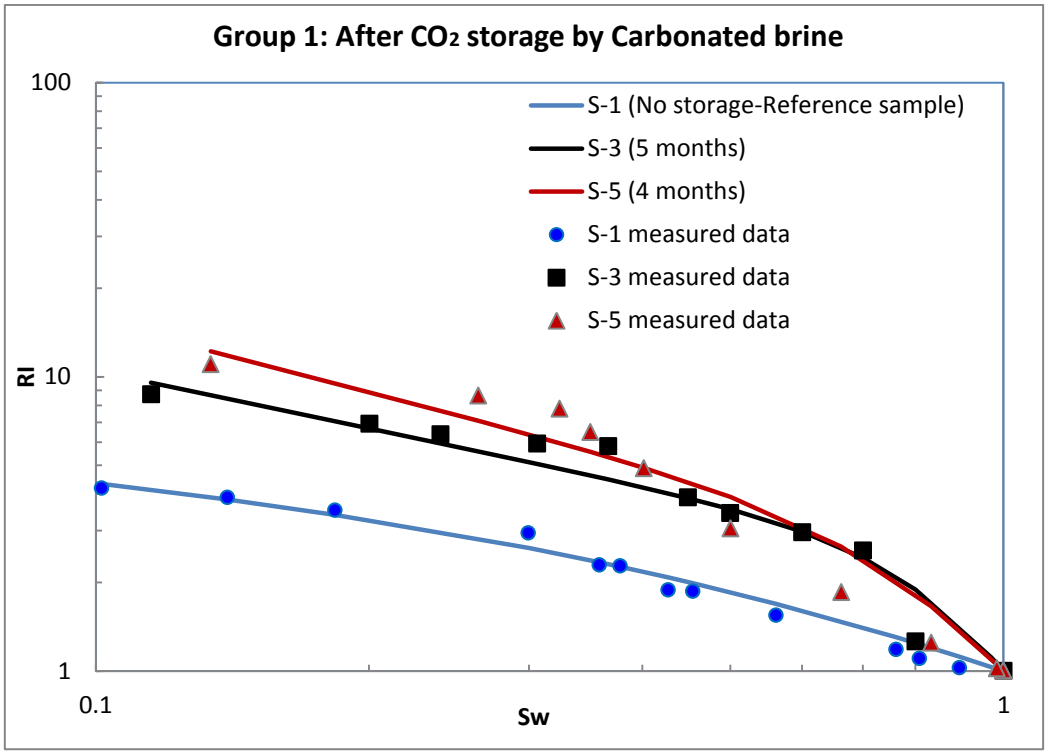

Figure 4-31 Resistivity index - S_w plots for group 1 samples (CO_2 storage by carbonated brine)

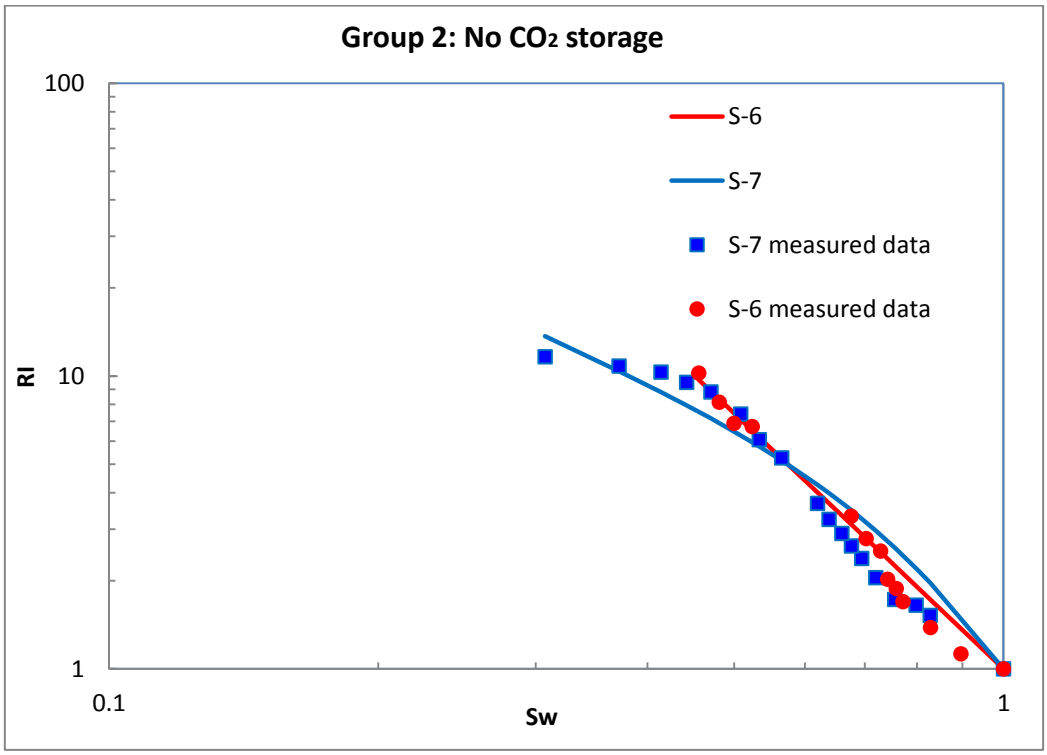

Figure 4-32 Resistivity index - S_w plots for group 2 samples (No CO_2 storage)

Table 4-4 Saturation exponents for group 1 samples

	n1	n2	α
No Storage			
S-1	1.46	0.25	0.58
Post storage			
S-2	1.65	0.73	0.68
S-3	5.68	0.65	0.73
S-4	3.51	0.43	0.69
S-5	4.66	0.79	0.67

Table 4-5 Porosity and permeability at pre and post storage conditions

	Pre-Storage		Post-Storage	
	K (mD)	ϕ (%)	K (mD)	ϕ (%)
S-1	320	18.13		
S-2	346	16.50	133	18.39
S-3	310	17.69	145	19.47
S-4	459	17.69	138	19.35
S-5	325	18.30	141	19.56

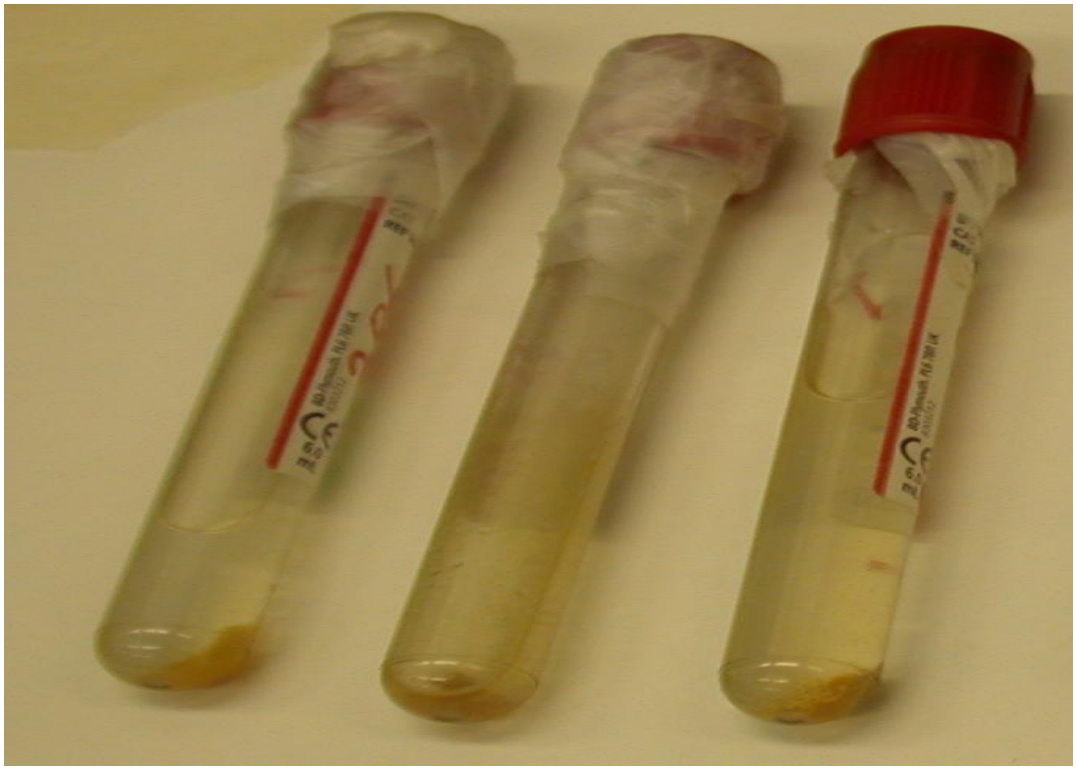

Figure 4-33 Precipitates seen at the bottom of brine collected from some samples after CO_2 storage

Table 4-6 Cementation factor for storage samples*.

	S-1	S-2	S-3	S-4	S-5
ω_1	0.183	0.165	0.177	0.177	0.183
ω_2		0.184	0.195	0.193	0.196
m_1	1.444	1.498	1.532	1.319	1.367
m_2		1.381	1.393	1.295	1.340

*Subscript 1 and 2 represent before and after storage

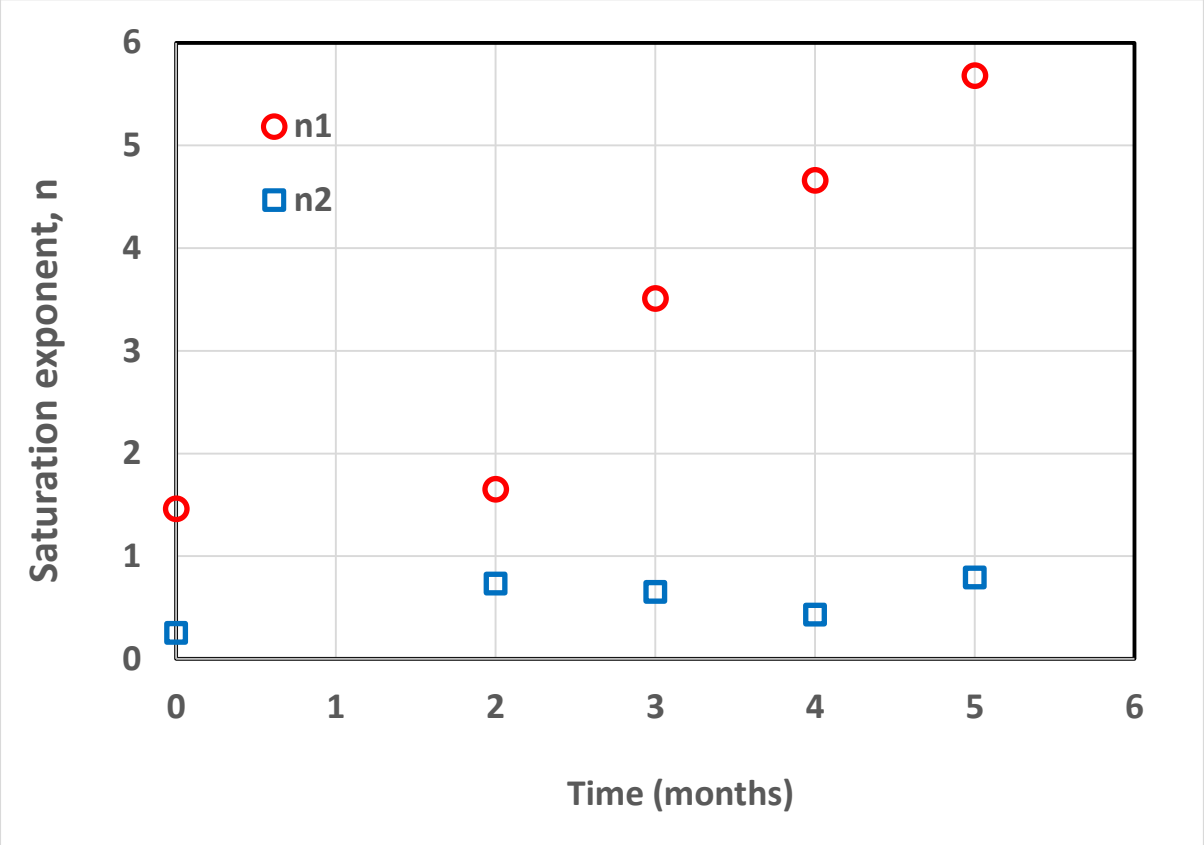

Figure 4-34 Saturation exponent as a function of storage time

CHAPTER 5

NMR and MICP SPECTROSCOPIC STUDY OF CARBONATE PORE STRUCTURE AFTER LABORATORY CO_2 STORAGE

In this chapter, the effect of CBRI on the pore geometry of storage rocks is investigated using NMR and MICP techniques.

5.1 Nuclear magnetic resonance (NMR)

Nuclear magnetic resonance (NMR) spectroscopy measures the relaxation time of hydrogen molecules in a rock pore after they have been excited by magnetic pulse. An electromagnetic pulse is turned on and off in a systematic fashion to excite the hydrogen molecules. When the pulse is turned off, hydrogen molecules relax back to their previous positions. The resulting signal generated by the relaxing molecules in a single pore is called spin-echo which the NMR equipment measures. The NMR signal (M) obeys the exponential decay described by equation 5-1 [114]. NMR signal is a function of time, M (t). A_o is the amplitude of initial signal, while T_2 is the decay time.

$$M\ (t) = A_o e^{\frac{1}{T_2}} \qquad 5\text{-}1$$

T_2 comprises of several components (Eq. 5-2) namely bulk relaxation (T_{2bulk}), molecules diffusion in gradient (T_{2DG}), and surface relaxation (T_{2s}). T_2 measurements reveal pore sizes and their population.

$$\frac{1}{T_2} = \frac{1}{\mathrm{T_{2bulk}}} + \frac{1}{\mathrm{T_{2DG}}} + \frac{1}{\mathrm{T_{2s}}} \qquad 5\text{-}2$$

In laboratory experiments, the effect of diffusion gradient and bulk relaxation is negligible; hence T_2 in equation **5-1** becomes surface relaxation (T_{2s}). T_{2s} is a measure of the time it takes for molecules to relax on the wall of the pores. The smaller the distance between the pore wall and the hydrogen molecules the faster the relaxation time, and vice versa. T_{2s} is thus related to pore radius according to Equation **5-3**

$$\frac{1}{\mathrm{T}_{2s}} = \rho\frac{s}{v} = \rho\frac{3}{r} \qquad 5\text{-}3$$

The term s/v is the surface to volume ratio which is also related to the effective pore radius (Equation 5-3) and ρ is surface relaxivity. In a multimodal pore system where different pore types exist, different NMR signal decay exponents exist for each pore type. Figure 5-1 [114] shows a typical NMR signal versus time and the associated T_2 distribution for hydrogen molecules in a heterogeneous formation having micro, meso, and macro pore systems. Micro pores have the smallest volumes and thus the shortest T_2. Meso pores are next followed by macro pores which have the longest T_2. These pore size distributions are thus distinct on the T_2 relaxation spectroscopy.

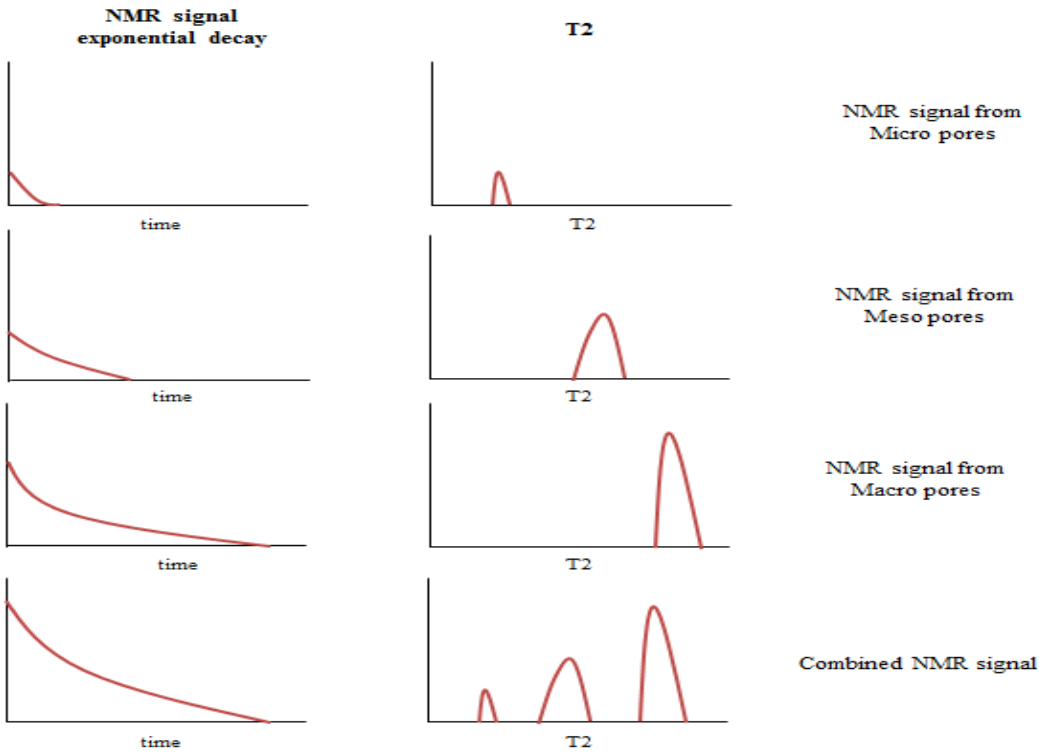

Figure 5-1 Typical NMR T2 distribution for a heterogeneous pore system (modified from [114])

5.2 Mercury Injection Capillary Pressure (MICP)

MICP test was conducted on the sample using the Micrometrics Auto Pore IV 9500 Series (Figure 4-7). Mercury was injected into the sample at an incremental pressure of 1.5 psi using nitrogen gas as the displacing medium to complete the low pressure stage at 30 psi. The injection pressure was released to the atmosphere and the penetrometer removed and weighed with the sample and mercury in place to determine the assembly weight and sample bulk volume. The sample was then loaded into the high-pressure chamber for the high pressure stage terminating at 60,000 psig injection pressure. The injection pressure was relieved and the penetrometer removed completing the test.

5.3 Results and Discussions

The effect of dissolution of rock grains caused by CO_2 in formation brine was investigated using NMR and MICP. It was observed from both NMR (Figure 5-2 through Figure 5-5) and MICP (Figure 5-6 through Figure 5-9) that there is a redistribution of pores and pore sizes for all samples after CO_2 storage. This was caused by the creation of new pores (micro) due to partial dissolution of soluble grains and the expansion of some micro pores (to form macro pores), and also by the closure of some small pores and pore throats by precipitates generated according to equations **2-10** to **2-15** discussed earlier. The redistribution resulted in increased porosity and decreased permeability in all the storage samples (Table 4-5). This is in accordance with other published works in the literature [73-76]. X-ray fluorescence spectroscopy (Figure 5-10) was used to characterize the precipitates deposited at the bottom of brine effluents collected after storage (Figure 4-33). Analysis of the brine effluents also showed change in brine composition (Table 5-1). It can be concluded from the discussed results that dissolution of rock matrix occurred since precipitates of carbonate minerals and change in brine chemistry are the evidence of rock dissolution [64] and also that pore structure and pore geometry changed as indicated by NMR and MICP results.

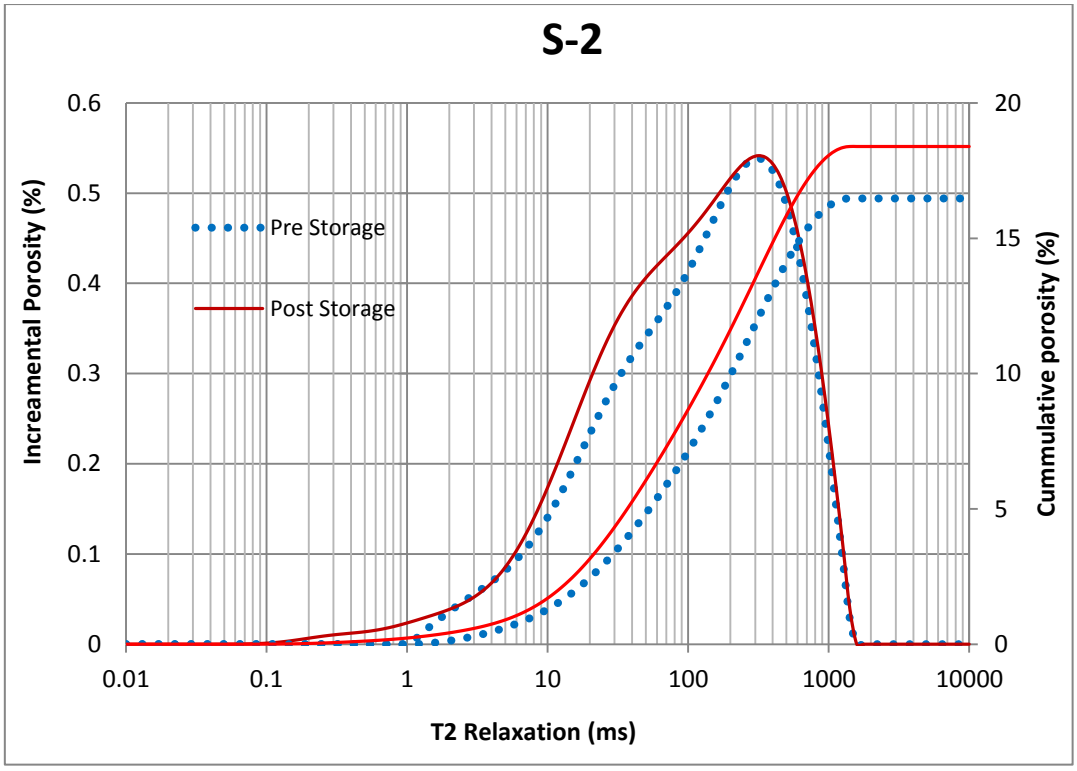

Figure 5-2 NMR porosity showing increase in porosity after CO2 storage in sample S-2

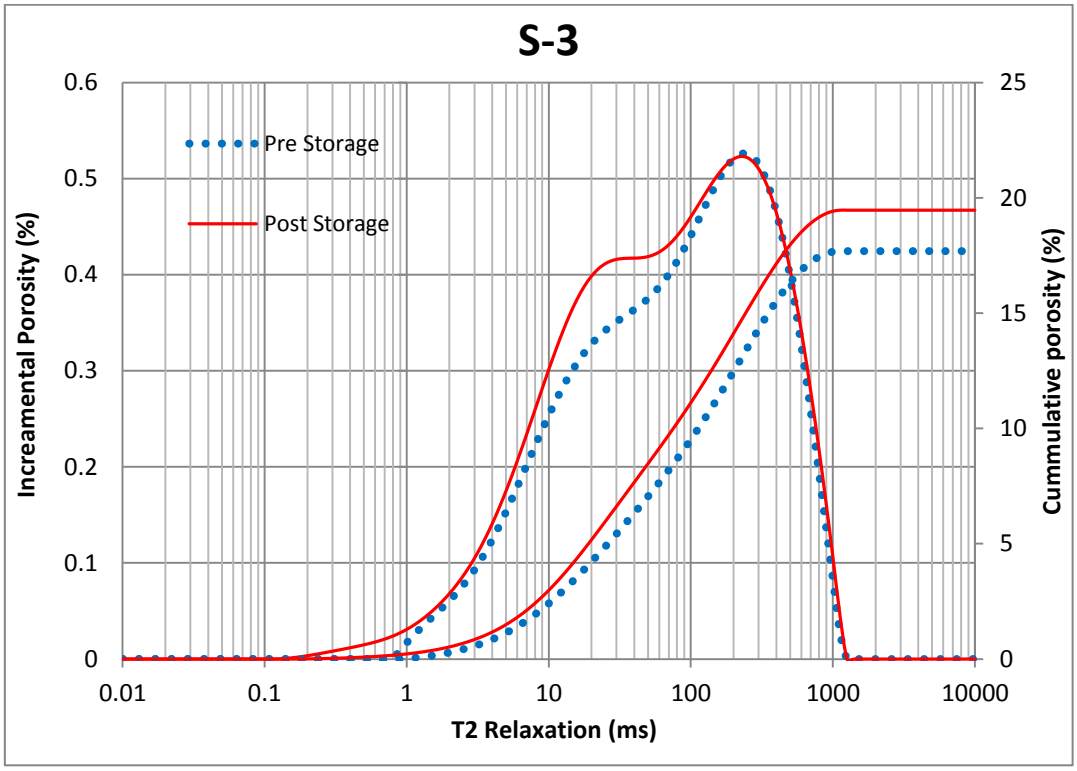

Figure 5-3 NMR porosity showing increase in porosity after CO2 storage in sample S-3

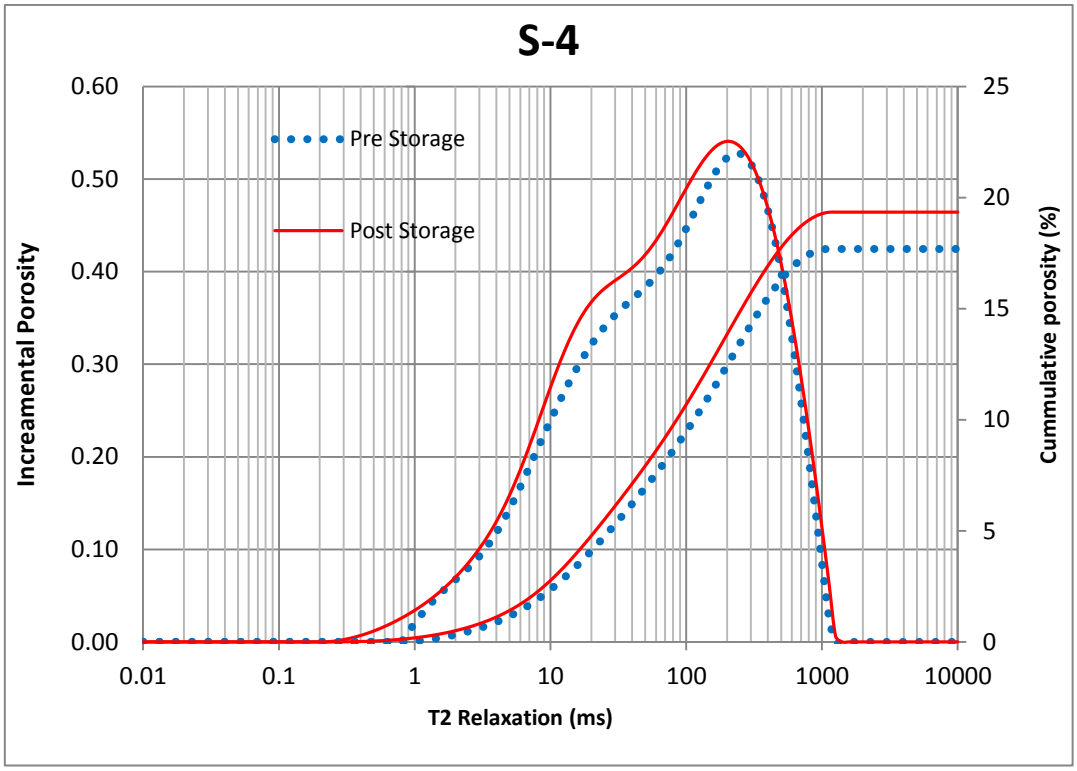

Figure 5-4 NMR porosity showing increase in porosity after CO2 storage in sample S-4

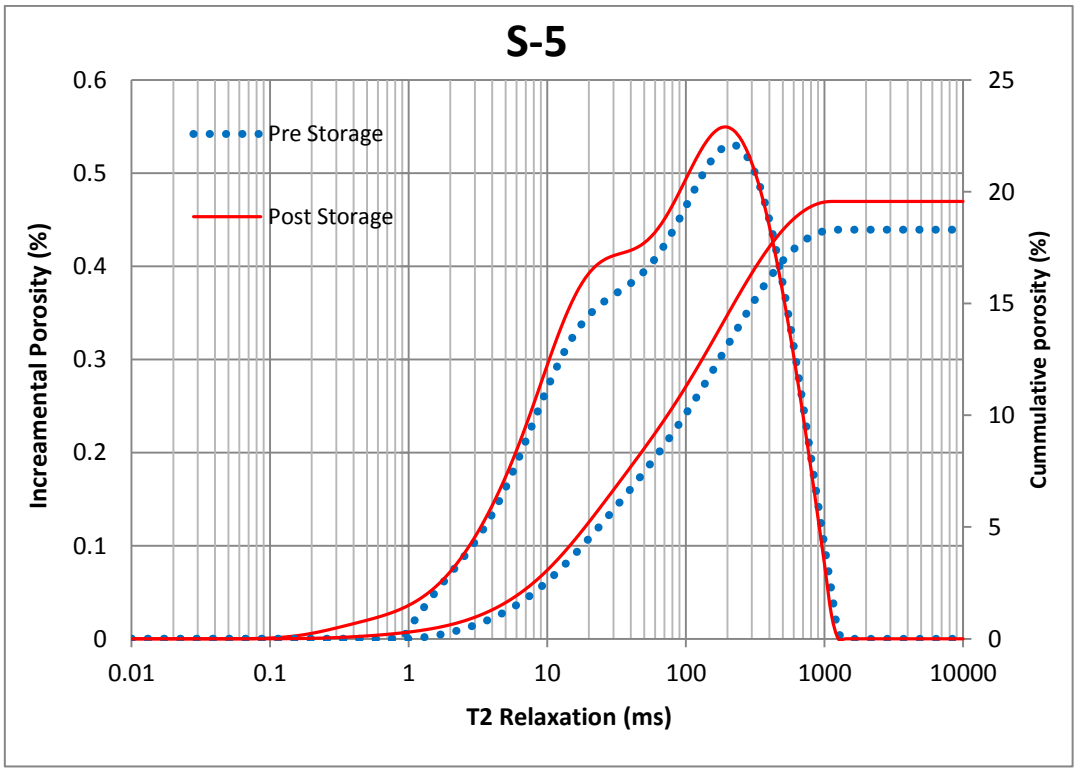

Figure 5-5 NMR porosity showing increase in porosity after CO2 storage in sample S-5

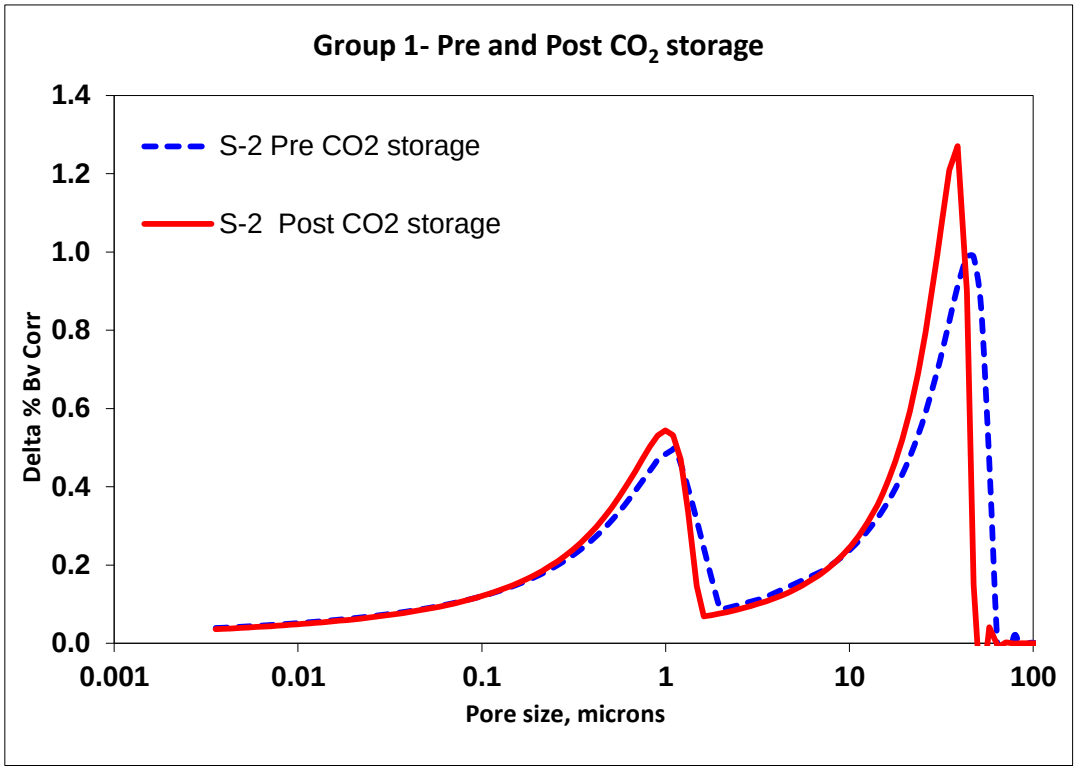

Figure 5-6 MICP pore size distribution for Pre and Post CO2 storage for sample S-2

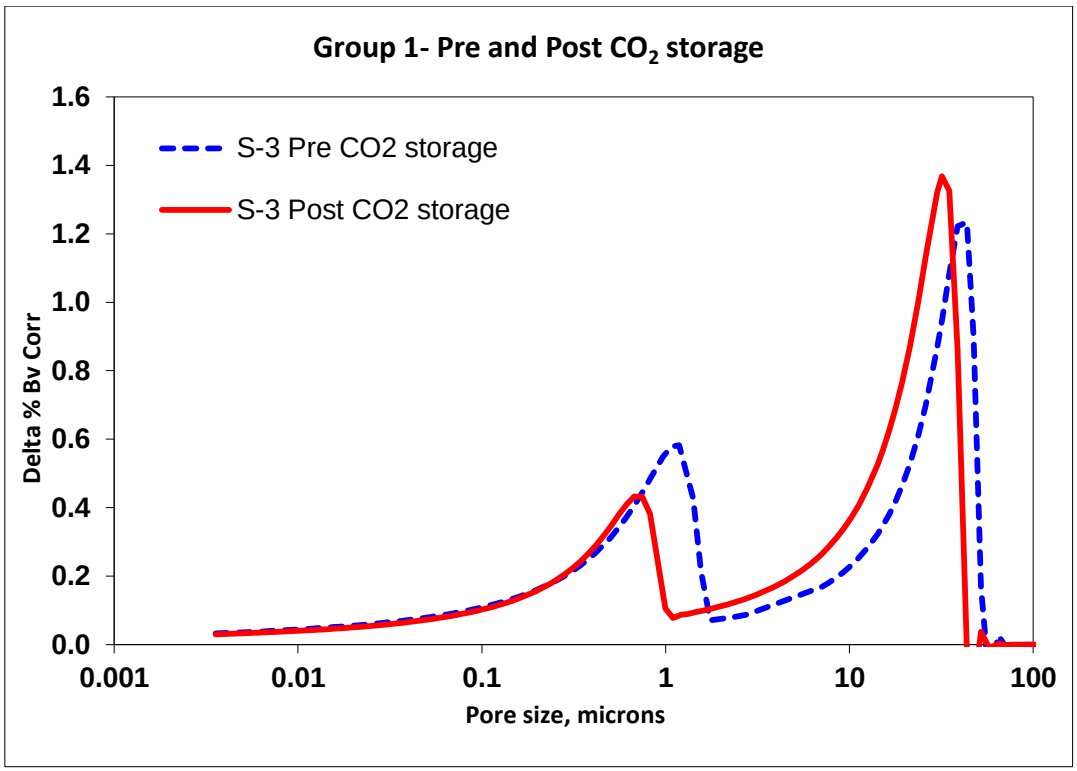

Figure 5-7 MICP pore size distribution for Pre and Post CO2 storage for sample S-3

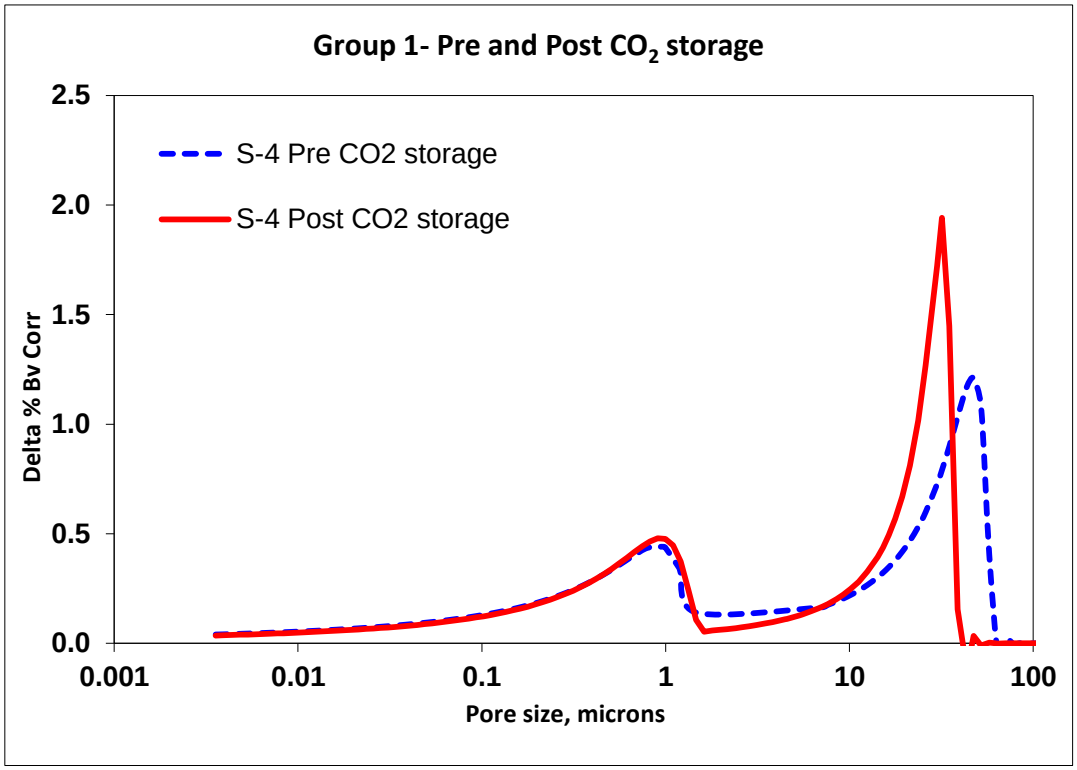

Figure 5-8 MICP pore size distribution for Pre and Post CO2 storage for sample S-4

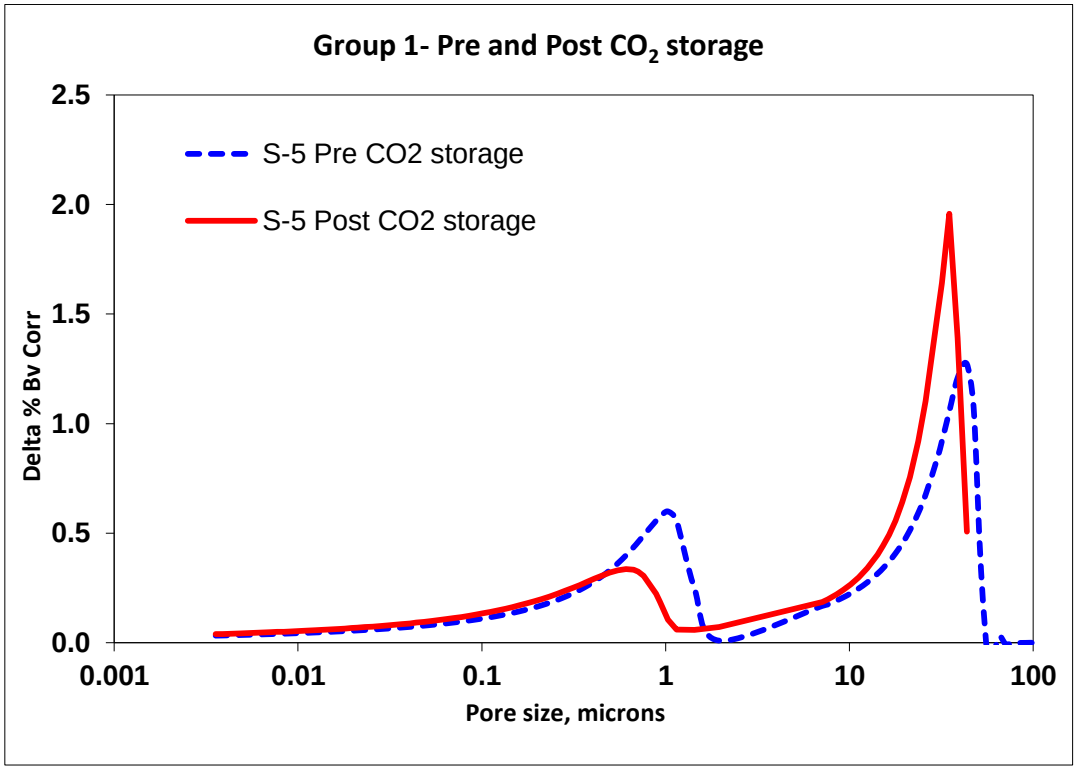

Figure 5-9 MICP pore size distribution for Pre and Post CO2 storage for sample S-5

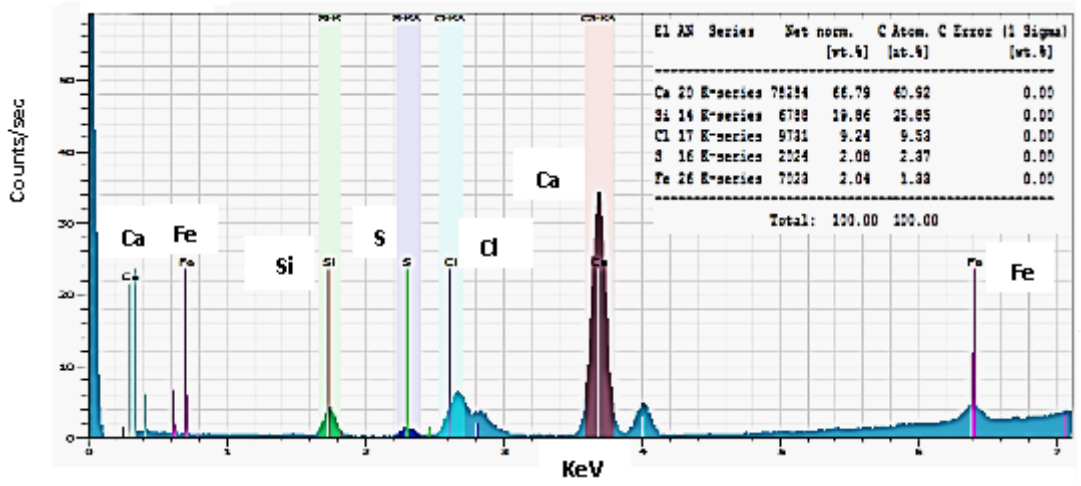

Figure 5-10 XRF Spectroscopy on precipitates collected at the bottom of post CO_2 storage brine

Table 5-1 Brine analysis

Pre CO_2 Storage, mg/l		
Components	Pure Brine	Post CO_2 Brine
Na	17462	19035
Mg	317	351
Ca	3570	3983
Cl	35879	37666
SO_4	365.5	290.8
HCO_3	34.5	85.7
CO_3	4434	18669
TDS	**62,062**	**80,081**

CHAPTER 6

RESISTIVITY INDEX HYSTERESIS

In this section, two systematic laboratory approaches to estimate the saturation exponents of rocks undergoing different displacement processes during CO_2 EOR process are presented. In the laboratory determination of I_R-S_w relationship, the displacement process must mimic the actual displacement process in the reservoir in order to avoid the effect of hysteresis. Hysteresis is a phenomenon used to describe differences in saturation exponents obtained from a given core when resistivity index measurements were plotted against saturation during drainage and imbibition [37]. Two types of hysteresis have been identified namely- displacing phase dependent and displacing cycle-dependent hysteresis [115]. Phase-dependent hysteresis is said to have occurred when the I_R-S_w plot for oil displacing brine is different for brine displacing oil. It is dependent on which phase is displacing the other. Cyclic dependent hysteresis on the other hand is cycle dependent regardless of whether the displacing phase and the displaced phase are the same. For example the I_R-S_w trend for oil displacing brine is different for successive displacements in the same rock [106].

Effect of hysteresis on saturation exponent has been reported in the literature. Longeron et al. [116] carried out laboratory experiments in which water wet brine saturated core samples were flushed with oil and then with brine and finally with oil again under the same experimental condition. The I_R-S_w plot and 'n' was different for each cycle. Gray et al. [117] compared saturation exponent derived from constant injection rate with that derived from constant pressure method. They found similarity in the two methods in water wet samples while disparity in oil wet samples were attributed to difficulty in achieving uniform

brine saturation across samples. Similarly, Jing et al. [118] studied the effect of cycle-dependent hysteresis on some rock samples (oil wet and water wet). The cores were fully saturated with brine and oil was injected to displace the brine until irreducible water saturation. The cores were then water flooded to displace the oil until no more oil was produced. This was followed by another cycle of oil displacing brine. Their results showed that the cores' saturation exponents in the second cycle were significantly lower than in the first cycle. This phenomenon was more pronounced in the water wet samples. Al-Kaabi et al. [119] also investigated phase dependent hysteresis on saturation exponent in sandstone using a double membrane experimental set up. Their results showed that saturation exponent is higher in second drainage cycle (oil displacing brine) than in the first drainage. However, second water flood (imbibition) and third drainage tend to agree with first water flood and second drainage respectively. They also showed that saturation exponent is similar for constant pressure and constant rate desaturation schemes. It is not clear whether their samples were water wet or oil wet. Variable saturation exponent can also be caused by inappropriate laboratory procedures.

In this present study, different displacement scenarios and their effect on saturation exponent in a carbonate rock formation undergoing CO_2-EOR were investigated. Different displacement scenarios are identified and investigated for hysteresis. They are: oil displacing brine (initial oil migration); brine displacing oil (water flooding); second cycle of oil displacing brine (trapped oil bank movement); CO_2 displacing brine at remaining oil saturation (ROS) (CO_2-EOR); and third cycle of oil displacing brine (trapped oil bank movement across carbon dioxide/oil/brine/rock interaction (COBRI) surfaces). Two laboratory methods were used to study these effects. The dimensions and properties of the samples used are given in Table 6-1.

Table 6-1 Sample properties

ID	L (cm)	D (cm)	Dry weight (g)	Sat Weight (g)	Bulk Vol. (cc)	He. Pore Vol. 500psi (cc)	He Porosity (%)	Air Permeability, k (mD)
103	6.82	3.735	161.4	175.65	74.77	14.47	19.359	528
106	7.09	3.743	167.9	182.35	77.96	14.60	18.719	354

Table 6-2 Crude oil properties

Crude oil properties		
Density, ambient (g/cc)	0.85	
API	34.39	
Viscosity (cp)	13.08	
Refractive Index	1.65	
SARA Analysis:	**Component**	**%Wt**
	Asphaltenes(n-C6 insoluables)	3.49
	Saturates	35.36
	Aromatics	49.51
	Polars	11.64

Three sets of desaturation experiments were conducted for resistivity index measurement with each test consisting of several steps. The experiments mimic different displacement processes in the history of a hydrocarbon reservoir undergoing CO_2-EOR. The objective of the experiments is to investigate the effect of cyclic and phase dependent hysteresis on saturation exponent. We focused on resistivity index in the decreasing S_w direction (i.e. drainage) since CO_2 sequestration in depleted hydrocarbon reservoirs is in this direction too. In each experiment, the initial oil migration process into the reservoir whereby invading oil displaces initial water saturation to irreducible water saturation was replicated. This was then followed by water flooding to displace oil until no more oil is produced by water flooding (ROS). The three experiments below focused on three different

EOR/displacement scenarios (where by S_w decreases) after water flooding and their effect on I_R - S_w relation.

6.1 Experiment 1: Sample IL-103

This experiment mimics CO_2-EOR displacement. Sample IL-103 was used for this test. Two different tests were conducted. The first represents oil initial migration into the reservoir and the second test simulates CO_2 displacement process after water flooding.

6.1.1 First S_w decreasing test

The experiment started with crude oil displacing brine at different capillary pressures until irreducible water saturation. A water wet porous plate with entry pressure of about 700 psig was placed at the outlet end of the core while oil displaces the brine from the other end. Brine production was measured and monitored using a 1/8 in. tygon tube. Core resistivity and the corresponding average brine saturation were continuously measured at different time intervals until no more brine is produced from the core outlet. The experiment was conducted at a temperature of 45^{o}C and a net overburden pressure of 2000 psig. This desaturation process represents initial oil migration into a reservoir. The resistivity index plot is used to estimate water saturation from well logs in virgin zones. Next, the core was water flooded with water injection through the water wet porous plate and oil is produced from the other end. Oil production was monitored and measured using a glass burette. Water flooding stopped after no more oil was produced. Saturation exponent derived from this test can be used to estimate water saturation from resistivity logs derived from invaded zones during drilling, transition zone, and water flooded areas.

6.1.2 Second S_w decreasing test

This test mimics CO_2-EOR process. A back pressure of 1300 psig was applied at the other end of the porous plate while CO_2 was used to displace brine at ROS from the other end of the core. Since, the water wet porous plate is only permeable to water and not oil, only brine was produced from the core during different capillary pressures. CO_2 transfer cell driven by a syringe pump was used to deliver CO_2 into the core at pressures of 1300 psig and above in small increments and the maximum differential pressure between the ends of the core is limited by the porous plate entry pressure. Prior to CO_2 injection, the brine pressure in the core was slowly raised to 1300 psig and the differential pressure across the porous plate was monitored to ensure that it does not exceed the plate entry pressure. Similarly, the overburden pressure was accordingly increased to maintain a net overburden pressure of about 2000 psig. Final overburden pressure was 3300 psig. Resistivity and brine production were recorded at intervals. Saturation exponent derived from this test can be used to estimate water saturation from well logs taken from CO_2-EOR fields for CO_2 monitoring in sequestration project.

6.2 Experiment 2: Sample IL-106

The objective of this test is to investigate the effect of COBRI on saturation exponent after oil bank movement in an EOR process [120]. That is some oil bank may migrate and displace some brine in locations where COBRI took place earlier during CO_2 flooding. This is required for water estimation from resistivity log in CO_2-EOR fields.

6.2.1 First S_w decreasing test

Sample IL-106 was used for this test. The same procedure was repeated as in previous experiment. The core was then allowed to age with oil saturation for several weeks after which water flooding began.

6.2.2 CO_2 Storage in Depleted Reservoir

CO_2 was injected into the brine saturated core at ROS. In this case the outlet valve was closed while CO_2 was injected until CO_2 pressure reaches 2000 psig and the inlet valve was closed to allow CO_2/oil/brine/rock interaction. Valves were closed for about 4 weeks. Pore pressure was seen to be rising during this period and the outlet valve had to be intermittently opened to bleed off pressure in excess of 2000 psig. During the first pressure bleeding, only CO_2 was bled. Oil mixed with CO_2 was produced in all subsequent pressure bleeding. After successive bleeding, pressure rose again and the outlet valve had to be intermittently opened to bleed off pressure in excess of 2000 psig. Brine was not visibly produced with oil. In order to ascertain that brine was not produced together with crude oil during the huff n puff style of oil production during pressure bleeding, all produced oil were cumulatively collected in a small test tube until the end of the test. The test tube was monitored for several days in an upright position to see if some brine would segregate from the oil. This was not the case.

6.2.3 Second S_w decreasing test

A second water flooding was carried out to mimic water flooding after CO_2 huff n puff to produce ROS. This was then followed by another oil-displacing-brine test to mimic trapped oil bank migration after CO_2 huff n puff into zones where COBRI took place. Again resistivity and corresponding brine saturation were measured and the displacement continued until S_{or} was achieved.

6.3 Results and Discussions

6.3.1 Experiment 1

Figure 6-1 shows the resistivity log during aging and water flooding process for sample IL-103. The resistivity index data for the two displacements are presented on a log-

log plot shown in Figure 6-2. It can be seen from Figure 6-2 that the slope of the resistivity index plot (saturation exponent, n) in the first cycle (oil displacing brine) is higher than the second cycle (CO_2 displacing brine at ROS). Although the reverse is expected since the rock surface is expected to have changed from water wetness to oil wetness as can be seen in the changing resistivity with time during aging (Figure 6-1). Similar phenomenon was observed in experiment 2.

6.3.2 Experiment 2

Figure 6-3 shows the resistivity log during aging and water flooding process for sample IL-106. Effect of aging on wettability is evident from the plot where the resistivity at the end of aging is significantly higher than at the beginning of aging. The core was then water flooded after aging as seen by the decrease in resistivity. The core outlet valve was closed while CO_2 was injected into the water flooded core after equilibrium was attained. The inlet valve was closed after CO_2 injection at 2000 psig. Figure 6-4 is the resistivity versus time as CO_2 reacts with oil, brine, and rock.

Resistivity index plot (Figure 6-5) for this experiment shows a higher saturation exponent for the second cycle of oil displacing brine compared to the first cycle.

The increased saturation exponent in the second cycle in this experiment can be attributed to wettability change to oil wetness caused by deposition of polar compounds from the crude oil onto the rock surface.

Figure 6-6 combines experiments 1 and 2 to represent a single rock formation since the two samples are of the same rock type as confirmed by NMR and MICP data and also by the first cycle oil migration. The data is overlapping for both samples (Figure 6-6). Results from this experiment showed that saturation exponent can differ in all the desaturation cases

and using the appropriate I_R-S_w plot will reduce error in S_w estimation. A parametric study done below makes the effect of the error on water saturation estimation clearer.

6.3.3 Parametric Study

Assuming the following typical well log data and considering resistivity log was taken in a location where some trapped oil banks are moving across a region pre-flooded with CO_2. Also assuming that the current water saturation measured from core analysis on core sample taken from around well logging location is 0.546 (note that this value was taken from the third cycle data, it is just intended to make clear the error of using wrong displacement process in a field evaluation of brine saturation).

R_t = 45.93 ohm.m

R_w = 0.44 ohm.m @ 22.4 ^oC

Porosity = 19%

Formation temperature = 45 ^oC

The saturation exponent for each displacement scenario was estimated using Fluery's dual porosity conductivity model [68] (Eq **4-14**). It can be seen from Table 6-3 that the third cycle (Oil bank movement after COBRI) gives the best estimation of water saturation because the displacement process is representative of actual field process. The first cycle under estimated brine saturation about 17% while the second cycle under estimated it by 41%.

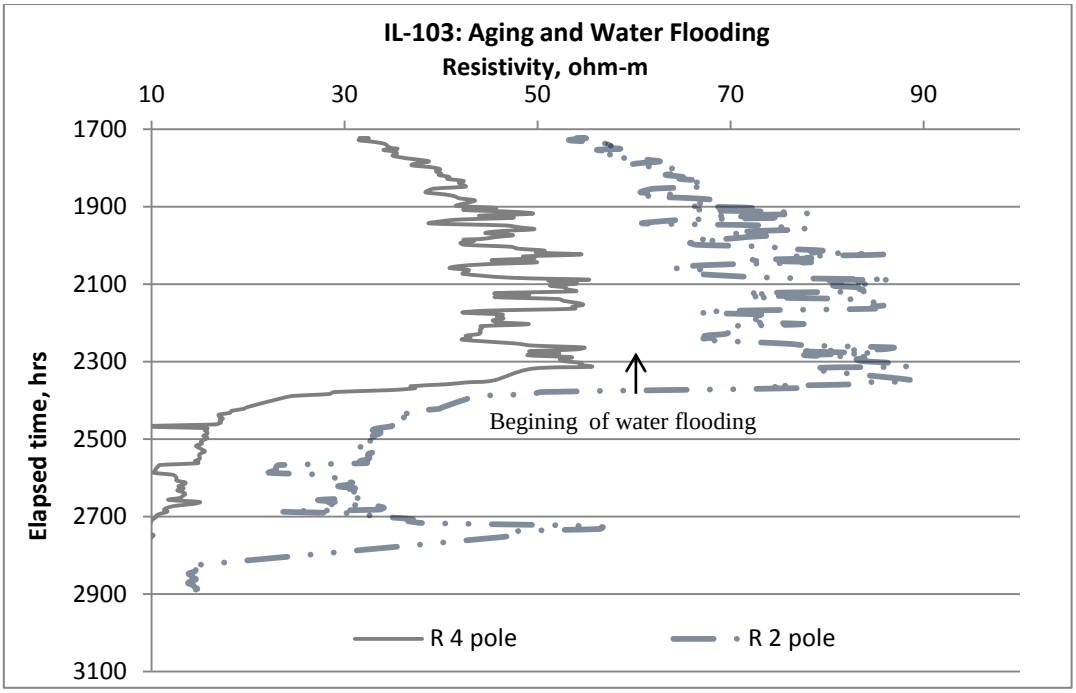

Figure 6-1 Resistivity log during aging and water flooding of sample IL-103

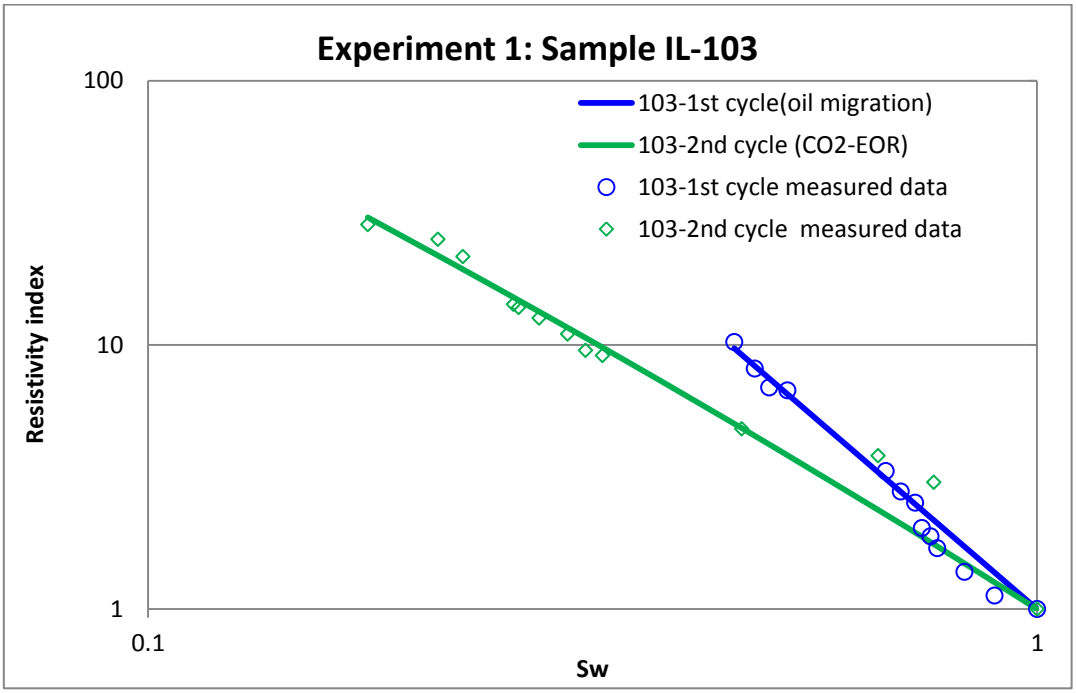

Figure 6-2 Resistivity index versus brine saturation for sample IL-103 in Experiment 1

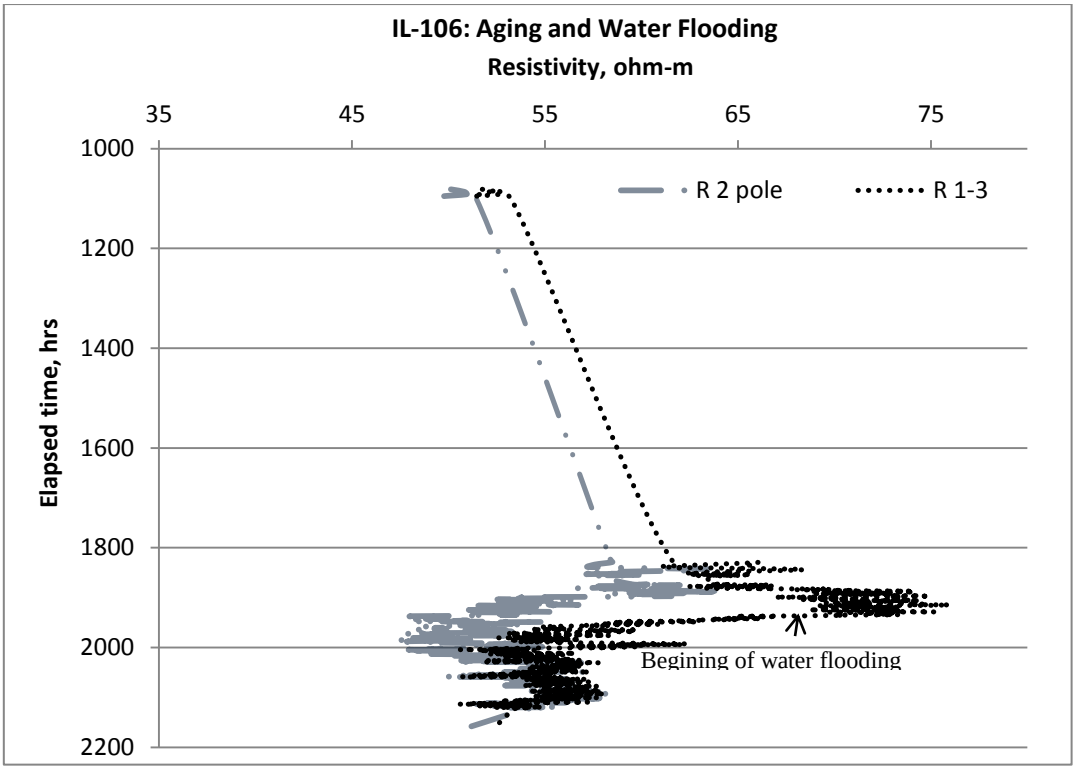

Figure 6-3 Resistivity log during aging and water flooding in sample IL-106

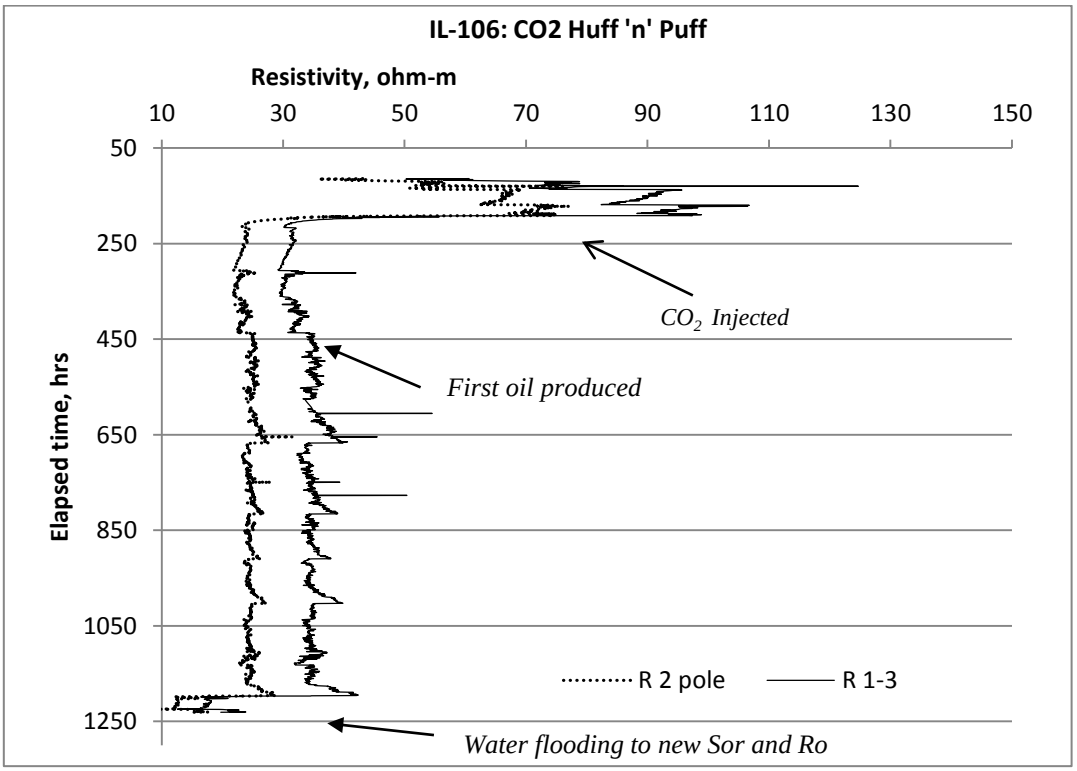

Figure 6-4 Resistivity log during CO_2 huff n puff in sample IL-103

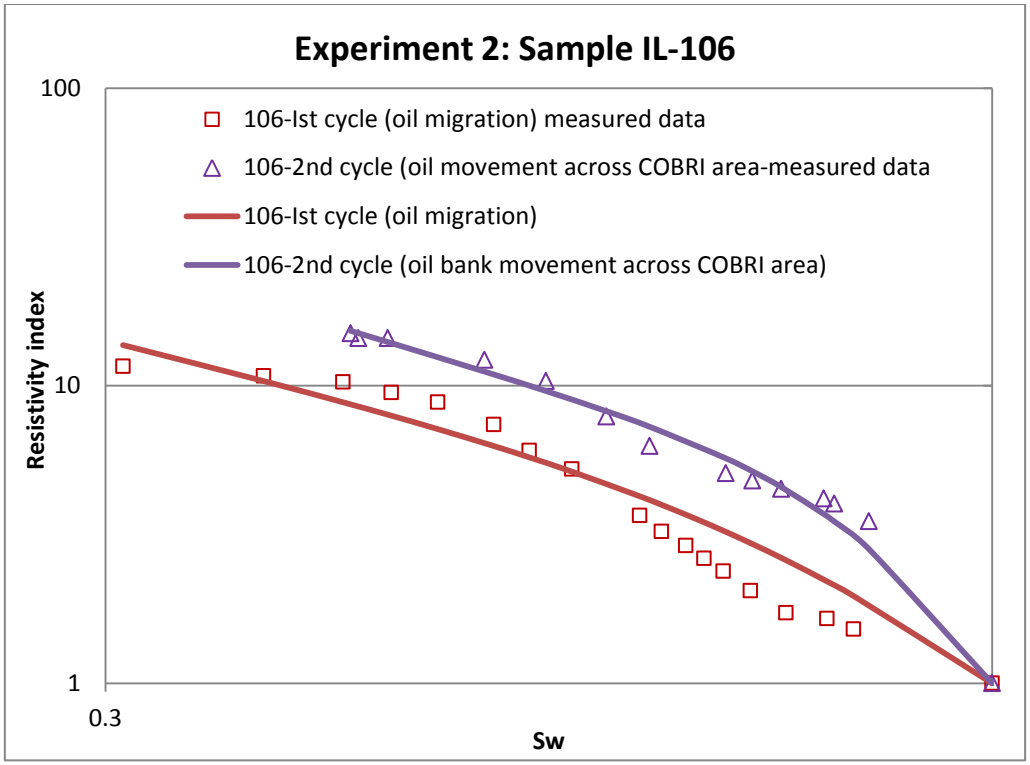

Figure 6-5 Resistivity index versus brine saturation for sample IL-106 in Experiment 2

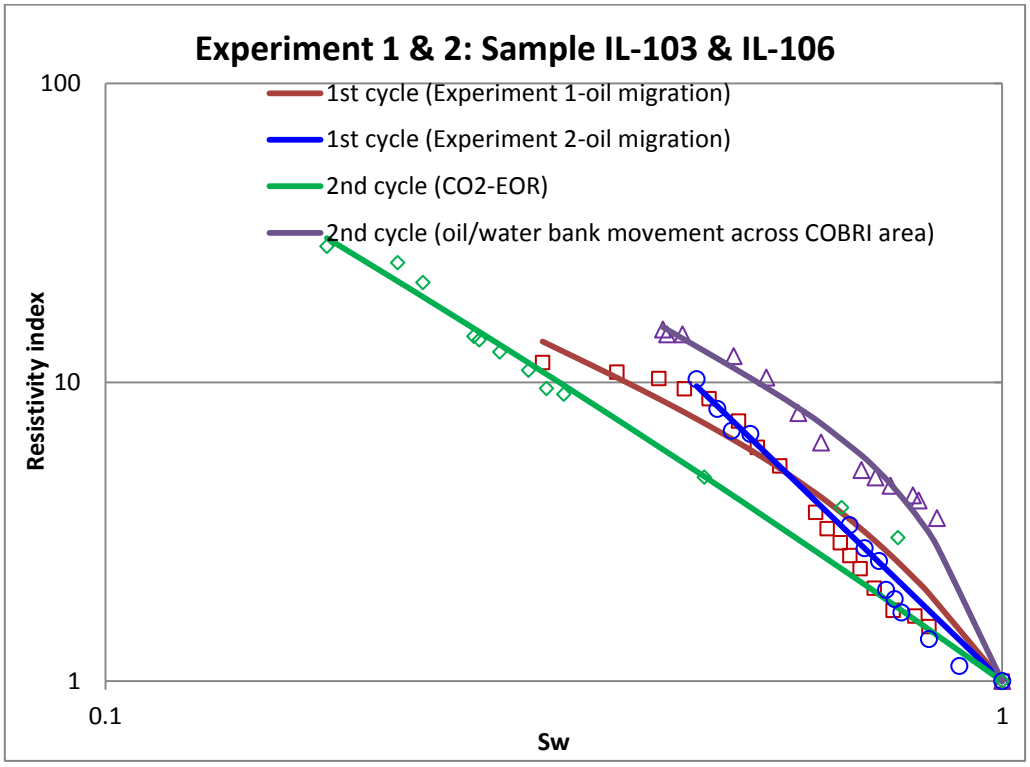

Figure 6-6 Resistivity index versus brine saturation for various displacement scenarios in the life of a CO_2-EOR carbonate reservoir

Table 6-3 Effect of hysteresis on water saturation in CO_2-EOR field

Displacement scenario	n1	n2	∝	Sw	%Error
1st cycle (first oil migration)	2.90	0.74	0.79	0.456	16.519
1st cycle (first oil migration)	2.85	0.68	0.55	0.453	17.045
2nd cycle (oil movement across COBRI area)	9.81	1.70	0.45	0.324	40.963
3rd cycle (CO2-EOR)	2.54	1.63	0.79	0.546	0.000

CHAPTER 7

PROPOSED RESISTIVITY AND TEMPERATURE LOGS FOR SCALE MONITORING

Electrical resistivity of rocks depends on: water saturation; type of ions and ionic strength; temperature; and cation exchange capacity. As a result, high resolution electrical resistance tomography has been successfully used to monitor subsurface migration of various fluids and contaminants, leakage detection, and monitoring of cap rock integrity [121-123].

During CO_2 sequestration, current industry practice is to log resistivity as a function of depth in many observation wells drilled around an injection well and in strategic locations across the reservoir. The objectives of such logs include: evaluation of reservoir performance, detection of leaks and flow path, and understanding geophysical and geochemical interaction of CO_2 with rock and rock fluids. Scale deposition at the wellbores and in near bore vicinity greatly reduce rock permeability and CO_2 injectivity into the reservoir thereby necessitating remedial action and increase in project cost. We show here that such logs can be used further when combined with temperature logs to give an indication of CO_2 rock brine interaction essentially the onset of mineral precipitation process which is an important and long term objective of CCS project. We hereby present a laboratory investigation of the applicability of combined and continuous log of resistivity and temperature as a function of time for oilfield scale monitoring. We also propose the continual use of already drilled observation wells and electric logging facilities to log electrical resistivity and formation temperature as a function of time and depth. Results showed that drop in formation resistivity does not necessarily

mean migration of CO_2 away from the location but can also indicate dissolution of rock grains. A base line log recorded prior to CO_2 injection allowed us to track onset of dissolution and precipitation. Deflection away from the baseline either inwards or outwards during the period of storage marks two distinct reaction phenomenon; dissolution and precipitation. Our hypothesis was justified by results of geochemical analysis of pre storage brine (the base line log) and post storage brine and also by petrographic study of the cores. Several other tests were also run to ensure consistency. This study is new compared to previous works in the following sense: Many previous works have focused on the applicability of electrical resistivity measurements to track carbon dioxide (CO_2) migration by way of resistivity change as a function of CO_2 saturation changes during CO_2 sequestration. Many others also studied the effect of CO_2 injection on the petro-physical and electrical properties of rocks. Previous works of these types in the literature [11-13, 65, 124-127] use continual flow of fluid in and out of the sample and such flow experiments lasted for few hours. They did not consider what happens with formation resistivity after a longer experimental period.

7.1 Experimental set up

The objective of this experiment is to investigate the applicability of online resistivity log in tracking fluid rock interaction such as dissolution and precipitation of rock grains during CO_2 sequestration in saline carbonate aquifer. Carbonate rock samples collected from the same rock quarry of Indiana limestone with recorded high level of homogeneity (see Table 7-1).

Figure 7-1 is the set up for CO_2 storage and resistivity measurements. Pure CO_2 was injected into brine saturated carbonate core samples at CO_2 pressure of 2000 psig under confining pressure and reservoir temperature of 45^0C. Prior to loading samples in the temperature control bath (or test cell), each sample was placed in a Viton sleeve embedded

with two electric potential electrodes (Figure 7-2). Two stainless steel caps at both ends of the core served as the current electrode as well as core inlet and outlet. The core samples were wrapped with Teflon tape such that only a part of the samples that will be in contact with the potential electrodes are left open (as in Figure 4-22). This served to reduce and delay CO_2 diffusion through the Viton sleeve. Core inlet valve was connected to a CO_2 source by steel tubing and fittings. A pressure gauge connected to the CO_2 line was used to monitor CO_2 pressure during storage. CO_2 was injected into the brine saturated sample until pore pressure reached 2000 psig at an overburden pressure of 2500 psig and temperature of 45^oC. A pump connected to the test cell delivered the overburden oil from the oil tank to the test cell while a heater wrapped around the cell heated the oil to the desired temperature. Both the core inlet and outlet valves were closed after CO_2 injection while a LCR meter connected to the test cells coupled with a data acquisition system and a computer allowed for continuous monitoring of rock resistivity with time as the CO_2, brine, and rock interact. CO_2 pressure was also monitored and recorded with time. Core temperature was also measured with time using thermocouple installed in the test cell. CO_2 was allowed to age in the core samples for a period of between 60 to 90 days. At the end of storage brine samples were collected in a test tube for post storage brine analysis. The core samples were also cleaned and prepared for porosity and permeability measurements.

Table 7-1 Samples' dimensions and properties

ID	L (cm)	D(cm)	Bulk Vol. (cc)	He Porosity (%)	Air permeability, k (mD)
IL-1	7.064	3.736	77.43	17.790	423
IL-2	7.034	3.741	77.37	18.367	324
IL-3	6.815	3.737	74.76	19.458	536
IL-4	6.603	3.735	72.35	19.354	652

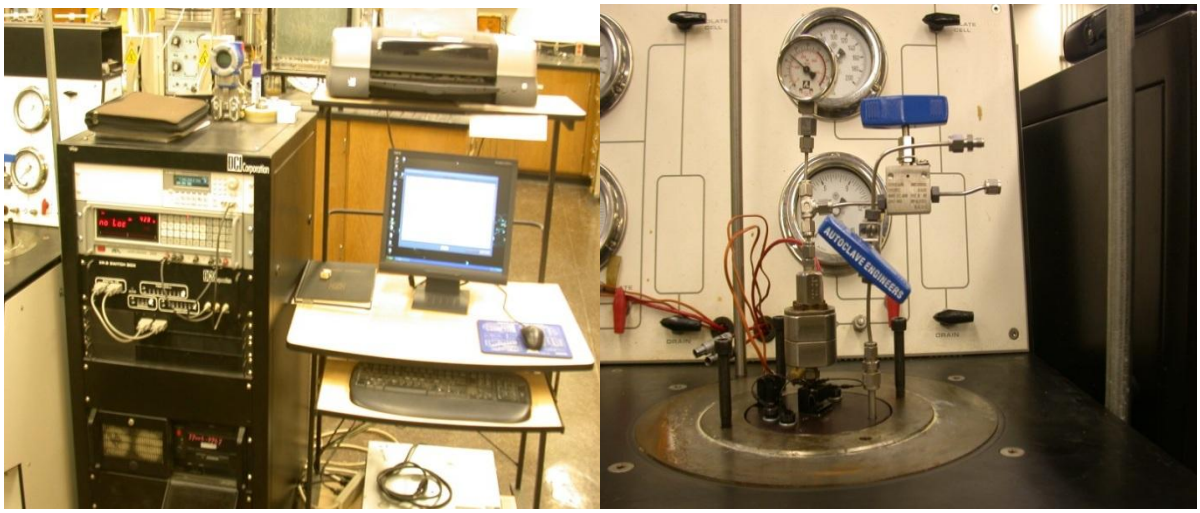

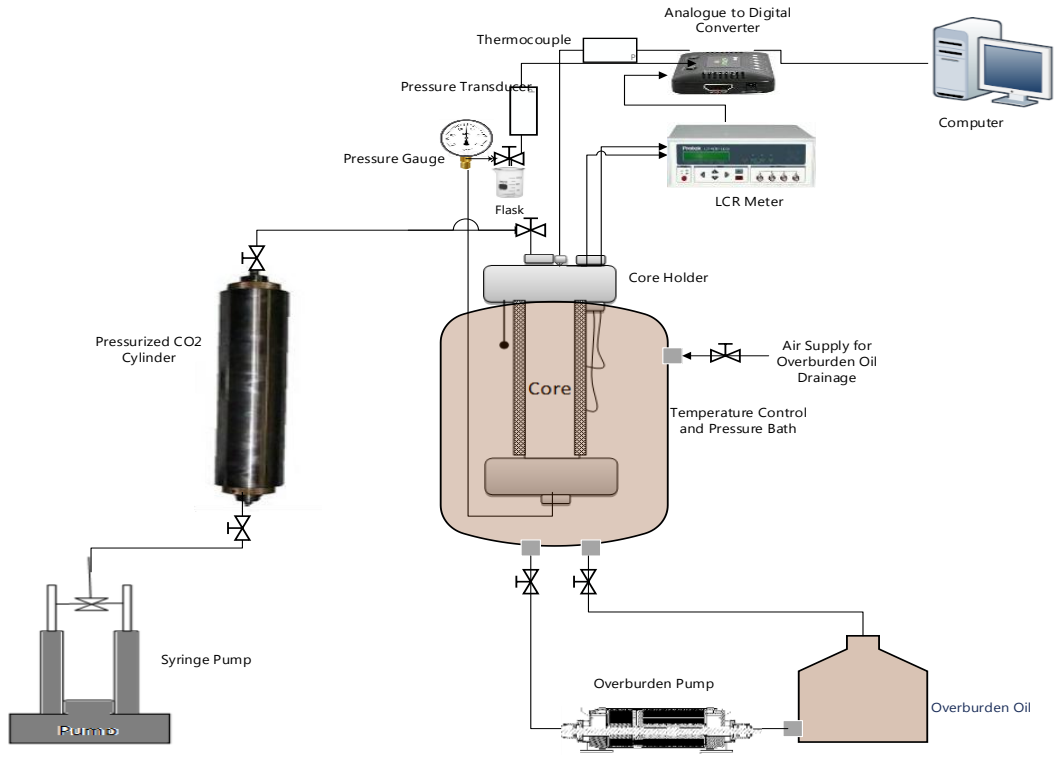

Figure 7-1 CO2 sequestration and online resistivity measurement system

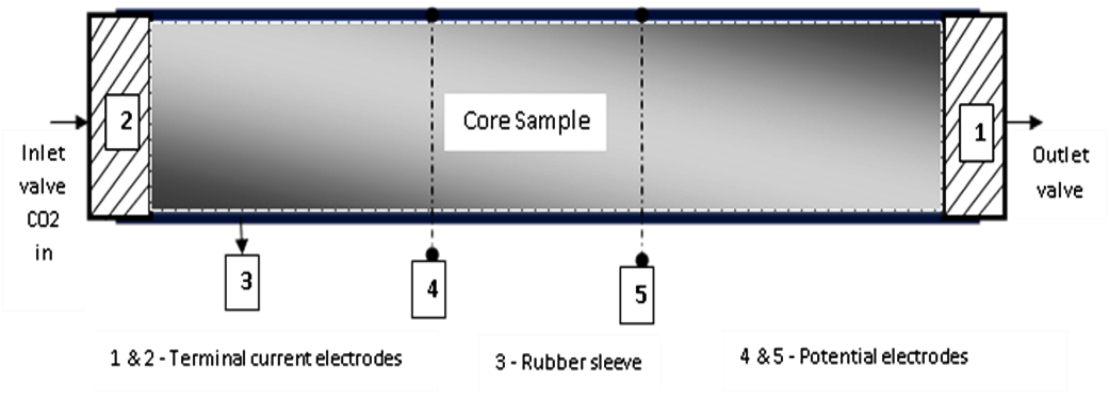

Figure 7-2 Core holder with rubber sleeve

7.2 Results and Discussions

Combined logs of resistivity and temperature with time for all samples are shown in Figure 7-3 through Figure 7-7. It was observed that the resistivity and temperature logs remain fairly constant after CO_2 injection until after about 150 hours when the log deflected to the left. The log prior to deflection was then taken as the base log (red line) for all the CO_2 storage experiments. Figure 7-3 and Figure 7-4 show the combined resistivity and temperature log for CO_2 storage in sample IL-1 and IL-2 respectively. The two logs (resistivity and temperature) showed similar trends in both samples tested. Electrical resistivity signature was constant prior to CO_2 injection and later increased slightly in response to CO_2 influx and remained constant again around this resistivity value until after quite a number of days (4 – 6 days in both experiments) when constant resistivity pattern deflected from the base line to the left suggesting the onset of chemical reactions between the three phases- CO_2, brine, and carbonate grains. The resistivity returned back to the base line after some days and remained on the base line for quite some time until late storage time when a second deflection this time to the right was observed again. Two major deflections were thus visible and a return to the base line after the first deflection observed in the two tests could provide very important information about CO_2/brine/rock interaction (CBRI). One distinct deflection was consistent in the temperature log and that is the deflection to the left

from the base log at the same time the resistivity log deflected to the left. The temperature log also returned to base log at the same time the resistivity log did. Petrophysical core analysis prior to and after CO_2 storage and post brine geochemical analysis helped to interpret the observed trends. The analysis confirmed minor grain dissolution and the presence of calcite minerals in brine effluents which is a by-product of the interaction.

Accurate interpretation of the observed and consistent trends is needed to understand the relationship between CBRI and rock resistivity and temperature. A possible explanation for this observation is that the deflection to the left (reduction) of both resistivity and temperature signifies the dissolution process which is endothermic [128, 129] resulting in lower temperature during the dissolution period (Figure 7-3 and Figure 7-4). The duration of dissolution is controlled by the duration at which CO_2 is trapped in the core pores space before being consumed by diffusion through the sleeve or by dissolution process. Equations 7-1 to 7-5 describe the CO_2 brine rock interaction processes in a carbonate formation [130].

$$CO_2 + H_2O \leftrightarrow H_2CO_3 \quad 7\text{-}1$$

$$H_2CO_{3\,(aq)} \leftrightarrow H^+_{(aq)} + HCO_3^-{}_{(aq)} \quad 7\text{-}2$$

$$CaCO_3 + H^+ \leftrightarrow Ca^{2+}_{(aq)} + CO_2^-{}_{(aq)} + H_2O \text{ (calcium, } CO_2\text{, and water source)} \quad 7\text{-}3$$

$$Ca^{2+}_{(aq)} + HCO_3^-{}_{(aq)} \leftrightarrow H^+_{(aq)} + CaCO_{3\,(s)} \text{ (calcite precipitate)} \quad 7\text{-}4$$

$$Mg^{2+}_{(aq)} + HCO_3^-{}_{(aq)} \leftrightarrow H^+_{(aq)} + MgCO_{3\,(s)} \text{ (magnesite)} \quad 7\text{-}5$$

Dissociation of H_2CO_3 formed from Equation **7-1** will trigger forward reaction and more CO_2 is dissolved in brine. Dissociation results in the formation of bicarbonate radicals and hydrogen radicals (Equation **7-2**) which further increases the acidity of the brine. Protons

(H+) formed after dissociation of bicarbonate will leach out cations from the carbonate rock minerals according to Equation (7-3) to produce free Calcium ions in solution. The reaction of bicarbonate radicals (produced from Eq. **7-2**) with reactive calcium radicals (produced from Equation **7-3**) leads to the formation of stable minerals (Equation 7-4). Equation **7-4** is the reversible reaction of Equation **7-3**. It occurs at higher pH occasioned by reduced volume of dissolved CO_2 in brine or because the rate of ionization of carbonic acid does not keep up with the pace of consumption of hydrogen ions - note that Carbonic acid is a weak acid and does not completely ionize. In that case the reversible reaction (Equation **7-4**) occurs simultaneously with forward reaction until equilibrium. Equilibrium is said to be achieved when both forward and backward reactions (in Equation 7-3 or Equation 7-4) occur at the same rate or when no reaction is going on. Ionization and leaching of calcium ion from carbonate grain surfaces are all endothermic processes, i.e. heat is taken from the surrounding to break calcium carbonate bonds. This explains the lower temperature observed in the temperature log in all the CO_2 storage experiments. It can be seen that at these low temperature periods, the resistivity logs were also seen to deflect to the left (lower resistivity). This means the brine is more conductive during the period due to increase in the population of free radicals that helped to conduct electricity more than the brine before addition of more ions to the brine. During the reversible reaction (Equation 7-4), the ionic strength is reduced leading to the increase in resistivity seen in the resistivity log. Resistivity continues to decrease until equilibrium state when the resistivity became constant. Later during storage when CO_2 pressure dropped significantly, the pH increased significantly too and this resulted in more precipitation and more ions taken out of solution. The result is a further increase in resistivity seen at the last stage of CO_2 storage. In all the CO_2 storage experiments, ionization or leaching of carbonate grains started at about 150 hours while precipitation started after pressure dropped below 800 psig.

In order to investigate if the observed trend was as a result of CBRI, pure Nitrogen was stored in another core sample (IL-3) at the same storage condition as CO_2. Figure 7-5 is the resistivity and temperature log of this sample (IL-3). The resistivity and temperature signature was seen to be different from that of CO_2 storage. Resistivity and temperature logs were seen to be relatively constant as no major deflection from the base line were seen. This is so because Nitrogen is an inert gas which is soluble in water without any further chemical reaction with water or the surrounding carbonate grains.

Figure 7-6 is the log of CO_2 storage in a core saturated with brine containing 3% chelating agent (ethylene di-amine tetra-acetic acid, EDTA). EDTA absorbs metal radicals such as calcium ions from solution immediately they are leached out of carbonate grains and binds them onto itself to form stable chelates making them non-reactive and nonconductive. At high CO_2 pressure when the pH of brine solution is low, leaching started as seen from the temperature log, the resistivity effect was the reverse from previous CO_2 storage without a chelating agent. Resistivity log deflected to the right while the temperature log deflected to the left as before signifying dissolution of calcium carbonate which is an endothermic process. The higher resistivity or deflection to the right is due to the fact that the chelating agent absorbed the calcium radicals as they are produced while hydrogen ion (that contributes to electric current) is continuously depleted during the process at a rate faster than they are produced. It could be seen at this period of chelation that the resistivity log is constant. At low CO_2 pressure, the effect of precipitation on resistivity was seen by increase in resistivity (deflection to the right of the base line) in Figure 7-3 and Figure 7-4. Such effect could not be seen here as the reactive radicals have been long absorbed by the chelating agent right from the start. This is why the increase resistivity effect was not seen at low CO_2 pressure but rather a decrease in resistivity. A decrease in resistivity or deflection to the left is believed to

be due to the fact that the EDTA saturation point was reached and it could no longer absorb more calcium radicals, hence the radicals moved freely conducting current at this stage.

In another experiment pure brine was stored in a sample at the same condition of CO_2 and N_2 storage in order to ascertain that the reason for the observed trends is as a result of the type of stored fluids and their interaction with the rock minerals. Figure 7-7 shows that resistivity and temperature logs were constant throughout the period of brine storage. This further confirms that the observed deflection pattern in CO_2 storage is as a result of CBRI.

Core samples were cleaned, dried, and measured for post storage porosity and permeability. Porosity was found to increase in CO_2 storage samples (18.4% for IL-1, 19.3% for IL-2) while permeability reduced from 423 mD to 201 mD in sample IL-1 and from 324 mD to 297 mD in sample IL-2. Reduction in permeability is due to blockage of pore throats by precipitates formed after CBRI.

7.3 Post CO_2 storage brine analysis

Inductively coupled plasma-atomic emission spectrometer (ICP-AES) analysis of brine prior to CO_2 storage and post CO_2 storage showed a difference in salinity content (see Table 7-2). Precipitates were also seen at the bottom of brine effluents collected is test tubes (Figure 7-8). XRF analysis (Figure 7-9) on these precipitates confirmed they are calcium carbonates

7.4 Significance and Field Applicability

Maximum fluid production and/or injection require(s) effective scale management. Effective scale management involves reduction and monitoring of scale formation. Currently scale inhibitors are injected to minimize scale formation while monitoring techniques used to evaluate rate of scale deposition rely on produced fluids to the surface. There is no reliable

online monitoring technique available for monitoring the extent of scale formation. This method can detect in real time the dissolution of carbonates and scale formation at reservoir conditions. Online monitoring technique such as the one proposed in this paper can be used to test the performance of injected scale inhibitors. Trends obtained will inform operators of eminent scale problem and thus allow them to take rapid corrective measures which reduce costs of scale related system failure. It does not require a new installation but uses already installed downhole sensors without the need for additional supporting equipment. Since temperature and resistivity sensors are normally installed in many locations down hole, scale formation at its earliest stage can now be monitored in-situ and in real time across the reservoir. Resistivity and temperature logging must therefore start early and continuously in order to track different stages of CBRI and in order to rightly interpret resistivity values.

7.5 Limitations of Study

Limitations include CO_2 storage in saline or depleted reservoirs and in static or near static conditions. It has not been tested in the presence of oil and in sandstones. It is only applicable to porous media and has not been applied to pipe lines and other surface facilities.

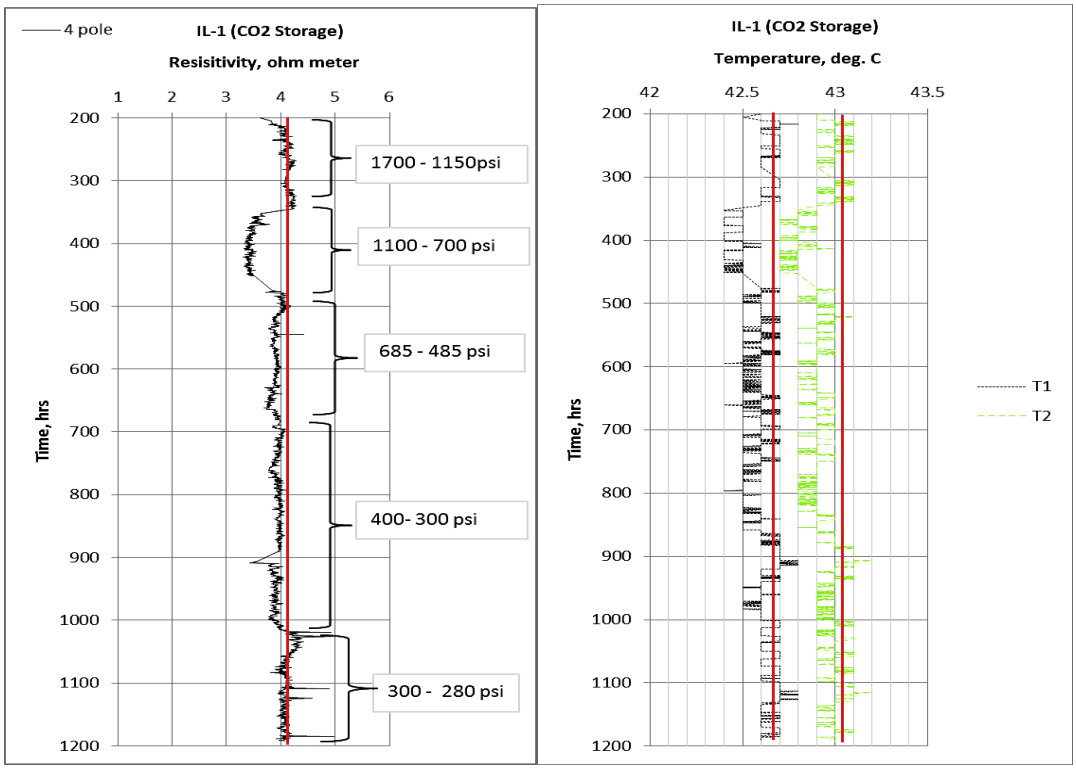

Figure 7-3 Resistivity and temperature log during CO_2 storage in saline aquifer (IL-1)

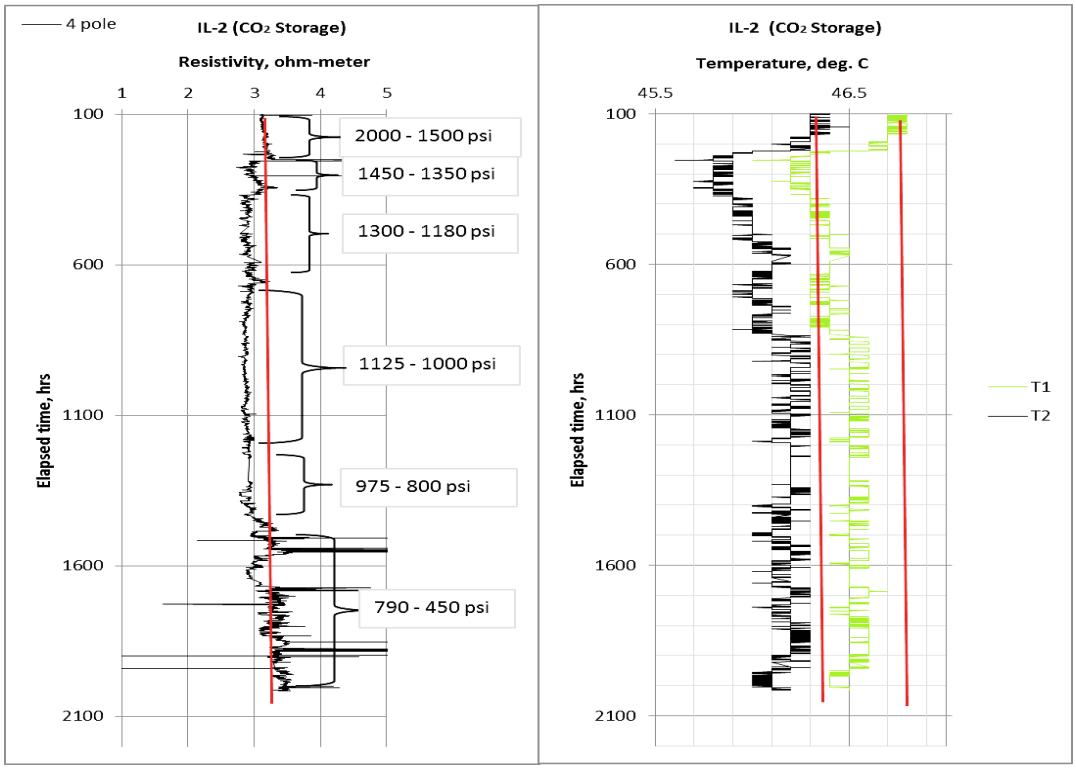

Figure 7-4 Resistivity and temperature log during CO_2 storage in saline aquifer (IL-2)

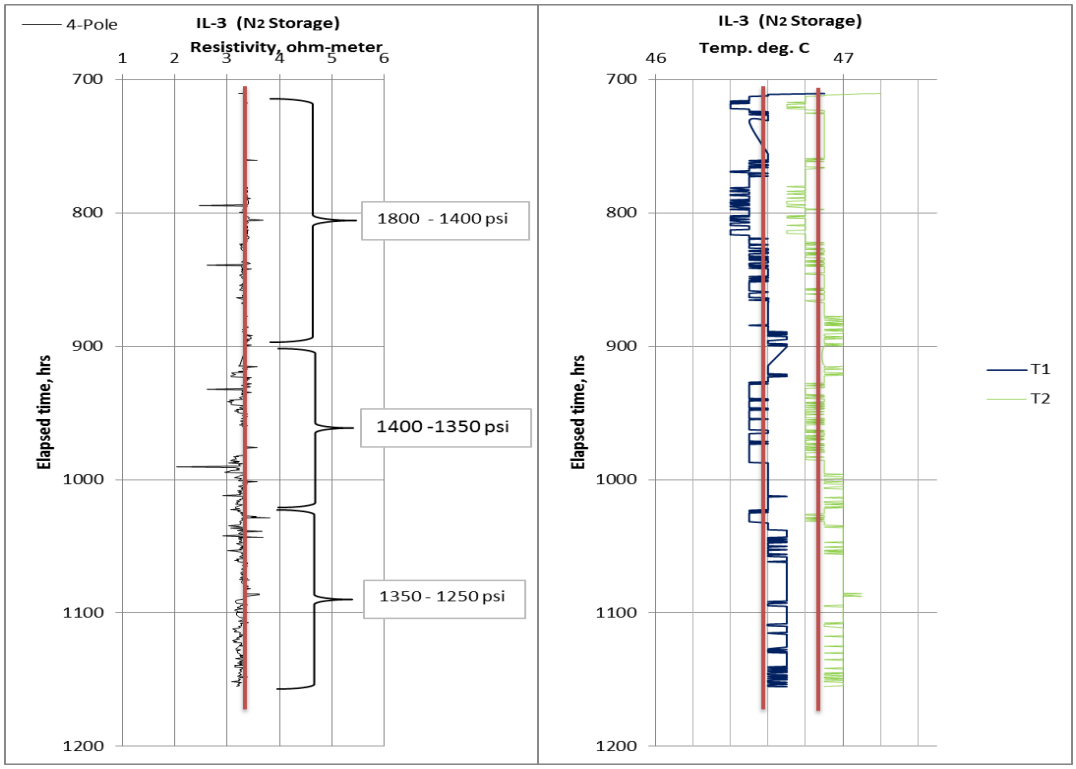

Figure 7-5 Resistivity and temperature log during Nitrogen storage in Saline sample IL-3

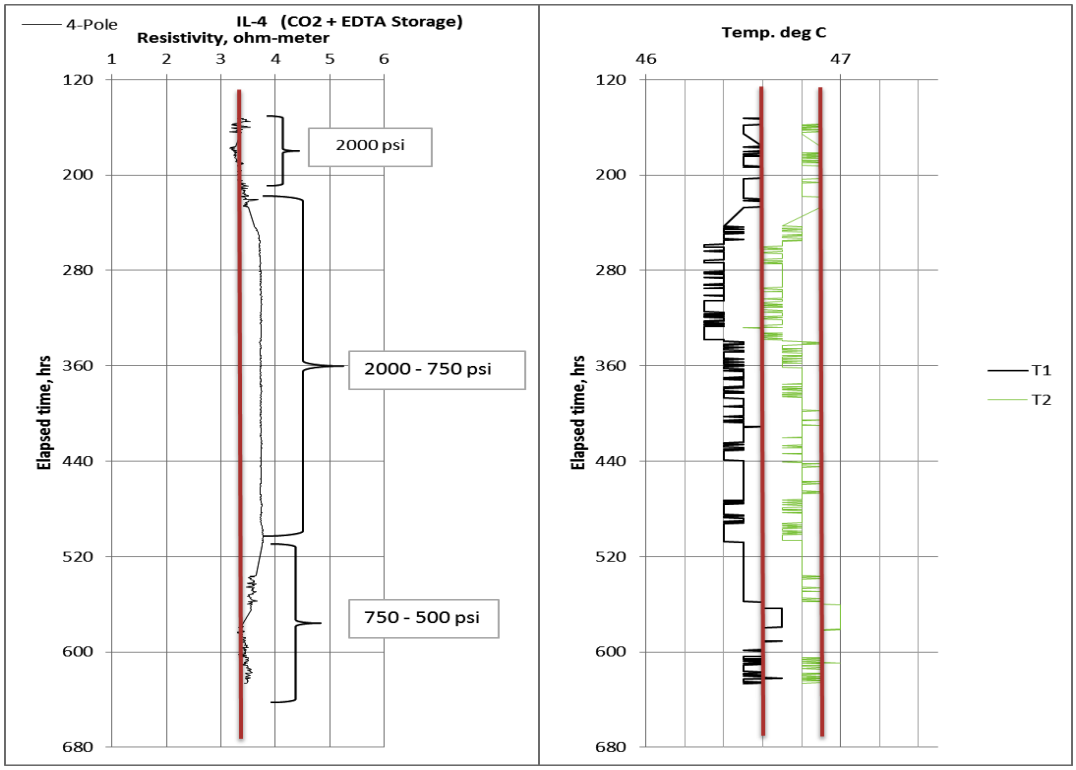

Figure 7-6 Resistivity and temperature log during CO_2+ EDTA storage in Saline Sample IL-4

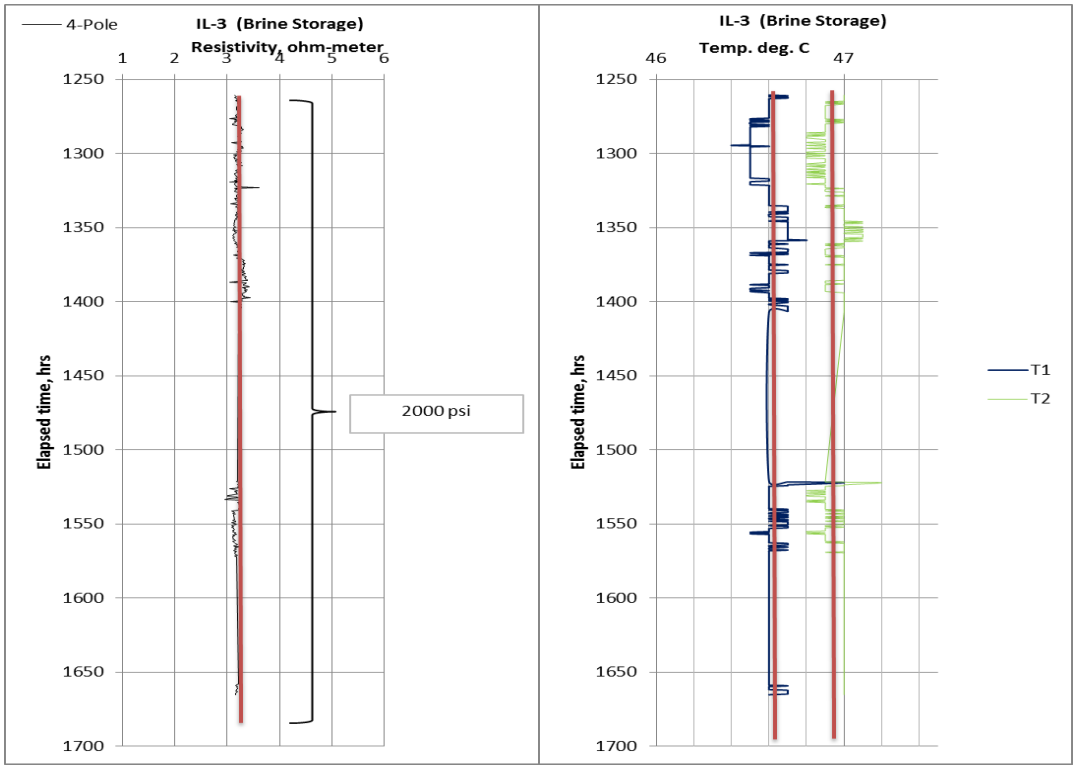

Figure 7-7 Resistivity and temperature log during brine storage in sample IL-3 at 2000 psig

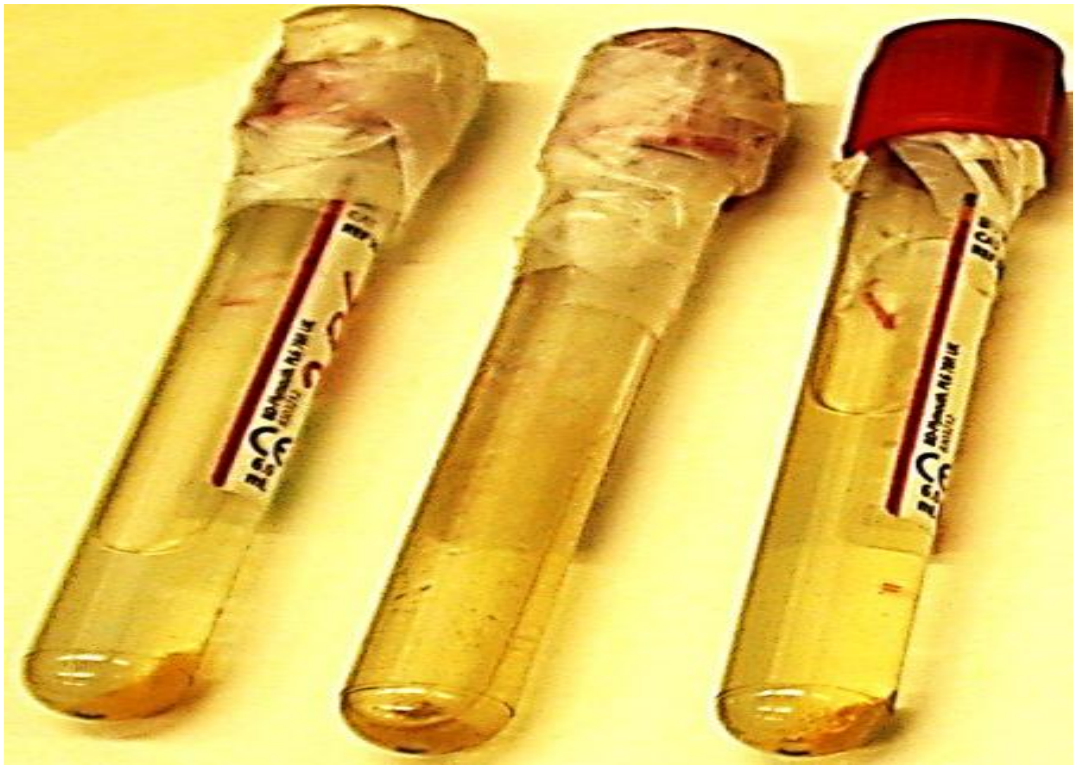

Figure 7-8 Precipitates seen at the bottom of test tube containing post CO_2 storage brine

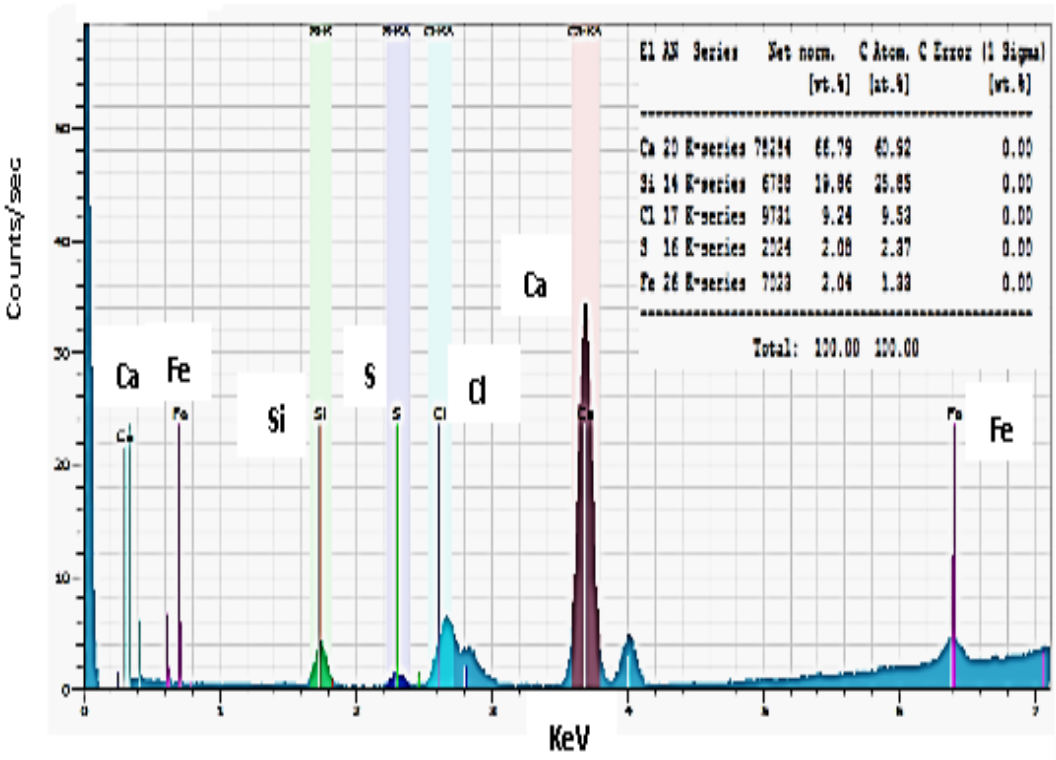

Figure 7-9 XRF Analysis on precipitates showed 61% calcium

Table 7-2 Brine analysis

Pre CO_2 Storage, mg/l		**Post CO_2 Storage, mg/l**	
Components	Pure Brine	IL-2	IL-1
Na	17462	19035	19002
Mg	317	351	344
Ca	3570	3983	3866
Cl	35879	37666	37801
SO_4	365.5	290.8	318.7
HCO_3	34.5	85.7	58.7
CO_3	4434	18669	8946
TDS	**62,062**	**80,081**	**70,336**

CHAPTER 8

CONCLUSIONS AND RECOMMENDATIONS

8.1 Conclusions

A suite of extensive laboratory measurements and analysis of carbonate cores has been performed for the purpose of understanding the long term effects of CO_2 sequestration in saline aquifers and during CO_2-EOR. Carbonate rock samples were prepared and characterized using nuclear magnetic resonance (NMR), mercury injection capillary pressure (MICP), porosimeter, and permeameter. Two experiments were designed and utilized to inject and store carbon dioxide in some rock samples for an average period of 3 months at reservoir conditions. The main focus of the study was the understanding of the electrical resistivity behaviour of carbonate rocks during CO_2 storage. The following conclusions can thus be derived from this study.

1. Resistivity index measurements made on all samples generally showed concave curves at low water saturation typical of non-Archie rocks except in few experiments that terminated at high water saturation (chapter 6). The deviation from the straight line type of Archie rocks was due to the presence of micro pore structures which act as parallel electrical path at low brine saturation. Dual porosity conductivity (DPC) model [68] was found to be the best model for the measured resistivity index.

2. CO_2 storage samples showed increase in saturation exponent compared to samples in which CO_2 was not sequestered. The increase in saturation exponents depend on the degree of CO_2/brine/rock interaction and also on the duration of storage in each sample. Increase in saturation exponent can be attributed to reduction in the

population of micro pores after CO_2 storage. Carbonic acid formed after dissolution of CO_2 in brine dissolved some grains and expands micro surfaces. This assertion was confirmed by NMR and MICP done prior to and after CO_2 sequestration. The results showed change in pore geometry and increase in porosity after CO_2 sequestration. XRF analysis on precipitates collected from the bottom of post CO_2 storage brine effluents confirmed that the precipitates were calcium carbonates, hence, another indication of rock dissolution.

3. Based on the laboratory investigation of the effect of CBRI on electrical resistivity logs, it was observed that resistivity measurements and temperature logs were affected by rock fluid interaction when fluid saturation was kept constant. Further investigations revealed that resistivity and temperature logs responded in certain fashion during rock grain dissolution and in another manner during precipitation. Upon this observation, resistivity logs combined with temperature logs have been proposed for monitoring rock fluid interaction and scale formation. At the field scale, we proposed the continual use of already drilled observation wells and their electric and temperature logging facilities to log electrical resistivity and formation temperature as a function of time and depth. However, the technique has not been tested under dynamic conditions. It has also not been tested in the presence of oil, in sandstones, pipe lines, and other surface facilities.
4. A systematic laboratory procedure was used to investigate hysteresis effect in I_R-S_w relationship in rock samples undergoing CO_2-EOR. We observed that saturation exponent differed in all the displacement scenarios investigated. Hence, using the correct I_R-S_w plot for appropriate displacement process will reduce reserves evaluation error.

8.2 Recommendations

A longer and effective CO_2 storage is important in order to determine the equilibrium time in which no more dissolution and precipitation takes place even with the presence of CO_2. This was not achieved in this work because CO_2 could not be trapped indefinitely as a result of its corrosive and diffusive nature.

Further development of the proposed monitoring technique is necessary and requires more complex laboratory experiments. Incorporation of an online pH meter during the CO_2 storage will help to match or correlate increase in pH to resistivity and temperature log as increase in pH is known to favor scale formation. The discussed experiments should be conducted for pipelines and tanks to confirm whether the same trends can be observed.

REFERENCES

1. Kiehl, J.T., and Kevin, E. T *Earth's annual global mean energy budget.* Bulletin of the American Meteorological Society, 1997. **78**(2): p. 197–208.
2. Benson, S.M., and Cole, D. R., *CO_2 Sequestration in Deep Sedimentary Formations.* Elements, 2008. **4**(5): p. 325–331
3. *IPCC*, *IPCC Special Report on Carbon Dioxide Capture and Storage*, W.G. III, Editor 2005, Intergovernmental Panel on Climate Change: Cambridge University Press, Cambridge, UK, and New York. p. 1-443.
4. Bachu, S., *Screening and Rankng of Sedimentary Basins for Sequestration of CO2 in Geological Media in Response to Climate Change.* Environmental Geology, 2003. **44**: p. 277-289.
5. Wang, S., Lee, M., Park, M.K., and Kim, J, *Box Experiments on Monitoring the CO2 Migration in a Homogeneous Medium Using Electrical Resistivity Survey.* Geoscience Journal, 2010. **14**(1): p. 77-85.
6. Torp, T.A., and Gale, J. *Demonstrating Storage of CO2 in Geological reservoirs:The Sleipner and SACS Projects*. in *Proceedings of the 6th International Conference on Greenhouse Gas Control Techologies*. 2003. Pergamon, Amsterdam.
7. Bachu, S., *Sequestration of CO_2 in geological media: criteria and approach for site selection in response to climate change.* Energy Conversion & Management, 2000. **41**: p. 953-970.
8. Korbol, R., and Kaddour, A., *Sleipner Vest CO2 Disposal injectionof Removed CO2 into the Utsira Formation.* Energy Convers. Mgmt, 1995. **36**: p. 509-512.
9. Shiraki, R., and Dunn, T.L, *Experimental study on water-rock interactions during CO_2 Flooding in the Tensleep Formation, Wyoming, USA.* Applied Geochemistry, 2000. **15**: p. 265-279.
10. Gaus, I., *Role and impact of CO_2 rock interactions during CO_2 storage in sedimentary rocks.* International Journal of Greenhouse Gas Control 2010. **4**: p. 73–89.
11. Wang, S., and Jaffe, P.R, *Dissolution of a mineral phase in portable aquifers due to CO_2 releases from deep formations; effect of dissolution kinetics.* Energy Conversion and Management, 2004. **45**: p. 2833–2848.
12. Christensen, N.B., Sherlock, D., and Dodds, K., *Monitoring CO2 Injection with Cross hole Electrical Resisitivity Tomography.* Exploration Geophysics, 2006. **37**: p. 44-49.
13. Ramirez, A.L., Newmark, R.L., and Daily, W.D, *Monitoring Carbondioxide Floods using Electrical ResistanceTomography (ERT): Sensitivitty Studies.* Journal of Environmental and Engineering Geophysics, 2003. **8**: p. 187-208.
14. Giese, R., Henninges, J., Lüth, S., Morozova, D., Schmidt-Hattenberger, C., Würdemann, H., Zimmer, M., Cosma, C., Juhlin, C., and CO2 SINK Group, *Monitoring at the CO2 Sink Site: A Concept Integrating Geophysics, Geochemistry and Microbiology.* Energy Procedia, 2009. **1**(2009): p. 2251–2259.
15. Nakatsuka, Y., Xue, Z., Garcia, H., and Matsuoka, T, *Experimental Study on Monitoring and Quantification of Stored CO2 in Saline Formation using Resistivity measurements.* International Journal of Greenhouse Gas Control, 2010. **4**: p. 209-216.
16. Graham, J.W., *Reverse Wetting Logging.* Trans. AIME, 1958. **213**.
17. Haro, C.F., *The Equations Archie Forgot: Anisotropy of the Rocks.* SPE Reservoir Evaluation and Engineering, October, 2010: p. 823-836.
18. Herrick, D.C., *Conductivity Models, Pore Geometry, and Conduction Mechanisms*, in *SPWLA Twenty-Ninth Annual Logging Symposium, June 5-8,* 1988.
19. Worthington, P.F., and Pallat, N, *Effect of Variable Saturation Exponent on the Evaluation of Hydrocarbon Saturation.* SPE Formation Evaluation, December, 1992(December): p. 331-336.

20. Wyllie, M.R.J., and Rose,W.D, *Comments in the Relation Between Electrical Resistivity and Brine Saturation in Reservoir Rocks.* Journal of Petroleum Technology, 1949.
21. Carter, L.S., and Power, H.H, *The Relationship Between Resistivity and Brine Saturation in Reservoir Rocks*, in *Petroleum Engineeringy*1951, University oTexas. p. 1-17.
22. Mungan, N., and Moore, E.J, *Certanin Wettability Effects on Electrical Resistivity In Porous Media.* The Journal of Canadian Petroleum, January-March, 1968: p. 20-25.
23. Swanson, B.F., *Microporosity in Reservoir Rocks: Its Measurements and Influence on Electrical Resistivity.* The Log Analyst, 1985. **November-December, 1985** p. 42-60.
24. Rasmus, J.C., *A Summary of the Effects of Various Pore Geometries and Their Wettabilities on Measured and In-situ Values of Cementation and Saturation Exponents* The Log Analyst, 1987(March-April, 1987): p. 152-164.
25. Worthington, P.F., .Pallatt, N., and Toussaint-Jackson, J. T *Influence of Microporosity on the Evaluation of Hydrocarbon Saturation.* SPE Formation Evaluation, June, 1989: p. 203-209.
26. Crane, S.D., *Impacts of Microporosity, Rough Pore Surfaces and Conducttve Minerals on-Saturation Calculations from Electric Measurements: an Extended Archie's Law* in *SPWLA 31st Annual Logging Symposium. June 24-27. 1990*1990.
27. Waxman, M.H., and Smits, L.J.M *Electrical Conductivities in Oil Bearing Shaly Sands.* SPE Journal, June, 1968: p. 107-122.
28. Diederix, K.M., *Anomalous Relationships Between Resist Ivity Index And Water Saturations In The Rotliegend Sandstone (The Netherlands)*, in *Spwla Twenty.Third Annual Logging Symposium, July 6-9, 1982*1982.
29. Han, M., Tariel, V., Youssef, S., Rosenberg, E., Fleury, M., and Levitz, P. *The Effect of the Porous Structure on Resistivity Index Curves. An Experimental and Numerical Study*. in *SPWLA 49 th Annual Logging Symposium held in Edinburgh, Scotland, May 25-28, 2008.* . 2008. Edinburgh, Scotland, : Society of Petrophysicists and Well Log Analysts (SPWLA)

30. Dixon, J.R., and Marek, B.F, *The Effect of Bimodal Pore Size Distribution on Electrical Properties of Some Middle Eastern Limestones*, in *65th Annual Technical Conference and Exhibition of the Society of Petroleum Engineers held in New Orleans, LA, September 23-26, 1990*1990.
31. Suman, R.J., and Knight, R.J, *Effects of Pore Structure and Wettability on the Electrical Resistivity of Partially Saturated Rocks—A Network Study.* Geophysics, July-August, 1997. **62**(4): p. 1151–1162.
32. Moore, J., *Laboratory Determined Electrical Logging Parameters of the Bradford Third Sand.* Production Monthly, 1958. **22**(5): p. 30-39.
33. Donaldson, E.C., and Bizerra, M.J, *Relationship of Wettability to the Archie Saturation Exponent*, in *3rd International UNITAR/UNDP Heavy Crude and Tar Sands Conference*1984, United Nations Institute for Training and Research, Information Centre for Heavy Crude and Tars: New York. p. 664-684.
34. Keller, G.V., *Effect of Wettability on the Electrical Resisitance of Sand.* Oil and Gas Journal, 1953. **51**(34): p. 62-68.
35. Sweeney, S.A., and Jennings, H. V, *The Electrical Resistivity of Preferentially oil Wet Carbonate Rocks.* Production Monthly, 1960. **24**(7): p. 29-32.
36. Anderson, W.G., *Wettability Literature Survey- Part 3: The Effects of Wettability on the Electrical Properties of Porous Media.* Journal of Petroleum Technology, December, 1986: p. 1371-1377.
37. Sharma, M.M., Garrouch, A., and Dunlap, H. F, *Effects of Wettability, Pore Geometry, and Stress on Electrical Conduction in Fluid Saturated Rocks.* The Log Analyst, September-October, 1991: p. 511-526.

38. Dicker, A.I.M., and Bemelmans, W.A. *Models for Stimulating the Electrical Resistance of Porous Media*. in *25th Annual Logging Symposium Transactions*. 1984. Society of Professional Well log Analysts.
39. Sweeney, S.A., and Jennings, H. V, *Effect of Wettability on the Electrical Resistivity of Carbonate Rock from Petroleum Reservoir.* J. Phys. Chem, May, 1960. **64**(5): p. 551-553.
40. Morgan, W.B., and Pirson, S.J. *The Effect of Fractional Wettability on the Archie Saturation Exponent*. in *Trans., SPWLA, Fifth Annual Logging Symposium*. 1964. Midland, TX: SPWLA.
41. Rust, C.F., *A Laboratory Study of Wettability Effects on Basic Core Parameters, Paper SPE 986-G*, in *SPE Venezuela Annual Meeting*1957: Caracas.
42. Schmid, C., *The Wettability of Petroleum Rocks and Results of Experiments to Study the Effects of Variations in Wettability of Core Samples.* Erdol und Kohle-Erdgas-Petrochemie, 1964. **17**(8): p. 605-609.
43. Licastro, P.H., and Keller, G.V, *Resistivity Measurements as a Criterion for Determining Fluid Distribution in the Bradford Sand.* Producers Monthly, May, 1953: p. 17.
44. Lasswell, P.M., *Core Analysis for Electrical Properties.* Petrophysics, 2006. **47**(3): p. 191-213.
45. Richardson, J.G., Perkins, F.M., and Osoba, J.S, *Differences in the Bahavior of Fresh and Aged East Texas Woodbine Cores* Trans. AIME, 1955. **204**: p. 86-91.
46. Ara, T.S., Talabani, S., Vaziri, H. H., and Islam, M. R. *In-Depth Investigation of the Validity of the Archie Equation in Carbonate Rocks*. in *SPE Production and Operations Symposium held in Oklahoma City, Oklahoma, 24–27 March*. 2001.
47. Trantham, J.C., and Clampitt, R.L *Determination of Oil Saturation after Water Flooding in an Oilwet Reservoir-The North Burbank Unit, Tract 97 Project.* Journal of Petroleum Technology, May, 1977: p. 491-500.
48. Winn, R.H., *The Fundamentals of Quantitative Analysis of Electric Logs*, in *Symposium on Formation Evaluation, AIME*1955.
49. Verwer, K., Eberli, E. P., and Weger, R. J, *Effects of Pore Structure on Electrical Resistivity in Carbonates.* AAPG Bulletin, 2011. **95**(2): p. 175-190.
50. Winsauer, W.O., Shearin,H.M., Masson, P.H., and Williams, M, *Resistivity of Brine Saturated Sands in Relation to Pore Geometry.* Bulletin of America Association of Petroleum Geologist, 1952. **36**(2).
51. Schlumberger, *Log Interpretation Charts, 1984 Edition*. 1984, Sugar Land, Texas, USA.
52. Mahood, B.C., and Boyd, D.A, *Formation Factor Relationships of Western Canada*, in *SPWLA Annual Logging Symposium*1993: Calgary.
53. Aguilera, R., *Naturally Fractured Reservoirs, second edition, 521*. 1995, Tulsa: Pennwell Books.
54. Lucia, F.J., *Carbonate Reservoir Characterization, 68*. Vol. 68. 1999, Berlin: Springer-Verlag.
55. Ragland, D.A., *Trends in Cementation Exponents (m) for Carbonate Pore Systems.* Petrophysics, 2002. **43**(5): p. 434-446.
56. Longeron, D., and Yahya, F. *Laboratory Measurements of Cementation Factor and Saturation Exponent Under Reservoir Conditions on Asab Reservoir Rock Samples*. in *5th Annual Society of Core Analysis Technical Conference*. 1991. San Antonio, Texas.
57. Salem, H.S., and Chilingarian, G.V, *The Cementation Factor of Archie's equation for Shaly Sandstone Reservoirs.* Journal of Petroleum Science and Engineering, 1999. **23**: p. 83-93.
58. Javadpour, F., *CO2 Injection in Geological Formations: Determining Macroscale Coefficients from Pore Scale Processes.* Transport in Porous Media, 2009. **79**(1): p. 87-105.
59. White, C.M., Strazisar, B.R., Granite, E.J., Hoffman, J.S., and Pennline, H.W, *Seperation and Capture of CO2 from Large Stationary Sources and Sequestration in Geological Formations-Coalbeds and Deep Saline Aquifers.* Journal of the Air and Waste Management Association, 2003. **53**(645-715).

60. Alotaibi, M.B., Nasr-El-Din, H.A., and Fletcher, J.J, *Electrokonetics of Limestone and Dolomite Rock Particles.* SPE Reservoir Eval. & Eng., October, 2011: p. 594-603.
61. Mitchell, M.J., Jensen, O.E., Cliffe,. K. A., and Maroto-Valer, M.A, *A model of carbon dioxide dissolution and mineral carbonation kinetics.* Proceedings of the Royal Society A, 2011. **466**: p. 1265-1290.
62. Kharaka, Y.K., Cole, D.R., Hovorka, S.D., Gunter, W.D., Knauss, K.G., and Freifeld, B.M, *Gas-Water-Rock Interactions in Frio Formation following CO_2 Injection: Implications for the Storage of Greenhouse Gases in Sedimentary Basins.* Geology, 2006. **34**(7): p. 577- 580.
63. Wildenborg, A.F.B., and Van der Meer, L.G.H. *The Use of Oil, Gas, and Coal Fields as CO2 Sinks*. in *Intergovernmental Panel on Climate Change, Working Group III: Mitigation of Climate Change, Workshop on Carbon Dioxide Capture and Storage*. 2002. Regina, Canada.
64. Kaszuba, J.P., Janecky, D.R., and Snow, M.G, *Carbon dioxide reaction processes in a model brine aquifer at 200^0 C and 200 bars: implications for geologic sequestration of carbon.* Applied Geochemistry 2003. **18**(2003): p. 1065–1080.
65. Nakatsuka, Y., et al., *Experimental study on CO2 monitoring and quantification of stored CO2 in saline formations using resistivity measurements.* International Journal of Greenhouse Gas Control, 2010. **4**(2): p. 209-216.
66. Kiessling, D., et al., *Geoelectrical methods for monitoring geological CO2 storage: First results from cross-hole and surface–downhole measurements from the CO2SINK test site at Ketzin (Germany).* International Journal of Greenhouse Gas Control, 2010. **4**(5): p. 816-826.
67. Bust, V.K., Oletu, J. U., and Worthington, P.F., *The Challenges for Carbonate Petrophysics in Petroleum Resource Estimation.* SPE Reservoir Evaluation and Engineering, February, 2011: p. 25-34.
68. Fleury, M., *Resistivity in Carbonates: New Insights* in *SPE Annual Technical Conference and Exhibition held in San Antonio, Texas, 29 September–2 October*2002. p. 1-9.
69. Honarpour, M.M., Djabbarah., N.F., and Sampath, K., *Whole-Core-Analysis-E|xperience and Challenges.* SPE Reservoir Evaluation and Engineering, December, 2005: p. 460-469.
70. Sen, P.N., *Resistivity of Partially Saturated Carbonate Rocks with Mocroporosity.* Geophysics, 1997. **62**(2): p. 415-425.
71. Zemke, K., Liebscher, A., and Wandrey, M, *Petrophysical analysis to investigate the effects of carbon dioxide storage in a subsurface saline aquifer at Ketzin, Germany (CO_2 SINK).* International Journal of Greenhouse Gas Control, 2010. **4**: p. 990-999.
72. Kjoller, C., Weibel, R., Bateman, K., Laier, T., Nielsen, L.H., Frykman, P., and Springer, N, *Geochemical impacts of CO_2 storage in saline aquifers with various mineralogy – results from laboratory experiments and reactive geochemical modelling* Energy Procedia., 2011. **4**: p. 4724–4731.
73. Lu, P., Fu, Q., Seyfried Jr., W.E., Hereford, A., and Zhu, C, *Navajo Sandstone–brine–CO_2 interaction: implications for geological carbon sequestration.* Environ Earth Sci, 2011. **62**: p. 101–118.
74. Gunter, W.D., Perkins, E.H. and Hutcheon, I., *Aquifer disposal of acid gases: modeling of water-rock reactions for trapping of acid wastes.* Applied Geochemistry, 2000. **15**: p. 1085-1095.
75. Perkins, E., Czernichowski-Lauriol, I., Azaroual, M. and Durst, P. *Long term predictions of CO2 storage by mineral and solubility trapping in the Weyburn Midale reservoir*. in *7th International Conference on Greenhouse Gas Control Technologies*. 2005. Oxford: Elsevier,.
76. Parry, W.T., Forster, C.B., Evans, J.P., Bowen, B.B., and Chan, M.A, *Geochemistry of CO2 Sequestration in the Jurassic Navajo Sandstone, Colarado Plateau, Utah.* Environ Geosci, 2007. **14**(2): p. 91-109.

77. Mathis, R.L., and Sears, S.O, *Effect of $C0_2$ Wasson (San Flooding on Dolomite Reservoir Rock, Denver Unit, Andres) Field, TX*, in *59th AnnualTechnical Conferenceand Exhibitionheld*1984, SPE 13132: Houston,Texas.
78. Morgenthaler, L.N., Lawson, J.B., Faircloth, R.J., and Berkshire, D.C, *Scale Prediction and Control in the Denver Unit CO2 Flood*, in *SPE Annual Technical Conference and Exhibition, Paper SPE 26603*1993: Houston, Texas, USA.
79. Wellman, T.P., Grigg, R.B., McPherson, B.J., Svec, R.K., and Lichtner, P.C. *Evaluation of CO2-Brine-Reservoir Rock Interaction with Laboratory Flow Tests and Reactive Transport Modelling*. in *International Symposium on Oilfield Chemistry*. 2003. Houston, Texas, USA.
80. Mohamed, I.M., and Nasr-El-Din, H.A, *CO_2 Sequestration in Dolomite Rock*, in *International Petroleum Technology Conference held in Bangkok, Thailand, 7-9 February* 2011. p. 1-26.
81. Alam, M.M., Hjuler, M.L., and Fabricius, I.L, *Impact of Supercritical CO2 Injection on Petrophysical and Rock Mechanics Properties of Chalk: An Experimental Study on Chalk from South Arne Field, North Sea* in *SPE Annual Technical Conference and Exhibition*2011, SPE 147056: Denver, Colorado, USA.
82. Xu, T., Apps, J.A., and Pruess, K, *Numerical Simulation to Study Mineral Trapping for CO2 Disposal in Deep Aquifers.* GeoChim Cosmochim Acta, 2004. **69**(6): p. 1435-1453.
83. Mohamed, I.M., Mahmoud, M.A., and Nasr-El-Din, H.A, *Effects of Pressure, CO_2 Volume, and the CO_2 to Water Volumetric Ratio on Permeability Change during CO_2 Sequestration. SPE Paper 136394* in *Abu Dhabi International Petroleum Exhibition & Conference, 1-4 November*2010: Abu Dhabi, UAE.
84. Wandrey, M., Fischer, S., Zemke, K., Liebscher, A., Scherf A.K., Vieth-Hillebrand, A., Zettlitzer, M., and Würdemann, H, *Monitoring petrophysical, mineralogical, geochemical and microbiological effects of CO exposure - Results of long-term experiments under in situ conditions* Energy Procedia, 2011. **4**: p. 3644–3650.
85. Omole, O., and Osoba, J.S, *Carbon Dioxide-Dolomite Rock Interaction During CO2 Flooding Process*, in *Petrol. Soc. Canadian Inst. Min. Metal, paper 83-34-17*1983: Banff, Alberta. p. 1-13.
86. Ross, G.D., Todd, A.C., and Tweedie, J.A. *The Effects of Simulated CO2 Flooding on the Permeability of Reservoir Rocks*. in *3rd European Symp. Enhanced Oil Recovery*. 1981.
87. Ross, G.D., Todd, A.C., Tweedie, J.A., and Will, A.G.S. *The Dissolution Effects of CO2 Brine Systems on the Permeability of U.K and North Sea Calcareous Sandstones* in *3rd Joint SPE/DOE Symp. Enhanced Oil Recovery, SPE/DOE 10685*. 1982.
88. Xiao, Y., Xu, T., and Pruess, K, *The Effect of Gas-Fluid-Rock Interactions on CO2 Injection and Storage: Insights from Reactive Transport Modelling.* Energy Proceedia, 2009. **1**(GHGT 9).
89. Wolcott, J.M., Monger, T. G., Sassen, R., and Chinn, E.W. *The Effect of CO2 Flooding on Reservoir Mineral Properties*. in *1989 SPE International Symposium Oilfield Chemistry, SPE 18467*. 1989.
90. Cerepi, A., Burlot, R., Galaup, S., Barde, J-P., Loisy, C., and Humbert, L., *Effect of Porous Solid Structures on the Electrical Behaviour: Prediction Key of Transport Properties in Sedimentary Reservoir Rock.* Studies in Surface Science Catalysis, 2002. **144**.
91. Eberli, G.P., Baechle, G.T., Anselmetti, F.S., and Ince, M.L, *Factors Controlling Elastic Properties in Carbonate Sediments and Rocks.* The Leading Edge, 2003. **22**(654-660).
92. Abousrafa, E.M., Somerville, J. M., Hamilton, S. A., Olden, P. W. H., Smart, B. D. G., and Ford, J, *Pore Geometrical Model for the Resistivity of Brine Saturated Rocks.* Journal of Petroleum Science and Engineering, 2009. **65**: p. 113-122.
93. Monger, T.G., and Fu, J.C. *The Nature of CO2 induced Organic Deposition*. in *1987 SPE Annual Technical Conference, SPE 16713*. 1987.
94. Monger, T.G., and Trujillo, D.E, *Organic Deposition During CO2 and Rich Gas Flooding.* SPE Reservoir Engineering, 1991. **6**: p. 17-24.

95. Nelson, P.H., *Pore-throat sizes in sandstones, tight sandstones, and shales.* AAPG Bulletin, 2009. **93**(3): p. 329–340
96. Vavra, C.L., Kaldi, J.G., and Sneider, R.M, *Geological Applications of Capillary Pressure; a Review.* AAPG Bulletin, 1992. **76**(6): p. 840-850.
97. Al-Asimi, M., Brown, G., Clancy, T., Cosad, C., Fitzgerald, J., Gabb, A., Ingham, J., and Kimminau, S, *Advances in Well and Reservoir Surveliance.* Oilfield Review, 2002/2003. **Winter**.
98. Smith, J.K., et al., *Real-Time and In-Situ Detection of Calcium Carbonate Scale in a West Texas Oil Field.* SPE Production & Facilities, 2004. **May**: p. 94-99.
99. Gunarathne, G.P.P. and R.W. Keatch, *Novel Techniques for Monitoring and Enhancing Dissolution of Mineral Deposits in Petroleum Pipelines*, 1996, Society of Petroleum Engineers.
100. Wyatt, D.F., Jacobson, L. A., Fox, P., *Use of Supplemental Curves From Pulsed Spectral Gamma Logs To Enhance Log Interpretation*, 1994, Society of Petroleum Engineers.
101. Bertrand, B., G. Ségéral, and P.O. Moksnes, *Detection and Identification of Scales Using Dual Energy / Venturi Subsea or Topside Multiphase Flow meters*, in *Offshore Technology Conference*2001, Offshore Technology Conference: Houston.
102. Bamforth, S., Besson, C., Stephenson, K., Whittaker, K., Brown, B., Catala, G., Rouault, G., Theron, B. , *Revitalizing Production Logging.* Oil field review, 1996. **8**(4): p. 44-60.
103. Morizot, A.P. and A. Neville, *A Novel Approach for Monitoring of CaCO3 and BaSO4 Scale Formation*, in *SPE second International Symposium on Oilfield Scale*2000, Society of Petroleum Engineers, Paper SPE 60189 Aberdeen.
104. Love, J.D. *Tapered single-mode fores and devices-Part 1: Adiabatic*. in *IEEE*. 1999.
105. Emmons, D.H., Graham, G. C., Holt, S. P., Jordan, M. M., and Locardel, B, *On-Site, Near-Real-Time Monitoring of Scale Deposition*, in *SPE Annual Technical Conference and Exhibition*1999, Society of Petroleum Engineers: New Orleans.
106. Elashahab, B.M., Jing, X. D., Archer, J. S., *Resistivity Index and Capillary Pressure Hysteresis for Rock Samples of Different Wettability Characteristics*, in *SPE Middle East Oil Show*1995, Society of Petroleum Engineers: Bahrain.
107. Clerke, E.A., Mueller, H.W., Philips, E.C., Eyvazzadeh, R.Y., Jones, D.H., Ramamoorthy, R., and Srivastava, A, *Application of Thomeer hyperbolas to Decode the Pore Systems, Facies, and Reservoir Properties of the Upper Jurassic Arab D Limestone, Ghawar Field, Saudi Arabia: A "Rosetta Stone" Approach.* Geoarabia, 2008. **13**(4): p. 113-160.
108. Clerke, E.A.a.P.R.M., *Thomeer Swanson excel spreadsheet and FAQ's and user comments*, in *SPWLA Carbonate Petrophysics Workshop*2004: Noordwijk, the Netherlands.
109. Eke, P., E., Naylor, M., Haszeldine, S., Curtis, A., *CO2/Brine Surface Dissolution and Injection: CO2 Storage Enhancement.* SPE Journal Paper, 2011: p. 41-53.
110. Duan, Z. and R. Sun, *An improved model calculating CO2 solubility in pure water and aqueous NaCl solutions from 273 to 533 K and from 0 to 2000 bar.* Chemical Geology, 2003. **193**(3–4): p. 257-271.
111. Duan, Z., et al., *An improved model for the calculation of CO2 solubility in aqueous solutions containing Na+, K+, Ca2+, Mg2+, Cl−, and SO42−.* Marine Chemistry, 2006. **98**(2–4): p. 131-139.
112. Amyx, J., D. Bass, and R. Whitney, *Petroleum Reservoir Engineering*. 1960, New York: McGraw-Hill Book Company.
113. Archie, G.E., *The Electrical Resistivity Log as an Aid in Determining Some Reservoir Characteristics.* Petroleum Transactions of AIME, 1942. **146**: p. 54–62.
114. *Routine core analysis, Pore size distributions. Application note 2* June 12 2014; Available from: http://www.magritek.com/products/spinsolve/.
115. Bouchard, A.J. and J.T. Hawkins, *Reservoir-engineering Implications Of Capillary-pressure And Relative-permeability Hysteresis.* The log Analyst, 1992. **July-August**: p. 415-420.

116. Longeron, D.G., M.J. Argaud, and J.P. Feraud, *Effect of Overburden Pressure and the Nature and Microscopic Distribution of Fluids on Electrical Properties of Rock Samples.* SPE Formation Evaluation, 1989. **June**: p. 194-202.
117. Gray, R., Trewin, B., Pallat, N., and Mitchell, P., *Comparison of Saturation Exponent Data by the Porous Plate and Continuous injection Technique with in-situ Saturation Monitoring*, in *Third European Core Analysis Symposium*1992: Paris.
118. Jing, X.D., Elashahab, B.M., and Archer, J.S. , *Experimental Investigation of the Effect of Wettability, Saturation History, and Overburden Pressure on Resistivity Index*, in *SPWLA 15th European Evaluation Symposium*1993, SPWLA Paper B: Stavanger, Norway.
119. Al-Kaabi, A.U., K. Mimoune, and H.Y. Al-Yousef, *Effect of Hysteresis on the Archie Saturation Exponent*, in *SPE 10th Middle East Oil Show & Conference*1997, Society of Petroleum Engineers: Manama, Bahrain.
120. Elashahab, B.M., Jing, X. D., Archer, J. S., *Resistivity Index and Capillary Pressure Hysteresis for Rock Samples of Different Wettability Characteristics*, 1995, Society of Petroleum Engineers.
121. Ramirez, A., Daily, W., Binley, A., LaBrecque, D., and Roelant, *Detection of leaks in underground storage tanks using electrical resistance methods.* Journal of Environmental and Engineering Geophysics, 1996. **1**(3).
122. Ramirez, W.D.a.A., *Electrical imaging of engineered hydraulic barriers.* Geophysics, 2000. **65**(1): p. 83-94.
123. Robin L. Newmark, A.L.R., William D. Daily, *Electrical Imaging EOR stimulation using steel-cased boreholes*, in *SPE/AAPG Western Regional Meeting*2000: Long Beach, California.
124. Seo, J.G. and D.D. Mamora, *Experimental and Simulation Studies of Sequestration of Supercritical Carbon Dioxide in Depleted Gas Reservoirs*, Society of Petroleum Engineers.
125. De Mago, M.C.N., *Effect of Flue-Gas Impurities on the Process of Injection and Storage of CO2 in Depleted Gas Reservoirs.* Journal of Energy Resources Technology, 2008. **130**(1).
126. Mohamed, I.M., J. He, and H.A. Nasr-El-Din, *Experimental Analysis of CO2 Injection on Permeability of Vuggy Carbonate Aquifers.* Journal of Energy Resources Technology, 2012. **135**(1): p. 013301-013301.
127. Nguyen, P., H. Fadaei, and D. Sinton, *Microfluidics Underground: A Micro-Core Method for Pore Scale Analysis of Supercritical CO2 Reactive Transport in Saline Aquifers.* Journal of Fluids Engineering, 2013. **135**(2): p. 021203-021203.
128. Boynton, W.V., Ming, D. W., Sutter, B., Arvidson, R. E. , Hoffman, J., Niles, P.B., Smith, P. *Evidence For Calcium Carbonate At The Phoenix Landing Site*. in *40th Lunar and Planetary Science Conference*. 2009. The Woodlands, Texas
129. Radha, A.V. and A. Navrotsky, *Thermodynamics of Carbonates.* Reviews in Mineralogy and Geochemistry, 2013. **77**(1): p. 73-121.
130. Daneshfar, J., R.G. Hughes, and F. Civan, *Feasibility Investigation and Modeling Analysis of CO2 Sequestration in Arbuckle Formation Utilizing Salt Water Disposal Wells.* Journal of Energy Resources Technology, 2009. **131**(2): p. 023301-023301.

Vitae

Name:	Abdulrauf Rasheed Adebayo
Nationality:	Nigeria
Date of Birth:	07/07/1977
Email:	raufrash@yahoo.com
Address:	Offa, Kwara, Nigeria
Academic Background:	Petroleum Engineering